TD

Piezoelectric Electrospun Nanomaterials as a Platform for Biological Applications

DOCTORAL THESIS

Huang Wei
DOCTORATE IN CHEMISTRY
SPECIALITY IN NANOCHEMISTRY

UNIVERSIDADE da MADEIRA
A Nossa Universidade
www.uma.pt

November | 2020

Piezoelectric Electrospun Nanomaterials as a Platform for Biological Applications

DOCTORAL THESIS

Huang Wei

DOCTORATE IN CHEMISTRY
SPECIALITY IN NANOCHEMISTRY

ORIENTATION

Pedro Filipe Duarte Louzeiro Pires

Piezoelectric Electrospun Nanomaterials as a Platform for Biological Applications

Thesis submitted to the University of Madeira for obtaining

the degree of Ph.D. in Chemistry

By Huang Wei

Under the supervision of Prof. Pedro Pires

Faculdade de Ciências Exatas e da Engenharia

Centro de Química da Madeira

Universidade da Madeira

Campus da Penteada 9000-390, Funchal – Portugal

November 2020

Acknowledgment

I remember myself as an ambitious and aspiring young master student with wonderful expectation when I first stepped into this fantastic island. Looking over the Madeira island for the first time from my flight, I had the feeling that I was going to make a big difference in this full of green and blue place. 5 years has passed and there comes graduation. The Madeira island is still beautiful as a paradise with amazing mountains, high cliffs, lava pools, exotic flowers, waterfall, and beaches, but my mindset and my understanding had significantly improved. Looking back, I experience ups and downs in my project as well as in my mindset. It was most experienced and tough period of my life. When I stayed on the bench near the port of Funchal, looking up the blue sky and ocean with my mind wandering around the universe. I believe I have gradually grasped how to become a good and independent researcher and gained invaluable understanding about myself. The whole of achievements from my Ph.D. career cannot happen without CQM members and other colleagues and friends.

I would like to thank my supervisor Prof. Pedro for his guidance and support during my Ph.D. project. I learned a lot from his deep thinking and intuitive explanation. Without his patience, motivation and knowledge, our challenging project, which involve the whole new idea of creating inverse piezoelectric device cannot complete.

I would also like to thank Prof. Shi from Donghua university, who support my critical project characterization and invaluable advice on my project. He is a great scientist to look up to and learn from. Besides Prof. Shi, I would like to thank Prof. Bai from Wuhan Textile University, who help me to finish one of most important piezoelectric characterization of my project. I still want to thank Prof. Lv from Suzhou university, who support my *in vitro* experiments.

I am also genuinely grateful to all my lab mates in CQM that I have had the pleasure of work with, especially. Ana Olival, Carla Miguel, Carla Alves, Dina Maciel, Mara Goncalves, Nadia Nunes, Rita Castro who support me directly in my Ph.D. project.

I also appreciate the help from Prof. Shi's lab members. That one year researching life with all of you is unforgettable memories. They are Xiao Tingting, Chen meixiu, Zhang Ni, Chen Huan, Zhu Wei, Sun Wenjie, Wang Xiaomeng, Ouyang Zhijun, Li Jin, Song Cong, Zhang Changchang, Xiao Yunchao, Fan Yu, Jia Liang, Xiong Zhijuan.

I still cannot forget the happiness from my flatmates and friends. Especially, Kenneth Kemp and Nadia Nudes. Our beautiful friendship is the most original power for me to overcome the hardest time.

Of course, Thanks must go to my lovely parents, sister, brother-in-law, niece and cousin. They tried their best to support and encourage me to do what I want. Without their constant support, I would never have had a chance to finish my Ph.D. or even to come study in Madeira.

Finally, I want to thank myself, never give up in the past 5 years and grow up to be an independent person.

These were the most experienced 5 years I have had. While challenging, it was undoubtedly exciting. Thank you to everyone I have met long the Ph.D. journey.

Sponsoring fund: This work was financially supported by the *Fundação para a Ciência e Tecnologia* (*FCT*) through the CQM different Strategic Projects (UID/QUI/00674/2013, UID/QUI/00674/2015, Pest-OE/QUI/UI0674/2019, and the CQM Base Fund - UIDB/00674/2020, Programmatic Fund - UIDP/00674/2020). The Madeira 14-20 Program and ARDITI - *Agência Regional para o Desenvolvimento da Investigação Tecnologia e Inovação*, respectively through the projects PROEQUIPRAM - *Reforço do Investimento em Equipamentos e Infraestruturas Científicas na RAM* (M1420-01-0145-FEDER-000008) and M1420-01-0145-FEDER-000005 - *Centro de Química da Madeira - CQM*$^{+}$ (Madeira 14-20 Program).

Abstract

Piezoelectric materials as new smart biomaterials show great potential for biological applications. Specifically, piezoelectric polyvinylidene fluoride (PVDF) electrospun nanofibers, possess outstanding properties, which provide many advantages in various healthcare applications.

We followed a systematic fabrication approach to create a new device for mechanical stimulation of cells, based upon the inverse piezoelectric effect from functionalized PVDF nanofibers, and tested it with different cell lines.

The major contents in this thesis are presented as follows:

(1) Fibers fabrication and characterization

Multi-walled carbon nanotubes (MWCNTs) were blended with PVDF to fabricate highly aligned PVDF/MWCNTs piezoelectric nanofibers. In this part we investigated the PVDF/MWCNTs nanofibers' properties, such as, morphology, alignment, crystal structure, mechanical properties, piezoelectric output voltage and cytotoxicity.

(2) Biological applications of inverse piezoelectric stimulation

To explore the effect of mechanical stimulation on cellular behavior, specifically, morphology, proliferation, migration and differentiation, we selected three cell line models: NIH3T3 cells as fibroblasts; PC12 cells as neuroblastic cells; mesenchymal stem cells. All cells were submitted to an inverse piezoelectric stimulation over 30 minutes per day, with 10 V amplitude at 5 Hz frequency driving signal.

It was found that inverse piezoelectric stimulation with PVDF/MWCNTs nanofibers, not just improved the proliferation of NIH3T3 cells, but also efficiently guided the cells migration.

In the part of neuroblastic cells investigation, the adhesion, proliferation and differentiation results of PC12 cells submitted to the inverse piezoelectric stimulation shown a great improvement.

In the study of mesenchymal stem cells (MSCs), the inverse piezoelectric PVDF/MWCNTs nanofibers could not improve the adhesion and proliferation of MSCs in early stage, but it improved the osteogenic differentiation.

Therefore, according to our results, we believe that inverse piezoelectric stimulation with aligned PVDF/MWCNTs nanofibers holds a great potential on wound healing, nerves regeneration and bone tissue engineering applications.

Keywords: electrospinning, piezoelectricity, nanofibers, biological applications

Resumo

Os materiais piezoelétricos apresentam um enorme potencial para aplicação como biomateriais inteligentes. As nanofibras de poli(fluoreto de vinilideno) [PVDF] piezoelétrico, possuem propriedades que as tornam vantajosas em várias aplicações biomédicas.

Utilizámos uma abordagem sistemática para criar um dispositivo inovador, para a estimulação mecânica de células, baseado no efeito piezoelétrico inverso de nanofibras de PVDF funcionalizadas, e testámo-lo em diferentes linhas celulares.

Apresenta-se em seguida o conteúdo principal desta tese:

(1) Fabricação e caracterização das fibras

Misturaram-se nanotubos de carbono de paredes múltiplas (MWCNTs) com PVDF, para produzir nanofibras com levado grau de alinhamento. Investigaram-se as propriedades das nanofibras de PVDF/MWCNTs, nomeadamente, a morfologia, alinhamento, estrutura cristalina, propriedades mecânicas, voltagem de saída e citotoxicidade.

(2) Aplicações biológicas do efeito piezoelétrico inverso

Para explorar os efeitos da estimulação mecânica no comportamento celular, especificamente, na morfologia, proliferação, migração e diferenciação, selecionámos três modelos de linhas celulares: células NIH3T3, como fibroblastos; células PC12, como modelo de células neuroblásticas; células estaminais mesenquimais. Todas as células foram submetidas a estimulação piezoelétrica inversa durante 30 minutos por dia, com um sinal de 10 V de amplitude e 5 Hz de frequência.

Verificou-se que a estimulação piezoelétrica inversa com nanofibras de PVDF/MWCNTs, além de melhorar a proliferação de células NIH3T3, também se mostrou eficiente para conduzir a migração celular.

No estudo de células neuroblásticas PC12 submetidas a estimulação piezoelétrica inversa, os resultados de adesão, proliferação e diferenciação mostraram um efeito positivo.

No estudo de células estaminais mesenquimais (MSCs) a estimulação com nanofibras de PVDF/MWCNTs não melhorou a adesão e proliferação das MSCs, mas melhorou a diferenciação osteogénica.

De acordo com os resultados obtidos, acreditamos que a estimulação piezoelétrica inversa com nanofibras de PVDF/MWCNTs, possui grande potencial para aplicações na cura de feridas, regeneração de nervos e aplicações de engenharia de tecido ósseo.

Palavras-chave: eletrofiação, piezoeletricidade, nanofibras, aplicações biológicas

Graphical Abstract

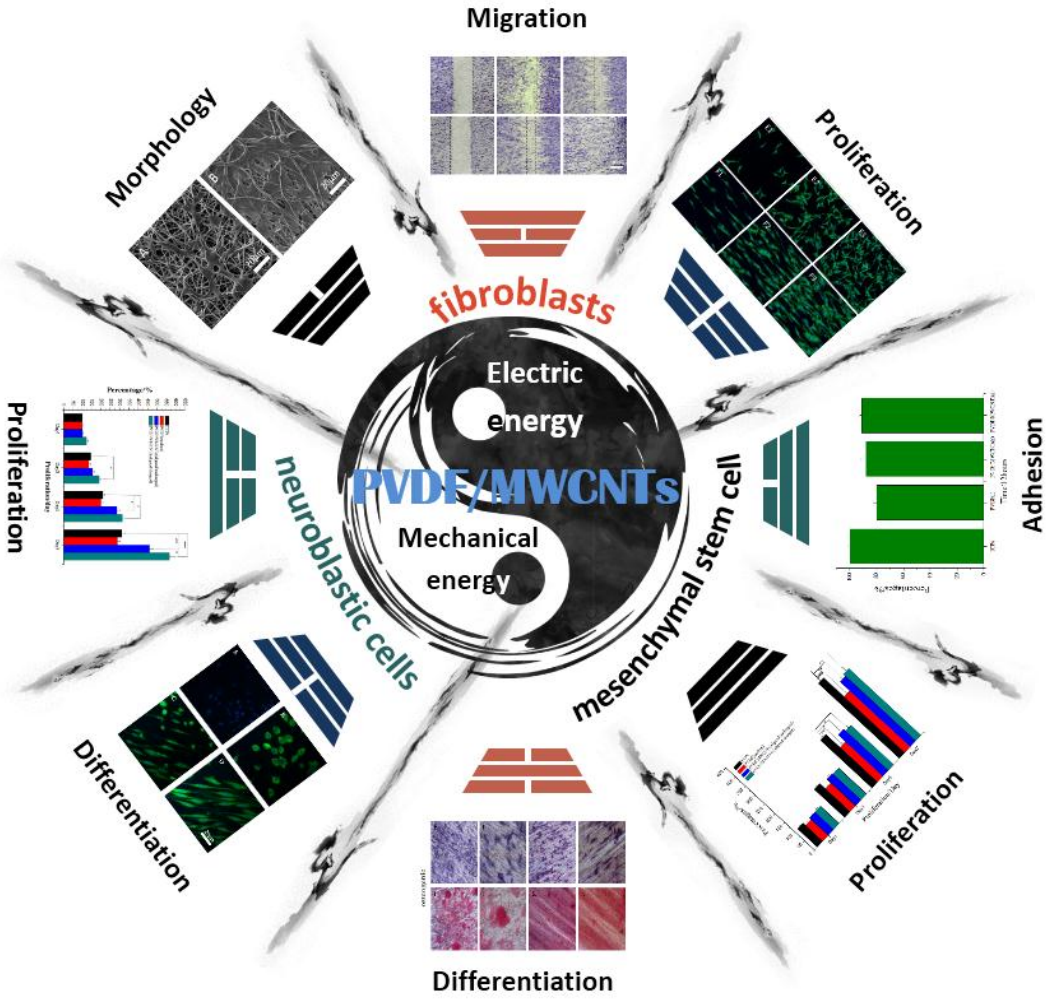

Abbreviations

3D	Three-dimensional
AA	Antibiotic-antimycotic
AlN	Aluminum nitride
ALP	Alkaline phosphatase assay kit
AMX	Amoxicillin
$BaTiO_3$	Barium titanate
BSA	Bovine Serum Albumin
CCK8	Cell counting Kit-8
CS	Chitosan
CNTs	Carbon nanotubes
DMEM	Dulbecco's Modified Eagle's Medium
DMF	Dimethylformamide
DOX	Doxorubicin
DMSO	Dimethyl sulfoxide
DAPI	4',6-diamidino-2-phenylindole
ECM	Extracellular matrix
F12	Hams F 12 nutrient medium
FBS	Fetal bovine serum
FFT	Fast Fourier transform
FTIR	Fourier transform infrared spectrophotometer
HPC	Hydroxypropyl cellulose
HS	Horse serum
IPSD	Inverse piezoelectric stimulation device
LAP	LAPONITE©
LSCM	Laser Scanning Confocal Microscopy
MSCs	Mesenchymal stem cells
MTT	3-[4,5-dimethyl-2-thiazolyl]-2,5-diphenyl-2H-tetrazolium bromide

MWCNTs	Multi-walled carbon nanotubes
NGF	Neural growth factor
NMP	N-methylpyrrolidone
PA	Polyamide
PAA	Polyacrylic acid
PAN	Polyacrylonitrile
PC	Polycarbonate
PCL	Polycaprolactone
PEO	Polyethylene oxide
PET	Polyurethane
PHB	Polyhydroxybutyrate
PI	Polyimide
PLA	Polylactic acid
PLGA	Poly(lactic-co-glycolic acid)
PLLA	Poly-L-lactic acid
PVA	Polyvinyl alcohol
PVDF	Polyvinylidene fluoride
P(VDF-TrFE)	Polyvinylidene fluoride-trifluoroethylene
PVP	Polyvinylpyrrolidone
PS	Penicillin-streptomycin
PU	Polyurethane
PZT	Lead zirconate titanate
REMA	Resazurin
SEM	Scanning electron microscope
TCPs	Tissue culture plates
TCH	Tetracycline hydrochloride
THF	Tetrahydrofuran
XRD	X-ray diffraction

Table of contents

Contents

List of figures

List of tables

Academic activities

Publications

Ph.D. project

1. Wei Huang, João Rodrigues, Xiangyang Shi, Pedro Pires. The inverse piezoelectric device development for biological applications. Patent (In preparation)

2. Wei Huang, Yuchao Xiao, Zhijun Xiong, Carla Alves, João Rodrigues, Xiangyang Shi, Pedro Pires. The effect of inverse piezoelectric stimulation on the behavior of fibroblasts. Paper (In preparation)

3. Wei Huang, Yuchao Xiao, Zhijun Xiong, Carla Alves, João Rodrigues, Xiangyang Shi, Pedro Pires. The effect of inverse piezoelectric PVDF/MWCNTs nanofibers stimulation on MSCs. Paper (In preparation)

The other works

4. W., Huang, Y. C., Xiao, X.Y., Shi. Construction of Electrospun Organic/Inorganic Hybrid Nanofibers for Drug Delivery and Tissue Engineering Applications. Advanced fiber materials 1, 32-45 (2019)

5. Y. Y., Yang, Z. P., Guo, W., Huang, W. L., Xu, S. J., Gu. Fabrication of multifunctional textiles with durable antibacterial property and efficient oil-water separation via in situ growth of zeolitic imidazolate framework-8 (ZIF-8) on cotton fabric. Applied surface science 503, 144079 (2020)

6. Y. Y., Yang, W., Huang, Z. P., Guo, Y. S., Zhang, W. L., Xu, S. J., Gu. Robust fluorine-free colorful superhydrophobic PDMS/NH2-MIL-125(Ti)@cotton fabrics for improved ultraviolet resistance and efficient oil-water separation. Cellulose 26, 9335-9348 (2019)

7. S. J., Gu, L., Yang, W., Huang, Y. M., Bu, W. L., Xu. Fabrication of hydrophobic cotton fabrics inspired by polyphenol chemistry. Cellulose 24, 2635-2646 (2017)

Conferences

1. Wei Huang, Xiangyang Shi, Pedro Pires. Piezoelectric PVDF/MWCNTs electrospun nanofibers as a platform for biological applications. 7th CQM Annual Meeting. Funchal, Portugal. 2020

2. Wei Huang, Xiangyang Shi, Pedro Pires. Comparison of cell behavior on PVDF/MWCNTs electrospun nanofibers with random and aligned configuration. 11th International Dendrimer Symposium. Funchal, Portugal. 2019

3. Wei Huang, Yunchao Xiao, Xiangyang Shi, Pedro Pires. The cells behavior of fibroblasts based on inverse piezoelectric nanofibers. International Conference on Biomedical Textile Materials, Shanghai, China, 2019.

Participation in advanced courses

Nanoschool 2016: "Principles and Applications of Fluorescence Spectroscopy" (8h, October **2016**). Lecturer: Prof. Fernando Lahoz, University of La Laguna (Spain).
Nanoschool 2015: "Bionanotechnology: From Bio to Nano & From Nano to Bio" (8h, October **2015**). Lecturer: Prof. Hiroshi Matsui, City University of New York (USA).

Other activities

Members of the Organizing Committee of Sino-France Healthcare Theranostics Forum. Shanghai, China. 2018

Chapter 1

1 Introduction

1.1 Electrospinning

1.1.1 History of electrospinning

Electrospinning as a viable fiber fabricating technique can be traced back to the beginning of 20th century. In 1902, John Cooley[1] and William Morton[2] obtained a pattern which generated powders or fibers through a high voltage apparatus. From this pioneering work, a series of techniques has been further developed, for example, John Zeleny[3] investigate the jet ejection at the tip of a metal capillary in 1914, Alton Formhals Anton[4] improved the equipment, moving toward the fabrication of cellulose acetate using acetone as the solvent. In 1938[5], the electrospun nanofibers were fabricated as the air filter for capturing aerosol particles. After this period of time, factory production of nanofibers as filter for gas mask applications were developed between 1950 and 1960[6]. Since the understanding of electrospinning was slowly developed, Geoffrey Taylor[7, 8] published a series of works which describe the process of polymer solution under the strong electric field. Specifically, the formation of Taylor cone was first reported in 1964. Until the 1990s, the word electrospinning was first introduced and this technique was described by Darrell Renenker and coworkers[9]. At the same time, electrospinning started to receive a lot of attention, especially many papers were published concerning the working parameters, such as, solution, ambient and instrumental parameters[10-12]. At beginning of this century, different types of electrospinning instruments were introduced and improved by several researchers[13-15] and new strategies were developed to control the structures and alignment of electrospun fibers. Nowadays, electrospun fibers hold a great potential in a series of applications (environment, catalysis, energy, photonics, electronics, biomedical applications etc.) due to their advantageous physical and chemical properties.

Table1 Brief summary of the development history of electrospinning

Year	Event	Researcher
1902	The fibers or powders was generated through a high voltage.	John Cooley and William Morton[1, 2]
1914	Investigation of jet ejection at tip of the metal capillary.	John Zeleny[3]
1938	Electrospun nanofibers were fabricated as the air filter.	Petryanov[5]
1950s, 1960s	Nanofibers as filter for gas mask applications.	
1964	Taylor cone was first reported.	Geoffrey Taylor[8]
1990s	Word Electrospinning was first introduced to describe this technique.	Darrell Reneker[10]
2000s	New strategies were developed and hold potential in series of applications.	

1.1.2 Mechanism of electrospinning

The typical electrospinning setup is relatively simple and can be summarized as follows: a high-voltage power supply, a syringe pump, a spinneret, and a conductive collector **(**Figure 1**)**.

In general, the electrospinning process can be divided into four main parts[16-21]: (1) when the applied power charges the solution until the electrostatic repulsion overcomes the surface tension, the formation of the Taylor cone is obtained. (2) From the apex of the Taylor cone, the charged jet is stretched and extends in a straight line[16]. (3) Due to the growth of unstable electrical bending, three different types (Fig. 2) of instabilities occur to electrically charged jet[17-21] (4) During the whole process of elongation, the jet solidifies and deposits to form fibers, which is caused by either solvent evaporation or the melt cooling.

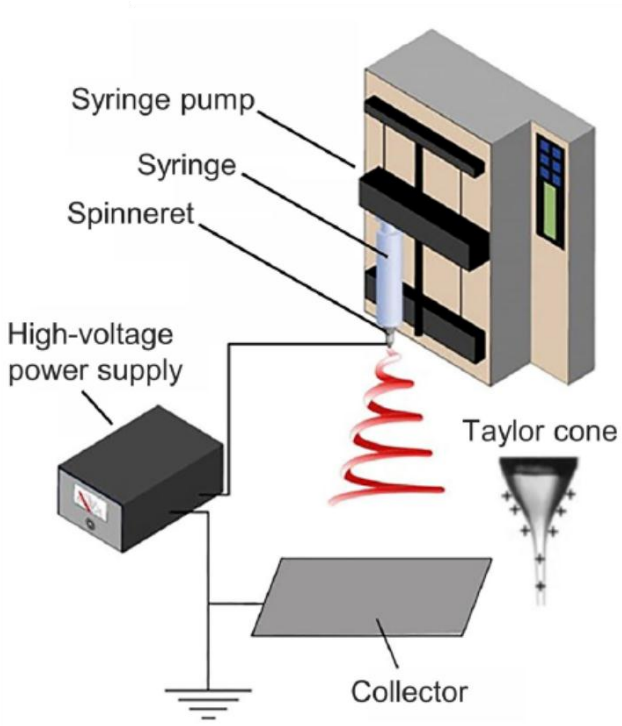

Fig. 1 Typical electrospinning setup

Effect of parameters on electrospinning

During the electrospinning process, there are several factors which affect the electrospun fibers, classified as the electrospinning parameters, solution and environmental parameters. The electrospinning parameters include the applied voltage, the flow rate of the solution, and the distance between the spinneret and collector. The

solution parameters include the viscosity, conductivity and concentration of polymer solution. The humidity and temperature of environment is still important for the electrospinning process. In order to gain a better understanding of the electrospinning technique and properties of electrospun fibers, it is necessary to explore the effects of all these governing parameters.

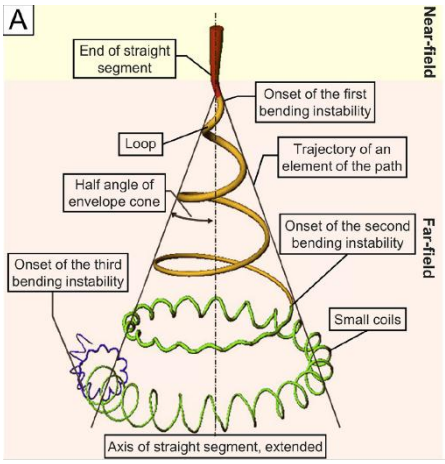

Fig. 2 Schematic of three different types of instabilities occur to electrically charged jet.[22] Reproduced with permission. Copyright 2019, American Chemical Society

In general, the applied voltage directly determines the electric charge distribution on the polymer jet, as well as the strength of the interactions between the jet and the electric field. Thus, the formation of thinner nanofibers usually result from increasing the applied voltage[23, 24]. However, the higher voltage may also induce more fluid ejection, increasing the diameter of electrospun fibers[25]. Furthermore, when the applied voltage increases beyond a critical value, the formation of beads and beaded electrospun fibers may occur. For example, Deitzel and coworkers represent the bead formation with an increase in the applied voltage using poly(ethylene oxide)/water [13].

Regarding the flow rate of the polymer solution, it still determines the morphology and diameter of electrospun fibers. We can always find a critical range which

corresponds to the minimum flow rate needed to maintain a balance between the leaving solution and replacement of that solution with a new one, during jet formation, for obtaining uniform and bead-less fibers[26]. Normally, a flow rate close to the minimum yields smaller diameter fibers while a flow rate close to the maximum will typically result in the formation of fibers with larger diameters.

The distance between the spinneret and collector determines the stage of instability at which the jet is deposited on the collector. Hence, a critical distance needs to be maintained for the full extension and solidification of the jet[27]. Generally, increasing the collecting distance will form smaller diameter fibers. However, when the distance is beyond a certain value, the morphology and diameter will not change because of the jet solidification.

The concentration of the polymer solution is another important effect on the fibers' morphology. As previous mentioned, during the stretching of the charged jet, a critical polymer concentration is a basic parameter for a stable electrospinning process. For example, when the concentration is not high enough, the entangled polymer chains break into fragments before depositing on the collector. Due to this fragmentation, the fibers morphologies always come with beads and beaded fibers. When the concentration of polymer solution is increased, the higher viscosity of the solution increases due to the chain entanglement among the polymer chains, which results in uniform electrospun fibers morphology. In addition, when the polymer concentration is beyond a critical value, the jet dries at the tip of the spinneret and blocks it, which results in beads or beaded fibers as well[28].

Furthermore, the electric conductivity of the solution plays a key role in fiber morphology. The coulomb force between the charges on the surface of the jet and additional force from the interaction with the electric field, are main driving force for the whole electrospinning process. When the of solution's conductivity is too low, the surface of the droplet cannot form a Taylor cone. When the conductivity increases

beyond a critical value, it hinders the formation of the Taylor cone. Normally, the increasing conductivity of the solution not only increases the charge on the surface of the droplet to form Taylor cone, but also decreases the diameter of the electrospun fibers [29]. In addition, adding salts (NaCl, KCl and KBr) to polymer solutions always increase the conductivity and results in thinner fibers[30].

Besides the electrospinning and solution parameters, the effect of temperature and humidity on the fiber characteristics is another important aspect in the electrospinning process. Humidity of the electrospinning environment affects the solidification process of the charged jet and therefore adjusts the fibers morphology and diameters. For instance, Pelipenko and coworkers[31] reported the different range of electrospun fibers diameter due to changes in humidity, using PVA, PEO and their blend solution PVA/hyaluronic acid(HA), PEO/chitosan(CS). The effects of temperature on the diameter of electrospun fibers are similar to humidity. Normally, increasing the temperature of the electrospinning environment causes the increase of the evaporation rate of the solvent and decreases the viscosity of the solution. Although these two effects work by two opposing principles, both lead to a decrease on the mean fiber diameter. For example, De Vrieze and coworkers reported the influence of temperature on the formation and the properties of nanofibers using cellulose acetate (CA) and poly(vinylpyrrolidone) (PVP)[32]. In addition, not only the temperature of the environment, but the different temperature of the collector also affects electrospinning. Kim and their group[33] reported the effect of collector temperature on the porous structure of electrospun fibers. Porous nature of nonwoven mats of PLLA dissolved in methylene chloride was significantly influenced by temperature of the collector.

1.1.3 Materials and methods of electrospinning

Materials

Since its beginning the electrospinning technique developed very quickly and various types of materials have been used to generate electrospun fibers. In general, organic polymer are the most common materials and are widely used. Normally, the organic polymers, including synthetic and natural, have been successfully explored to fabricate fibers from solution or melt electrospinning. Other than just using simple polymer solutions, composite materials have been also successfully electrospun into fibers, making use of sol-gel chemistry.

Natural polymers

Due to the good biocompatibility, natural polymers have been widely used in the field of biomedicine in recent years. However, since natural polymers are mostly polyelectrolytes, it is difficult to prepare natural polymer nanofibers by electrospinning process. Until now, the electrospun nanofibers of natural polymers are mainly polysaccharide biopolymers (cellulose and its derivatives[34], chitin[35], chitosan [36], hyaluronic acid[37], etc.) and proteins (collagen[38], gelatin[39], silk fibroin[40], elastin[41], fibrinogen[42], grain protein[43], etc.)

Synthetic polymers

In addition to natural polymer materials, synthetic polymers are more popularly used in electrospinning to prepare nanofibers. In recent years, dozens of different synthetic polymers have been prepared into nanofibers by electrospinning. One type are water-soluble polymers such as polyethylene oxide[44], polyvinyl alcohol [45], polyacrylic acid [46], polyvinylpyrrolidone [47], and hydroxypropyl cellulose [48]. The another type are degradable polymers such as polylactic acid [49], polyglutamic acid[50], polyhydroxybutyrate[51], etc. Furthermore, several polymers that are soluble in organic solvents have also been electrospun into nanofibers, such as polystyrene [52], polyacrylonitrile [53], polycarbonate[54], polyimide[55], polyethylene terephthalate [56], polyvinylidene fluoride[57], polyamide[58], etc.

Table 2 Natural polymers

Polymer	Solvent	
Cellulose	*N*,*N*-dimethyl acetamide (DMAc), *N*-methylmorpholine oxide (NMMO) and water	34
Chitin	1,1,1,3,3,3-hexafluoro-2-propanol (HFIP)	35
Chitosan	dilute hydrochloric acid, acetic acid, neat formic acid and trifluoroacetic acid	36
Hyaluronic acid	Dulbecco's modified eagle's medium (DMEM)	37
Collagen	1,1,1,3,3,3 hexafluoro-2-propanol (HFP)	38
Gelatin	Water, 2,2,2-trifluoroethanol	39
Silk fibroin	Water	40
Elastin	1,1,1,3,3,3-hexafluoro-2-propanol (HFIP)	41
Fibrinogen	1,1,1,3,3,3-hexafluoro-2-propanol (HFIP) and minimal essential medium (Earle's salts)	42
Grain protein	hexane	43

Table 3 Synthetic polymers

Polymer	Solvent	
Polyethylene oxide (PEO)	chloroform, ethanol, dimethylformamide (DMF) and water	44

Polyvinyl alcohol (PVA)	deionized water and acetic acid	[45]
Polyacrylic acid, (PAA)	deionized water and NaCl	[46]
Polyvinylpyrrolidone, (PVP)	ethanol and chloroform	[47]
Hydroxypropyl cellulose (HPC)	anhydrous ethanol	[48]
Polylactic acid, (PLA)	tetrahydrofuran (THF) and dimethylformamide (DMF)	[49]
Polycaprolactone, (PCL)	Dichloromethane and dimethylformamide (DMF)	[50]
Polyhydroxybutyrate, (PHB)	chloroform and dimethylformamide (DMF)	[51]
Polystyrene	dimethylformamide (DMF)	[52]
Polyacrylonitrile, (PAN)	dimethylformamide (DMF)	[53]
Polycarbonate （PC）	Chloroform, Tetrahydrofuran (THF) and Dimethylformamide (DMF)	[54]
Polyimide, (PI)	*N*,*N*-dimethyl acetamide (DMAc)	[55]
Polyurethane, (PET)	dichloromethane (CH_2Cl_2) and trifluoroacetic acid (TFA)	[56]

Polyvinylidene Fluoride, (PVDF)	dimethylformamide(DMF) and acetone	[57]
Polyamide (PA)	formic acid	[58]

Methods

In the early years, the most popular method was typically far-field electrospinning which includes a hollow needle as the spinneret at a long distance to the collector. However, the basic far-field electrospinning setup is unstable in nature as it relies on the chaotic whipping of liquid jets to generate nanofibers. A series of new electrospinning methods were developed in the last decade, which included near-field electrospinning, multi-needle array electrospinning and coaxial electrospinning (Figure 3). In addition, several researchers designed different collectors which expanded the capability of electrospinning.

Far-field electrospinning,

In general, the collecting distance of the conventional far-field electrospinning setup is around of 10-15 cm and the applied voltage is around of 15-30 kV. However, the distance between the spinneret and collector determines the different electrospinning stages and how the fibers will be deposited on the collector. Thus, during electrospinning with long distances, it is difficult to control the position of deposited electrospun fibers.

Near-field electrospinning

Unfortunately, the electrospinning setup is unstable by nature, as it relies on the chaotic whipping of liquid jets to generate nanofibers. Thus, near-field electrospinning was created such that the jet is impacted onto the collector as a straight segment[59]. In this case, the electric field is highly concentrated between the spinneret and collector,

and the applied voltage is much lower than far field electrospinning. The range of near filed electrospinning parameters are as follows: 0.6-3 kV of apply voltage, 0.01-1 ml/h of flow rate, and less than 500 μm of collecting distance.

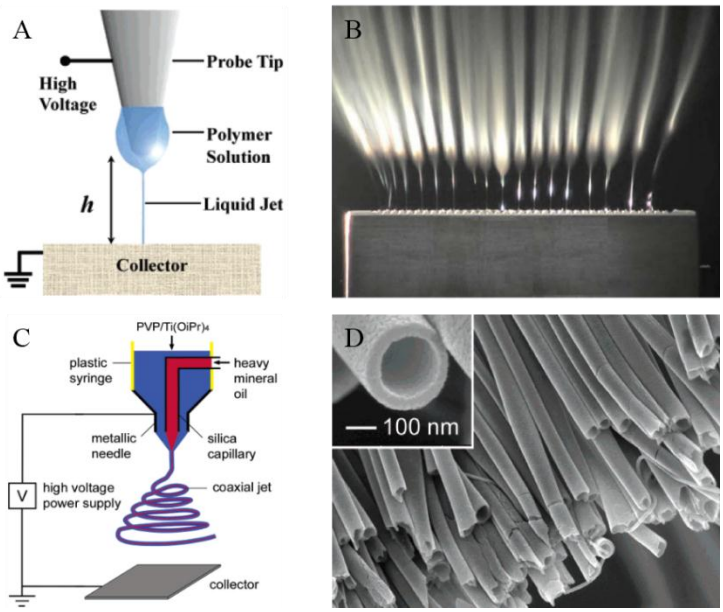

Fig. 3 Schematic of electrospinning techniques including (A) near field electrospinning.[59] (B) multi-needle array electrospinning[60] (C) coaxial electrospinning (D) hollow electrospun nanofibers[61]. Reproduced with permission. Copyright 2019, American Chemical Society.

Multi-needle array electrospinning

In order to improve the productivity, an array of spinnerets or multiple-spinneret electrospinning was designed to offer a straightforward route to mass production through use of polymer jets simultaneously ejected from many needles. However, in this case, the effect of the electric field and coulombic repulsion on the electrospinning process is more complicated than for single needles. The main important parameters of

multiple-spinneret electrospinning we should considered is the distance between the needles or nozzles[62, 63].

Coaxial electrospinning

In addition, coaxial electrospinning has also been used to prepare nanofibers, in which a coaxial spinneret composed of an outer and inner needle is commonly used [61]. By adjusting the flow rate of the inner and outer polymer solutions with different compositions, various nanofibers with varied morphologies can be obtained. There are several types of materials that have been incorporated into the core sheath nanofibers, such as polymers, metal salts, proteins, even cells/bacteria/viruses[64-68]. For example, Li has reported hollow nanofibers with walls prepared by electrospinning two immiscible liquids through a coaxial, two-capillary spinneret, followed by selective removal of the cores[69].

1.1.4 Applications of electrospinning materials

With the development of nanotechnology, electrospinning has become a simple and effective new processing technology that can produce nanofibers, which play a huge role in the fields of biomedical materials, filtration and protection, catalysis, energy, optoelectronics, food engineering, cosmetics, etc.[22].

In the field of biomedicine applications, the nanofibers' diameter of is always smaller than most cells, which can mimic the structure and biological functions of natural extracellular matrix. Most animal tissues are similar in form and structure to electrospun nanofibers. In this case, some electrospun materials have good biocompatibility and degradability, which can be used as a carrier into the human body. In addition, modified nanofibers have a large specific surface area and porosity and other excellent properties, therefore, it has attracted continuous attention of researchers in the field of drug controlled release, wound repair, biological tissue engineering and other aspects[22].

In the field of filtration applications, the filtration efficiency of the fiber filter material normally increases with decreasing of the fiber diameter. Therefore, reducing the fiber diameter becomes an effective method to improve the filtration performance of the fiber filter material. In addition to its small diameter, electrospun fibers have the advantages of small pore size, high porosity, and good fiber uniformity, which results in great application potential in the fields of gas filtration, liquid filtration and personal protection[70].

The electrospinning process can effectively regulate the fine structure of the fibers. Combined with low surface energy materials, materials with super-hydrophobic properties can be obtained. It is expected to be used in the outer layers of ships' hulls, the inner walls of oil pipelines, high-rise glass, automotive glass, etc. However, if the electrospun fiber material is to be applied in the above-mentioned self-cleaning field, it must improve its strength, abrasion resistance, and the binding fastness of the fiber membrane material to the base material.

In the field of catalysis[71], the catalyst particles with nanostructure can easily agglomerate, which affects its dispersibility and utilization rate. Therefore, the electrospun fiber material can serve as a template to uniformly disperse, while also exerting the flexibility and ease of operation of the polymer carrier. Furthermore, it is possible to use the surface recombination of catalytic materials and polymer micro-nano dimensions to produce a strong synergistic effect and improve catalytic efficiency.

Electrospun nanofibers have a higher specific surface area and porosity, which can increase the area of action between the sensing material and the detected object, which is expected to greatly improve the performance of sensors. In addition, electrospun nanofibers can also be used in energy, optoelectronics, food engineering and other fields[22].

1.2 Piezoelectricity

1.2.1 History of piezoelectric materials

In 1880, brothers Pierre and Paul-Jacques Curie discovered the direct piezoelectric effect in single crystal quartz which, under pressure, generated electrical charge[72]. Several other materials also exhibit this behavior. Also, most piezoelectric materials conversely show a geometric strain proportional to an applied electric filed. This converse piezoelectric effect was discovered by Gabriel Lippmann in 1881. After that, a number of piezoelectric materials were explored by several different researchers, such as barium titanate ($BaTiO_3$) ceramics, discovered independently by three groups, Wainner in 1942, Ogawa in 1944 and Vul in 1944, respectively[73-75]. Following the methodology taken for the barium titanate discovery, the perovskite isomorphic oxides such as $PbTiO_3$, and their solid solutions were intensively studied. Particularly, the discovery of antiferroelectrictiy in lead zirconate and the determination of the $Pb(Zr,Ti)O_3$ system phase diagram by E. Sawaguchi[76, 77]. After the discovery of barium titanate and PZT, in parallel to the PZT-based ternary solid solutions, complex perovskite structure materials were intensively synthesized and investigated in 1950s. Starting in the 1990s and continuing today, researchers focus on understanding the piezoelectric mechanism and developing advanced processing techniques, investigating the effect of dopants on physical properties.

1.2.2 Piezoelectric effect and piezoelectric materials

The piezoelectricity is used to describe the materials which generate the electric charge under an applied mechanical stress, which is called direct piezoelectric effect. The indirect or converse piezoelectric effect happens when the materials are subjected to an electrical field resulting on a mechanical strain. In piezoelectric materials, the relationship between induced charges per unit area and the applied stress is linear and

reversible. In this part we aim to introduce the most important organic and inorganic piezoelectric materials and their piezoelectric definition.

Inorganic piezoelectric material

The piezoelectric effect on inorganic materials is usually explained by the displacement of ions inside crystals. When the mechanical stress is applied on the materials, the atomic structure of the crystal changes, a dipole moment is generated due to the shifts or balance of ions in the structure. Nowadays, there are several different inorganic piezoelectric materials which are widely used in various of areas such as aluminum nitride (AlN), lead zirconate titanate (PZT).

AlN is a tetrahedral bonded semiconductor which has one N atom in the tetrahedral interstice surrounded by four Al atoms. In each interstice, since there is no symmetry center, when mechanical press is applied, the motion of the central atom results in a dipole moment[78, 79].

PZT is a non-centrosymmetric crystal structure and has a net nonzero charge in each unit cell of the crystal. When the mechanical is stress applied, the titanium ion inside the unit cell moves and the electrical polarity develops. Therefore, the unit cell shows an electric dipole[80].

Organic piezoelectric materials

Piezoelectricity in organic materials mainly originated from the reorientation of the molecular dipole[81, 82]. As organic piezoelectric materials are deformed under stress, the molecular chains are aligned following one direction, yielding or changing the net polarization so that it is able to present the piezoelectric behavior. The following part provides details on most popular organic piezoelectric materials such as PVDF, PLLA (poly-L-lactic acid), collagen and silk (Figure 4).

PVDF is the most popular organic piezoelectric material and is widely used in applications in different areas. In general, five different crystal phases (α, β, γ, δ, ε) have been reported, being α and β phase the most commonly used. In the α phase, the molecular chain is packed in the unit cell as a nonpolar crystal structure and the molecular dipoles are antiparallel. The β phase presents the best piezoelectric properties, because all the dipoles are parallel and contribute to the highest dipole moment per unit cell[83-85].

In the case of PLLA, four different crystal phases (α′, α, β, and γ) have been reported [86]. The piezoelectricity of PLLA is different from PVDF, which requires a β phase, since PLLA does not depend on the formation of a specific crystalline phase. Although elongated PLLA does not show any spontaneous polarization, it still exhibits large shear piezoelectric constants[87].

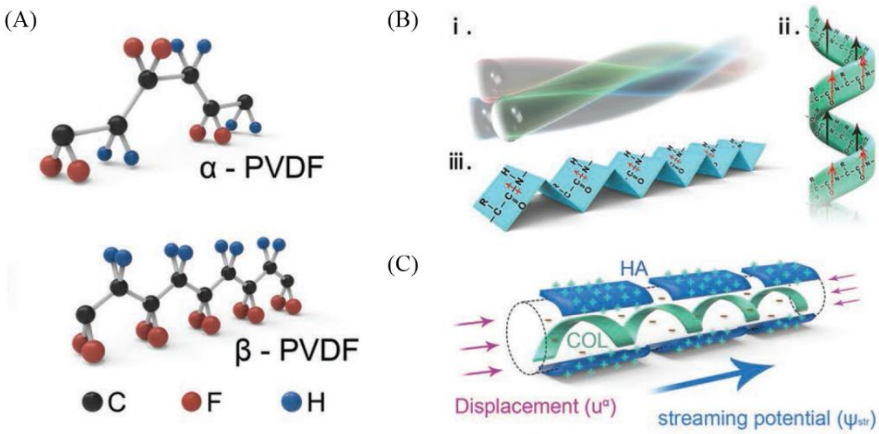

Fig. 4 Piezoelectric materials (A) α and β phase of PVDF. (B) (i) triple helix and (ii) longitudinal polarization in collagen. (iii) is silk β-sheets. (C) Natural nanocomposites, bone, collagen (COL)-hydroxyapatite (HA) biocomposite.[89] Reproduced with permission. Copyright 2020, Wiley-VCH.

Collagen is a biopolymer and one of the most important part of natural extracellular matrix (ECM). Collagen molecules exist as a spiral triple helix which self-assembles through extensive hydrogen bonding of amine and carbonyl functionalities and packs into a quasi-hexagonal lattice of crystalline fibrils[88]. Under mechanical stress, displacement of hydrogen bonds redistributes dipole moments toward the longitudinal axis of collagen molecules, thereby inducing permanent polarization.

The piezoelectricity of silk fibers was first reported by Harvey[90]. The silk fiber comprises a light chain (L-chain) and heavy chain (H-chain) polypeptides linked by a disulfide bond. The piezoelectricity is determined by the H-chain which consists of repeated hydrophobic domains and non-repeated hydrophilic domains. These domains are made of amino acids which are known to exhibit piezoelectricity[91, 92].

1.3 Biological applications of electrospun materials

Electrospun nanofibers hold a remarkably wide range of applications in industries such as semiconductors, protective materials, water purification and clean energy equipments. Nowadays, the most promising applications lie in the biological field which include tissue engineering, wound healing, drug delivery, diagnosis, biomimetics and others (Fig. 5). In this part, we aim to introduce the applications of nanofibers and piezoelectric materials which are most related to our research project.

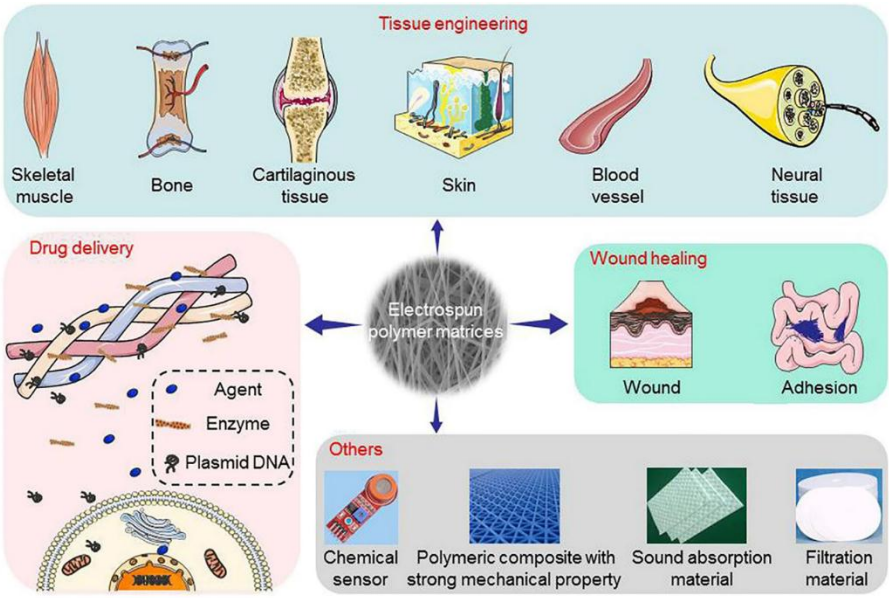

Fig. 5 Main biomedical applications of electrospun nanofibers.[93] Copyright 2019, Elsevier.

1.3.1 Tissue engineering

Electrospun nanofibers have been widely used as scaffold materials in simulating natural ECM, due to their composition and structure. Nowadays, different types of synthetic or natural polymer are used for tissue engineering. Particularly, natural ECM components such as collagen, elastin, and proteoglycans, can be fabricated alone or blended with other synthetic polymers to obtain nanofibers with a diameter of 50-500 nm. In addition, the different biomechanical and degradative nanofiber scaffolds are fabricated by adjusting the optimal blending ratio. The adhesive glycoprotein used to promote cell adhesion in the natural ECM components can also be directly coated on the nanofibers by physical adsorption or covalent bonding. In order to further establish a microenvironment for natural tissues, soluble biomolecules or growth factors present in the ECM can also loaded into the nanofibers (Fig. 6).

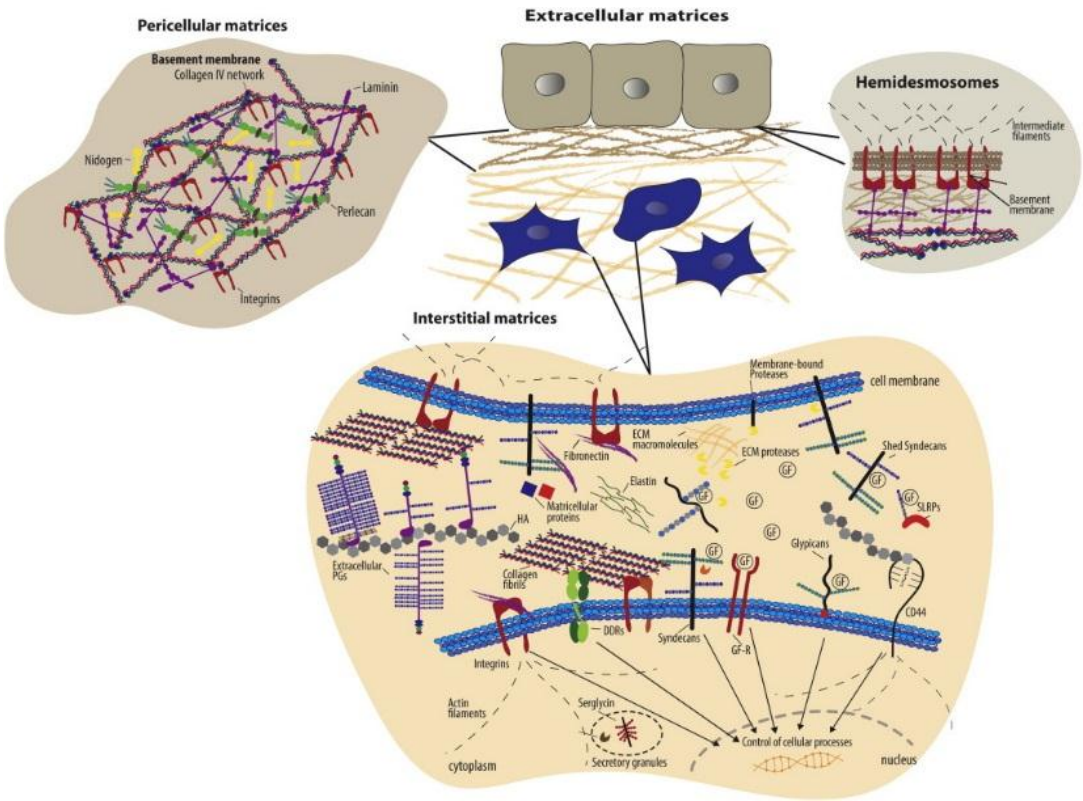

Fig. 6 Major extracellular matrices, their major components, and interactions with cells.[94] Copyright 2016, Elsevier.

Electrospun nanofibers are commonly used to simulate the structure of natural ECM. From a microscopic perspective, the surface topology of nanofibers can be flexibly adjusted, such as the diameter, orientation, porosity of the fibers and the structure or patterning of the fiber assembly. These topological structure signals can affect the cell behavior and fate, and ultimately determine the results of tissue regeneration. From a macroscopic perspective, the overall structure and dimensions of a nanofiber scaffold can also be adjusted to match the tissue with special shape, such as from single-layer structure to a multi-layer structure, or from a two dimensional nanofiber mesh to a three dimensional porous scaffold. Therefore, scaffolds based on electrospun nanofibers have great advantages in simulating the composition and structure of natural tissues, which can effectively regulate cell behavior and promote the regeneration of different types

of tissues. However, the porosity of the nanofiber scaffold prepared by traditional methods is usually smaller than natural ECM. In order to solve this problem, it is usually necessary to change the receiving device or post-process the prepared nanofibers to reduce the density of the fibers and expand the porosity of the nanofiber scaffold.

Neural tissue engineering

Neural tissue engineering shows new therapeutic opportunities for regenerating the damaged nervous tissues in transplantation[95]. In these studies, biomaterial scaffolds are usually required to provide a similar ECM for seeding and growth of nerve cells. In recent years, many advanced strategies for neural tissue engineering have been developed, especially in producing biocompatible nanofibrous scaffolds used to mimic the ECM. The current technologies have enabled control of the morphologies and the biochemical properties of nanofibers for tissue engineering[96]. Nowadays, various polymers have been used to fabricate nanofibrous scaffolds for neural tissue engineering, such as natural polymer, synthetic polymer, composite polymer and naturally and synthetic derived peptides.

For natural polymer nanofibrous scaffolds, natural polymer always exhibits better biocompatibility and lower immunogenicity than synthetic polymers. For instance, Faghihi and coworkers reported the fabrication of 3D gelatin nanofibrous scaffolds to evaluate the effects of retinoic acid on differentiation of human chorion derived MSCs into motor-neuron-like cells[97]. Alternatively, silk fibroin is one of natural proteins often used in fabricating electrospun nanofibers due to their great oxygen-water permeability and biodegradability. For example, PLGA/MWCNTs/silk fibroin nanofibers have been successfully produced for neuronal differentiation by Guo et, al [98]. Compared with natural polymers, synthetic polymers are important alternatives for developing scaffolds, allowing functionalization and parameter adjusting on the scaffolds for nerve cells growth. Among the various synthetic polymer scaffolds, polyester is one of the most popular biomaterials for electrospun nanofiber scaffolds. For example, Vicentini

has reported that PLLA blended with CNTs nanofibers can promote neurite outgrowth. In addition, graphene oxide was also employed to coat PLLA nanofibers. Furthermore, the researcher also revealed the addition of nerve growth factor into the nanofibrous scaffolds could improve the neurite growth and indicated a better performance in nerve regeneration.

For composite polymer nanofibrous scaffolds, the drawbacks of natural polymer and synthetic polymers can be improved. For example, Kuppan et al. demonstrated that cell adhesion and proliferation in the poly-(e-caprolactone) (PCL)/ gelatin nanofibers were more favorable than that in the pure PCL nanofibers[99]. In their study, they investigated an increase of actin, myosin heavy chain, collagen and elastin gene expression in human smooth muscle cells, which indicated that strong cell matrix interactions exist in random and aligned PCL/gelatin nanofiber scaffolds. Inspired by the dynamic self-assembly behavior of short peptides, people have tried to design scaffold with peptide motifs. For instance, peptides can self-assemble into α-helical, β-sheet or β-hairpin structures at the molecular structural level and form supramolecular structures for tissue engineering applications[100].

Bone tissue engineering

Bone tissue engineering is based on the understanding of bone structure, bone mechanics and tissue formation, which aims to develop new materials to induce formation of bone tissue. According to the advanced properties of electrospun nanofibers, which can mimic the natural ECM, the polymeric electrospun scaffolds are very versatile due to their flexibility in the chemical and physical properties, the ability to control morphology, structure and degradability rate, for bone tissue engineering. In general, the polymers which can be used in electrospinning for bone tissue engineering include natural polymer, synthetic polymers and polymer blends. The most common natural polymers which have been used for bone tissue engineering are collagen, chitosan, silk, gelatin, elastin, etc.[101, 102] For example, as natural polymer sources, type

I collagen is the major organic component of bone ECM, and has been considered as bone cell supporting matrix. Therefore, Venugopal has reported that collagen nanofibers could improve the mineralization of osteoblasts[103]. Silk fibroin has also been investigated as a potential scaffold due to its useful properties, such as, cell compatibility, degradability and minimal inflammatory reaction[104]. Li reported silk fibroin promoted the deposition of calcium phosphate minerals to form an apatite–silk nanocomposite[105].

Synthetic polymers have also been used to fabrication of biomaterials for tissue repair and drug delivery. Among the most commonly used synthetic polymers are poly(vinyl) alcohol (PVA), poly(caprolactone) (PCL), poly(lactic acid) (PLA), and poly(lactic-co-glycolic acid) (PLGA). For example, PVA is a biologically compatible material which is stable *in vivo* and has suitable biomechanical properties. Phromviyo has fabricated PVA electrospun nanofibers for hydrogen peroxide-triggered drug release for bone regeneration[106]. Being semi-crystalline and hydrophobic, PCL exhibits a slow degradation rate and great mechanical properties which make it a suitable material for bone scaffolds. Jing et al. fabricated the innovative shish-kebab structured PCL electrospun nanofibers that mimic the collagen fibrils present in bone ECM[67]. PLA is an aliphatic polyester biodegradable and compostable thermoplastic, made up of lactic acid, which can be obtained from renewable plant sources, such as starch and sugar. A number of studies shown that PLA can be used for fabrication of electrospun scaffolds for the regeneration of bone tissues[107].

Comparing to the limitations of natural polymers, such as poor processability and mechanical properties, the drawbacks of synthetic polymer, are mainly low hydrophilicity and lack of cell recognition sites. Therefore, the blending of natural and synthetic polymers plays an important role in bone tissue engineering, since it can endow good mechanical requirements as well as ECM topographic cues. For example,

Tiwari has reported heterogeneous electrospun polycaprolactone/polyethylene glycol membranes with improved wettability, biocompatibility and mineralization[108].

Skin tissue engineering

When a skin injury occurs, it is important to reestablish the skin structure and functions to assure the maintenance of body homeostasis. Even though skin holds the capacity of self-regeneration, some types of wounds do not recover well, as a consequence of extensive lesions or chronic wounds. To overcome this drawbacks and limitation, skin tissue engineering has been widely developed. Specifically, electrospun nanofibers have captured the attention of researchers due to their capacity to mimic the morphological characteristics of skin ECM. Moreover, the cell adhesion, migration, growth and differentiation, can be supported by nanofiber meshes, which are vital events for the occurrence of an effective wound healing process[109-114] (Fig. 7). In recent years, various polymers have been used to fabricate nanofibers for application on skin tissue engineering, such as synthetic polymers, natural polymers and blends of natural and synthetic polymers.

In general, synthetic polymers can be tailored to show excellent mechanical properties, thermal stability and appropriate degradation profile. For example, Khil fabricated polyurethane (PU) nanofiber meshes to be applied as skin substitutes which control the water vapor transmission rate, display a great oxygen permeability, and present fluid drainage ability[115]. Kumbar has reported that PLGA nanofibers shown great improvement on cells spreading, adhesion from their multiple layers, after 28 days in culture[49].

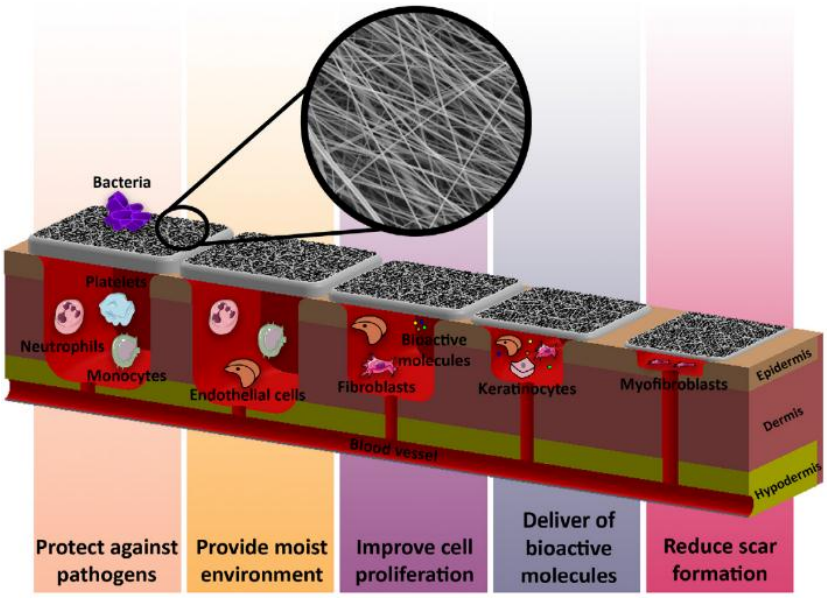

Fig. 7 The properties that electrospun nanofibers must display to be used in skin tissue engineering.[114] Copyright 2018, Elsevier.

In order to improve some limitations of synthetic materials, natural polymers hold a viable option due to their availability of peptide sequences at their surfaces, that can be recognized by the receptors on the cell surface, and subsequently trigger cell adhesion and proliferation. For example, Hyung used silk to fabricate electrospun nanofibers and evaluated their biological performance. They revealed that the silk fibroin nanofibers were able to induce a higher rate of epithelialization and collagen production, than commercially available dressings[116]. In addition, the most important natural ECM material, collagen, also has been used in wound dressing. Lin fabricated collagen nanofibers and evaluated its capacity to be used in the treatment of full thickness skin wounds induced in mice[117].

In recent years, blending electrospun synthetic and natural polymers has also become a promising strategy to improve the limitations of both synthetic and natural polymers. For instance, Venugopal shown that collagen and PCL blended nanofibers could promote cell adhesion and proliferation where the PCL nanofibers could not[118]. Zhou

produced carboxyethyl chitosan (CS)/PVA blended nanofibers to improve chitosan electro-spinnability and hold a great adhesion and proliferation results after 2 days fibroblasts culturing. In another study, PLGA is a common synthetic polymer to mix with natural polymers due to its good biocompatibility and degradation. For example, PLGA was combined with collagen to fabricate nanofibrous wound dressings that reproduce the native structure and biological function of skin ECM.

1.3.2 Drug delivery

In general, typical drug delivery systems are specific structures that can be loaded with molecules therefore acting as tools for the pharmaceutical administration process. Nowadays, it represents one of most promising methods in the biomedical investigations. Such materials hold capacity to transport a chemotherapeutic molecule to a desired area. Among several different nanoformulations, such as, liposomes, micelles and dendrimers, polymer nanoparticles have been widely reported as drug delivery systems[119]. Electrospun nanofibers hold a great potential in drug delivery due to their advantages of large specific surface area, good biocompatibility, easy fabrication and surface modification. Electrospun nanofibers have been used to encapsulate various types of drugs for different biomedical applications, in particular for antibacterial and antitumor applications[120, 121].

As an antibacterial drug delivery system, nanofibers usually combined with inorganic nanoparticles or antibacterial drugs, such as, amoxicillin (AMX) and tetracycline hydrochloride (TCH), can be encapsulated to form drug-loaded nanofiber systems[122, 123](Fig. 8). For instance, Qi investigated the use of HNTs/PLGA composite nanofibers for encapsulation and release of a model drug TCH[122]. In this study, they shown that the TCH release rate could be controlled by the content of TCH in the drug-loaded electrospun mats. In addition, Wang prepared PLGA/LAPONITE©/AMX composite electrospun nanofibers[123] (Fig. 8). In their research, AMX was incorporated

into the interlayer space of LAPONITE© (LAP), and the AMX-loaded LAP nanodisks with an optimized loading efficiency of 9.76% were incorporated with PLGA nanofibers. With the coexistence of both LAP interlayer space and the matrix-type of PLGA nanofibers, the release speed of AMX was significantly suppressed with biphasic and sustained manner.

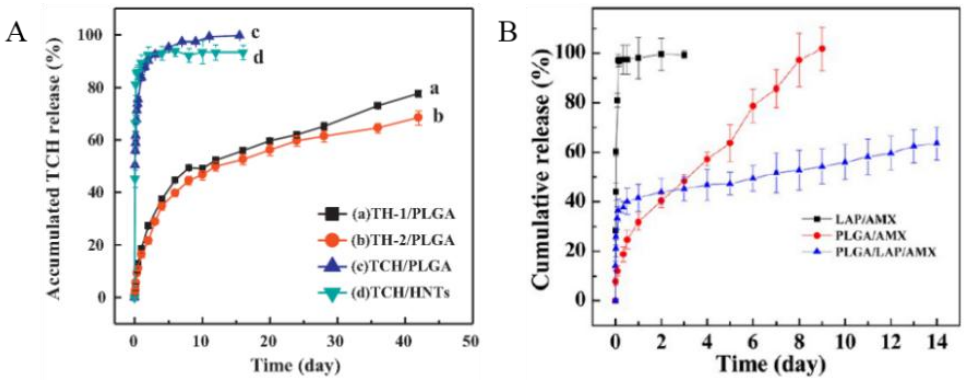

Fig. 8 is in vitro release profiles of TCH from (a) TH-1/PLGA, (b) TH-2/PLGA, (c)TCH/PLGA, (d) TCH/HNTs powders.[122] Reproduced with permission. Copyright 2013, Elsevier. B is in vitro release of AMX from LAP/AMX nanodisks, PLGA/AMX nanofibers, and PLGA/LAP/AMX nanofibers.[123] Reproduced with permission. Copyright 2012, American Chemical Society.

Besides antibacterial drug delivery, anticancer drugs have also been incorporated into nanofibers for therapeutic applications. For example, doxorubicin (DOX) is known as a highly efficient antineoplastic agent commonly used in the treatment of different cancers (such as Malignant lymphoma, breast cancer), although its use is often limited due to its undesirable cardiac toxicity, short half-life and low solubility in aqueous solutions[124]. For instance, Zheng reported the development of nano-hydroxyapatite (n-HA) doped PLGA nanofibers for DOX encapsulation, release and antitumor activity evaluation[125]. Similarly, Qi prepared PLGA nanofiber mats with DOX-loaded CNTs

that shown the same performance in terms of the controlled release of DOX, since DOX can be properly incorporated into the interior or onto the surface of CNTs[126].

1.3.3 Biological applications of electrospun piezoelectric nanofibers

Electrospun nanofibers that exhibit piezoelectric properties are a new generation of smart biomaterials which display electromechanical behavior by transforming the mechanical energy into electric energy and *vice versa*. As we know, piezoelectricity can be found in different parts of mammalian tissue, such as hair, bone, tendon, ligaments, cartilage, skin, dentin, collagen etc. It means piezoelectricity can be referred as a extended property of living tissue and plays an important role in various physiological phenomena[127]. For example, bone is a dynamic tissue which involves electromechanical processes due to its piezoelectric characteristics[128]. Nowadays, many applications for piezoelectric nanofibers, that involve interfaces with biological systems, represents an exciting area of rapid development. Specifically, it become a powerful biomaterial that can be interfaced with biological tissue and used for miniaturized bioelectronic and biomechanical devices. In general, polymer and lead-free ceramics are the most common materials used. The most important lead-free piezoceramic that possesses perovskite-like structure is barium titanate ($BaTiO_3$). The most common polymers entitled with piezoelectric properties and usable in contact with the human body is PVDF. Therefore, in this part, we aim to explain the recent biomedical applications of PVDF and lead-free ceramic electrospun nanofibers.

Biological applications of ceramic-based piezoelectric electrospun nanofibers

From all the natural or synthetic piezoelectric materials, the family of ceramics based upon lead titanate ($PbTiO_3$), lead zirconate titanate and lead lanthanum zirconate titanate ($PbZrxTi_1$-xO_3), are the ones that show the most significant piezoelectric effect. But their use for biomedical applications research is severely limited by the concerns about the toxic effect due to lead oxides[129, 130]. In recent years, piezoelectric ceramics

$BaTiO_3$ have widely employed for their also excellent piezoelectric properties. Especially, the absence of lead and their stability at high temperatures make it become an optimal candidate for bioengineering applications. Specifically, electrospun $BaTiO_3$ nanofibers have been considerably explored in the field of sensors and transducers for bioengineering.

The successful fabrication of electrospun $BaTiO_3$ nanofibers requires careful preparation of the precursors and annealing conditions. For example, hollow $BaTiO_3$ nanofibers have been fabricated for biosensor and actuators by Zhan, who co-electrospun the sol precursor of $BaTiO_3$ xerogel without any further polymer additive [131]. In addition, Zhan has reported $BaTiO_3$ nanofibers for transducer applications which show a correct management of both the hydrolysis and the polymerization of the sol solution can be beneficial to the topography of $BaTiO_3$ nanofibers. Furthermore, $BaTiO_3$ nanofibers also play an important role in the application of energy harvesting. For instance, Jalalian produced very large piezoelectric lead-free $BaTiO_3$ nanofibers with high aspect ratio in morphotropic phase boundary area which can be applied as piezoelectric nanogenerators[132].

Bioapplications of PVDF nanofibers

Organic piezoelectric electrospun nanofibers hold several different benefits over inorganic piezoelectric materials such as ceramic-based nanofibers, which include high biocompatibility, great flexibility and easy fabrication. Although organic piezoelectric materials often don't have a piezoelectric output comparable to inorganic ones, recent research suggests that its interface with biological systems makes them better functional materials in the field of implantable applications. In recent years, PVDF and its copolymers, such as polyvinylidene fluoride-trifluoroethylene [P(VDF-TrFE)] have been used due to their strong piezoelectric effect. In addition, the outstanding properties of PVDF-based polymers includes flexibility, transparency, good mechanical strength and high chemical resistance, which provide many advantages in various healthcare

applications. Especially, the electrospun PVDF-based nanofibers which hold great chemical stability, biocompatibility and durability in the human body, get lots of attention nowadays, becoming the most popular piezoelectric materials in many different areas. Therefore, in this part, we aim to introduce the main biological applications of PVDF-based electrospun nanofibers.

Tissue engineering

PVDF and its copolymers in the form of 3D scaffolds hold the ability to do electrical stimulation of cells and promote various types of tissue regeneration. As we know, the topography of biomaterials has a significant effect on cells behavior and cell morphology, therefore designing a suitable structure becomes important. Different 3D porous bioactive PVDF nanofibers, adjusted through careful control of the processing parameters, have been used for bone, muscle and nerve regeneration[133].

In the bone tissue engineering, the optimal bone repair remains a big challenge, especially in the case of the bone healing and defects. The main pathway to be explored in the next years will be to mimic tissue physiology with PVDF nanofibers or growth factors. Specifically, bone is a tissue with piezoelectric properties similar to those of quartz, primarily by virtue of collagen, the main component of the bone ECM. For this reason, the application of PVDF nanofibers in bone tissue engineering have been investigated. Specially, the role of electric signals in bone is not clear, the effect of PVDF nanofibers by their properties and structure in osteogenic process was studied by many researchers.

For instance, Damaraju produced 3D fibrous P(VDF-TrFE) scaffolds that were used for stimulation of human mesenchymal stem cells[134] (Fig. 9). In their work, they revealed the P(VDF-TrFE) nanofibers with high output voltage helped osteogenic differentiation and low voltage output helped chondrogenic differentiation. Furthermore, Wang also investigated the effect of P(VDF-TrFE) scaffolds undergoing the dynamic electric stimulation on mouse osteoblastic cell adhesion and

proliferation[135]. The highlights of their results shown the cells were elongated and oriented along the direction of nanofibers.

External electric fields have shown the potential effect on the neurite outgrowth and nerve regeneration. As with the research for promotion of bone tissue regeneration, electrospun PVDF nanofibers have also received considerable interest for nerve regeneration and neural tissue engineering. For example, Lee[136] fabricated aligned P(VDF-TrFE) nanofibers which significantly promoted neurite outgrowth and guidance of dorsal root ganglions, as compared to random fibers (Fig. 9). Furthermore, the differentiation of human neural stem cells was guided into mature neuronal cells by electrospun P(VDF-TrFE) nanofibers. Arinzeh revealed that the differentiation of human neural stem/precursor cells on electrospun PVDF scaffolds mostly induced the expression of neuron-like β-III tubuli[137]. In a similar work by Motamedi, aligned PVDF nanofibers doped with laser ablated Au nanoparticles showed an increase in the growth and adhesion of cells without any toxicity[138]. Hoop demonstrated that ultrasonic acoustic stimulation of piezoelectric PVDF membranes improved the neurite generation in PC12 cells[139].

Living biological tissue can generate endogenous electric potentials, which accelerates the process of wound healing by modulating migration, proliferation and differentiation of fibroblasts [140]. Collagen type I fibers are the most common and important in skin tissue, which contains mechanoceptors as sensorial cells. Therefore, the piezoelectric nanofibers were considered for skin tissue engineering. For example, Weber fabricated 3D P(VDF-TrFE) scaffolds and cultured human fibroblasts, which turn into perfectly spindle shaped cells after 1 week and show potential for skin regeneration[141]. Moreover, Wang[142] fabricated P(VDF-TrFE) nanofibers and used it for implanted energy harvester in SD rats. In their work, with great cytocompatibility and relatively large piezoelectric effect, fibroblasts grew and aligned perfectly along the nanofibers' direction and cell proliferation was promoted. Guo fabricated PU/PVDF

scaffolds with excellent mechanical and piezoelectric properties. Fibroblasts cultured on these scaffolds, under piezoelectric stimulation, showed enhanced migration, adhesion and secretion[143] (Fig. 9).

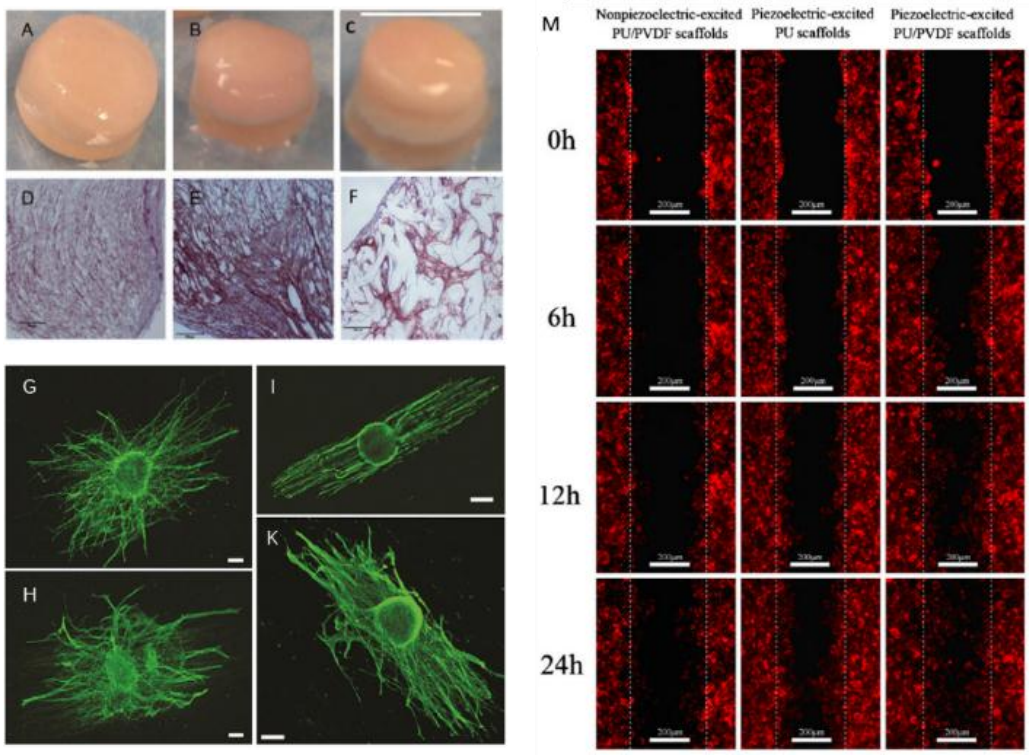

Fig. 9 A-F represent images of scaffolds after 28 days undergoing osteogenic differentiation in dynamic conditions, A is as-spun PVDF-TrFE, B is annealed PVDF-TrFE, C is PCL scaffolds, D-F is immunohistochemical staining for collagen type I[134]. Reproduced with permission. Copyright 2017, Elsevier. G-K represent confocal fluorescence images of DRG stained with phalloidin on random and aligned PVDF-TrFE nanofibers, G and H is cells on random fibers, I and K is cells on aligned fibers[136]. Reproduced with permission. Copyright 2011, Elsevier. M represent the fluorescence images of the migration of fibroblasts on the PU/PVDF nanofibers undergoing piezoelectric stimulation in 24 hours.[143] Reproduced with permission. Copyright 2012, Elsevier.

Biosensors

Nowadays, smart biosensors based on piezoelectric materials have received considerable attention, especially the piezoelectric nanofibers. Piezoelectric nanofibers are flexible and can deform under tiny applied forces, which makes them suitable candidates for detecting various mechanical and electric signals in biological tissue. For their durability, chemical inertia, and strong piezoelectric response, PVDF and copolymers have easily found applications as biosensors which were widely used in pressure sensing, healthcare monitoring and cell actuators.

Pressure sensing

For example, Persano fabricated a flexible, self-powered and lightweight pressure sensor made from aligned PVDF fibers. This device is capable of measuring small pressures (0.1 Pa) and could be valuable for applications in biomedical and wearable electronics[144]. In another work, Beringer used aligned P(VDF-TrFE) nanofibers interfaced with a flexible plastic substrate to produce a device which is able to evaluate voltage response[145].

Healthcare monitoring

Over the last few years, the PVDF biosensors demonstrated the capability for physiological signal monitoring, disease diagnosis and health assessment. Electronic skins have attracted attention for the applications in wearable sensors and healthcare monitoring system. For example, Liu produced a wearable self-powered PVDF sensor which can be used as a physiological signal recording system to measure respiration signals[146]. Park and co-workers have produced a bendable and stretchable P(VDF-TrFE) sensor which is able to identify the movement of the skin on the neck, induced by the pulsed behavior of the carotid[147].

Energy harvesting

In recent years, various advanced harvesters based on PVDF and copolymer nanofibers have shown significant developments. Using advanced electrospinning technology, flexible and large surface area PVDF and P(VDF-TrFE) nanofibers were fabricated. These fiber-based electronics are capable of being woven into textiles and capture energy from the human daily activities[148]. A large amount of research in biomechanical energy harvesting of discontinuous human activities has been reported.

For example, Ishida produced a shoe insole pedometer as the early stage toward the application of flexible energy harvesting, which include an organic pedometer circuit, a PVDF roll for pulse generation[149]. After that, a series of wearable insole or similar device was investigated. In other work, Liu et al. have produced random and aligned PVDF nanofiber meshes for energy harvesting. They reported that their cell-based energy harvester gave rise to a remarkable contractile response at cardiac level[150].

References

1. Cooley, J. F. Electro-spinning characterised by the electro-spinning apparatus. U.S. Pat. 692,631, **1902**.

2. Mortonp, W. Method of dispersing fluids. U.S. Pat. 705,691, **1902**.

3. Zeleny, J., On the Conditions of Instability of Liquid Drops, with Applications to the Electrical Discharge from Liquid Point. *Physical Review* **1914,** *3* (69),

4. Formahals, A. Process and apparatus for Preparing Artificial Threads. U.S. Pat. 1,975,504, **1934**.

5. Petryanov, The development of ailfiler for capturing aerosol particles. U.S. Pat. 2,349,950, **1938**.

6. Luo, C. J.; Stoyanov, S. D.; Stride, E.; Pelan, E.; Edirisinghe, M., Electrospinning versus fibre production methods: from specifics to technological convergence. *Chemical Society Reviews* **2012,** *41* (13), 4708-4735.https://doi.org/10.1039/C2CS35083A

7. Latham, J.; Roxburgh, I. W., Distintegration of pairs of water drops in an electric field. *Proceedings of the Royal Society of London Series a-Mathematical and Physical Sciences* **1966,** *295* (1440), 84.https://doi.org/10.1098/rspa.1966.0227

8. Taylor, G., ELECTRICALLY DRIVEN JETS. *Proceedings of the Royal Society of London Series a-Mathematical and Physical Sciences* **1969,** *313* (1515), 453.https://doi.org/10.1098/rspa.1969.0205

9. Fong, H.; Chun, I.; Reneker, D. H., Beaded nanofibers formed during electrospinning. *Polymer* **1999,** *40* (16), 4585-4592.https://doi.org/10.1016/s0032-3861(99)00068-3

10. Reneker, D. H.; Chun, I., Nanometre diameter fibres of polymer, produced by electrospinning. *Nanotechnology* **1996,** *7* (3), 216-223.https://doi.org/10.1088/0957-4484/7/3/009

11. Fong, H.; Reneker, D. H., Elastomeric nanofibers of styrene-butadiene-styrene triblock copolymer. *Journal of Polymer Science Part B-Polymer Physics* **1999,** *37* (24), 3488-3493.https://doi.org/10.1002/(sici)1099-0488(19991215)37:24<3488::aid-polb9>3.0.co;2-m

12. Bognitzki, M.; Czado, W.; Frese, T.; Schaper, A.; Hellwig, M.; Steinhart, M.; Greiner, A.; Wendorff, J. H., Nanostructured fibers via electrospinning. *Advanced Materials* **2001,** *13* (1), 70-+.https://doi.org/10.1002/1521-4095(200101)13:1<70::aid-adma70>3.3.co;2-8

13. Deitzel, J. M.; Kleinmeyer, J.; Harris, D.; Tan, N. C. B., The effect of processing variables on the morphology of electrospun nanofibers and textiles. *Polymer* **2001,** *42* (1), 261-

272.https://doi.org/10.1016/s0032-3861(00)00250-0

14. Li, D.; Xia, Y. N., Electrospinning of nanofibers: Reinventing the wheel? *Advanced Materials* **2004,** *16* (14), 1151-1170.https://doi.org/10.1002/adma.200400719

15. Zong, X. H.; Kim, K.; Fang, D. F.; Ran, S. F.; Hsiao, B. S.; Chu, B., Structure and process relationship of electrospun bioabsorbable nanofiber membranes. *Polymer* **2002,** *43* (16), 4403-4412.https://doi.org/10.1016/s0032-3861(02)00275-6

16. Collins, R. T.; Jones, J. J.; Harris, M. T.; Basaran, O. A., Electrohydrodynamic tip streaming and emission of charged drops from liquid cones. *Nature Physics* **2008,** *4* (2), 149-154.https://doi.org/10.1038/nphys807

17. Reneker, D. H.; Yarin, A. L.; Fong, H.; Koombhongse, S., Bending instability of electrically charged liquid jets of polymer solutions in electrospinning. *Journal of Applied Physics* **2000,** *87* (9), 4531-4547.https://doi.org/10.1063/1.373532

18. Shin, Y. M.; Hohman, M. M.; Brenner, M. P.; Rutledge, G. C., Experimental characterization of electrospinning: the electrically forced jet and instabilities. *Polymer* **2001,** *42* (25), 9955-9967.https://doi.org/10.1016/s0032-3861(01)00540-7

19. Yarin, A. L.; Koombhongse, S.; Reneker, D. H., Bending instability in electrospinning of nanofibers. *Journal of Applied Physics* **2001,** *89* (5), 3018-3026.https://doi.org/10.1063/1.1333035

20. Hohman, M. M.; Shin, M.; Rutledge, G.; Brenner, M. P., Electrospinning and electrically forced jets. II. Applications. *Physics of Fluids* **2001,** *13* (8), 2221-2236.https://doi.org/10.1063/1.1384013

21. Shin, Y. M.; Hohman, M. M.; Brenner, M. P.; Rutledge, G. C., Electrospinning: A whipping fluid jet generates submicron polymer fibers. *Applied Physics Letters* **2001,** *78* (8), 1149-1151.https://doi.org/10.1063/1.1345798

22. Xue, J.; Wu, T.; Dai, Y.; Xia, Y., Electrospinning and Electrospun Nanofibers: Methods, Materials, and Applications. *Chemical Reviews* **2019,** *119* (8), 5298-5415.https://doi.org/10.1021/acs.chemrev.8b00593

23. Hu, J. P.; Wang, X. F.; Ding, B.; Lin, J. Y.; Yu, J. Y.; Sun, G., One-step Electro-spinning/netting Technique for Controllably Preparing Polyurethane Nano-fiber/net. *Macromolecular Rapid Communications* **2011,** *32* (21), 1729-1734.https://doi.org/10.1002/marc.201100343

24. Sill, T. J.; von Recum, H. A., Electro spinning: Applications in drug delivery and tissue engineering. *Biomaterials* **2008,** *29* (13), 1989-2006.https://doi.org/10.1016/j.biomaterials.2008.01.011

25. Demir, M. M.; Yilgor, I.; Yilgor, E.; Erman, B., Electrospinning of polyurethane fibers. *Polymer* **2002,** *43* (11), 3303-3309.https://doi.org/10.1016/s0032-3861(02)00136-2

26. Megelski, S.; Stephens, J. S.; Chase, D. B.; Rabolt, J. F., Micro- and nanostructured surface morphology on electrospun polymer fibers. *Macromolecules* **2002,** *35* (22), 8456-8466.https://doi.org/10.1021/ma020444a

27. Matabola, K. P.; Moutloali, R. M., The influence of electrospinning parameters on the morphology and diameter of poly(vinyledene fluoride) nanofibers- effect of sodium chloride. *Journal of Materials Science* **2013,** *48* (16), 5475-5482.https://doi.org/10.1007/s10853-013-7341-6

28. Haider, S.; Al-Zeghayer, Y.; Ali, F. A. A.; Haider, A.; Mahmood, A.; Al-Masry, W. A.; Imran, M.; Aijaz, M. O., Highly aligned narrow diameter chitosan electrospun nanofibers. *Journal of Polymer Research* **2013,** *20* (4).https://doi.org/10.1007/s10965-013-0105-9

29. Sun, B.; Long, Y. Z.; Zhang, H. D.; Li, M. M.; Duvail, J. L.; Jiang, X. Y.; Yin, H. L., Advances in three-dimensional nanofibrous macrostructures via electrospinning. *Progress in Polymer Science* **2014,** *39* (5), 862-890.https://doi.org/10.1016/j.progpolymsci.2013.06.002

30. Wang, Z. J.; Li, Z. Y.; Liu, L.; Xu, X. R.; Zhang, H. N.; Wang, W.; Zheng, W.; Wang, C., A Novel Alcohol Detector Based on ZrO2-Doped SnO2 Electrospun Nanofibers. *Journal of the American Ceramic Society* **2010,** *93* (3), 634-637.https://doi.org/10.1111/j.1551-2916.2009.03480.x

31. Pelipenko, J.; Kristl, J.; Jankovic, B.; Baumgartner, S.; Kocbek, P., The impact of relative humidity during electrospinning on the morphology and mechanical properties of nanofibers. *International Journal of Pharmaceutics* **2013,** *456* (1), 125-134.https://doi.org/10.1016/j.ijpharm.2013.07.078

32. De Vrieze, S.; Van Camp, T.; Nelvig, A.; Hagstrom, B.; Westbroek, P.; De Clerck, K., The effect of temperature and humidity on electrospinning. *Journal of Materials Science* **2009,** *44* (5), 1357-1362.https://doi.org/10.1007/s10853-008-3010-6

33. Kim, C. H.; Jung, Y. H.; Kim, H. Y.; Lee, D. R.; Dharmaraj, N.; Choi, K. E., Effect of collector temperature on the porous structure of electrospun fibers. *Macromolecular Research* **2006,** *14* (1), 59-

65.https://doi.org/10.1007/bf03219069

34. Kim, C. W.; Kim, D. S.; Kang, S. Y.; Marquez, M.; Joo, Y. L., Structural studies of electrospun cellulose nanofibers. *Polymer* **2006,** *47* (14), 5097-5107.https://doi.org/10.1016/j.polymer.2006.05.033

35. Noh, H. K.; Lee, S. W.; Kim, J. M.; Oh, J. E.; Kim, K. H.; Chung, C. P.; Choi, S. C.; Park, W. H.; Min, B. M., Electrospinning of chitin nanofibers: Degradation behavior and cellular response to normal human keratinocytes and fibroblasts. *Biomaterials* **2006,** *27* (21), 3934-3944.https://doi.org/10.1016/j.biomaterials.2006.03.016

36. Ohkawa, K.; Cha, D. I.; Kim, H.; Nishida, A.; Yamamoto, H., Electrospinning of chitosan. *Macromolecular Rapid Communications* **2004,** *25* (18), 1600-1605.https://doi.org/10.1002/marc.200400253

37. Ji, Y.; Ghosh, K.; Shu, X. Z.; Li, B. Q.; Sokolov, J. C.; Prestwich, G. D.; Clark, R. A. F.; Rafailovich, M. H., Electrospun three-dimensional hyaluronic acid nanofibrous scaffolds. *Biomaterials* **2006,** *27* (20), 3782-3792.https://doi.org/10.1016/j.biomaterials.2006.02.037

38. Matthews, J. A.; Wnek, G. E.; Simpson, D. G.; Bowlin, G. L., Electrospinning of Collagen Nanofibers. *Biomacromolecules* **2002,** *3* (2), 232-238.https://doi.org/10.1021/bm015533u

39. Huang, Z. M.; Zhang, Y. Z.; Ramakrishna, S.; Lim, C. T., Electrospinning and mechanical characterization of gelatin nanofibers. *Polymer* **2004,** *45* (15), 5361-5368.https://doi.org/10.1016/j.polymer.2004.04.005

40. Jin, H. J.; Chen, J. S.; Karageorgiou, V.; Altman, G. H.; Kaplan, D. L., Human bone marrow stromal cell responses on electrospun silk fibroin mats. *Biomaterials* **2004,** *25* (6), 1039-1047.https://doi.org/10.1016/s0142-9612(03)00609-4

41. Boland, E. D.; Matthews, J. A.; Pawlowski, K. J.; Simpson, D. G.; Wnek, G. E.; Bowlin, G. L., Electrospinning collagen and elastin: Preliminary vascular tissue engineering. *Frontiers in Bioscience-Landmark* **2004,** *9*, 1422-1432.https://doi.org/10.2741/1313

42. Wnek, G. E.; Carr, M. E.; Simpson, D. G.; Bowlin, G. L., Electrospinning of nanofiber fibrinogen structures. *Nano Letters* **2003,** *3* (2), 213-216.https://doi.org/10.1021/nl025866c

43. Aceituno-Medina, M.; Mendoza, S.; Lagaron, J. M.; Lopez-Rubio, A., Development and characterization of food-grade electrospun fibers from amaranth protein and pullulan blends. *Food*

Research International **2013,** *54* (1), 667-674.https://doi.org/10.1016/j.foodres.2013.07.055

44. Son, W. K.; Youk, J. H.; Lee, T. S.; Park, W. H., The effects of solution properties and polyelectrolyte on electrospinning of ultrafine poly(ethylene oxide) fibers. *Polymer* **2004,** *45* (9), 2959-2966.https://doi.org/10.1016/j.polymer.2004.03.006

45. Nguyen, T. B. L.; Lee, B. T., Electrospinning of polyvinyl alcohol/gelatin nanofiber composites and cross-linking for bone tissue engineering application. *Journal of Biomaterials Applications* **2012,** *27* (3), 255-266.https://doi.org/10.1177/0885328211401932

46. Kim, B.; Park, H.; Lee, S. H.; Sigmund, W. M., Poly(acrylic acid) nanofibers by electrospinning. *Materials Letters* **2005,** *59* (7), 829-832.https://doi.org/10.1016/j.matlet.2004.11.032

47. Yan, E.; Huang, Z. H.; Xin, Y.; Zhao, Q.; Zhang, W., Polyvinylpyrrolidone/tris(8-quinolinolato) aluminum hybrid polymer fibers by electrospinning. *Materials Letters* **2006,** *60* (24), 2969-2973.https://doi.org/10.1016/j.matlet.2006.02.045

48. Shukla, S.; Brinley, E.; Cho, H. J.; Seal, S., Electrospinning of hydroxypropyl cellulose fibers and their application in synthesis of nano and submicron tin oxide fibers. *Polymer* **2005,** *46* (26), 12130-12145.https://doi.org/10.1016/j.polymer.2005.10.070

49. Kumbar, S. G.; Nukavarapu, S. P.; James, R.; Nair, L. S.; Laurencin, C. T., Electrospun poly(lactic acid-co-glycolic acid) scaffolds for skin tissue engineering. *Biomaterials* **2008,** *29* (30), 4100-4107.https://doi.org/10.1016/j.biomaterials.2008.06.028

50. Wutticharoenmongkol, P.; Sanchavanakit, N.; Pavasant, P.; Supaphol, P., Preparation and characterization of novel bone scaffolds based on electrospun polycaprolactone fibers filled with nanoparticles. *Macromolecular Bioscience* **2006,** *6* (1), 70-77.https://doi.org/10.1002/mabi.200500150

51. Correia, D. M.; Ribeiro, C.; Ferreira, J. C. C.; Botelho, G.; Ribelles, J. L. G.; Lanceros-Mendez, S.; Sencadas, V., Influence of Electrospinning Parameters on Poly(hydroxybutyrate) Electrospun Membranes Fiber Size and Distribution. *Polymer Engineering and Science* **2014,** *54* (7), 1608-1617.https://doi.org/10.1002/pen.23704

52. Pai, C. L.; Boyce, M. C.; Rutledge, G. C., Morphology of Porous and Wrinkled Fibers of Polystyrene Electrospun from Dimethylformamide. *Macromolecules* **2009,** *42* (6), 2102-2114.https://doi.org/10.1021/ma802529h

53. Chen, L.; Bromberg, L.; Schreuder-Gibson, H.; Walker, J.; Hatton, T. A.; Rutledge, G. C., Chemical protection fabrics via surface oximation of electrospun polyacrylonitrile fiber mats. *Journal of Materials Chemistry* **2009,** *19* (16), 2432-2438.https://doi.org/10.1039/b818639a

54. Krishnappa, R. V. N.; Desai, K.; Sung, C. M., Morphological study of electrospun polycarbonates as a function of the solvent and processing voltage. *Journal of Materials Science* **2003,** *38* (11), 2357-2365.https://doi.org/10.1023/a:1023984514389

55. Wang, Q. J.; Song, W. L.; Wang, L. N.; Song, Y.; Shi, Q.; Fan, L. Z., Electrospun polyimide-based fiber membranes as polymer electrolytes for lithium-ion batteries. *Electrochimica Acta* **2014,** *132*, 538-544.https://doi.org/10.1016/j.electacta.2014.04.053

56. Hadjizadeh, A.; Ajji, A.; Bureau, M. N., Nano/micro electro-spun polyethylene terephthalate fibrous mat preparation and characterization. *Journal of the Mechanical Behavior of Biomedical Materials* **2011,** *4* (3), 340-351.https://doi.org/10.1016/j.jmbbm.2010.10.014

57. Yee, W. A.; Kotaki, M.; Liu, Y.; Lu, X. H., Morphology, polymorphism behavior and molecular orientation of electrospun poly(vinylidene fluoride) fibers. *Polymer* **2007,** *48* (2), 512-521.https://doi.org/10.1016/j.polymer.2006.11.036

58. Supaphol, P.; Mit-Uppatham, C.; Nithitanakul, M., Ultrafine electrospun polyamide-6 fibers: Effect of emitting electrode polarity on morphology and average fiber diameter. *Journal of Polymer Science Part B-Polymer Physics* **2005,** *43* (24), 3699-3712.https://doi.org/10.1002/polb.20671

59. Sun, D.; Chang, C.; Li, S.; Lin, L., Near-Field Electrospinning. *Nano Letters* **2006,** *6* (4), 839-842.https://doi.org/10.1021/nl0602701

60. Lukas, D.; Sarkar, A.; Pokorny, P., Self-organization of jets in electrospinning from free liquid surface: A generalized approach. *Journal of Applied Physics* **2008,** *103* (8).https://doi.org/10.1063/1.2907967

61. Li, D.; Xia, Y., Direct Fabrication of Composite and Ceramic Hollow Nanofibers by Electrospinning. *Nano Letters* **2004,** *4* (5), 933-938.https://doi.org/10.1021/nl049590f

62. Zhou, F. L.; Gong, R. H.; Porat, I., Mass production of nanofibre assemblies by electrostatic spinning. *Polymer International* **2009,** *58* (4), 331-342.https://doi.org/10.1002/pi.2521

63. SalehHudin, H. S.; Mohamad, E. N.; Mahadi, W. N. L.; Afifi, A. M., Multiple-jet electrospinning

methods for nanofiber processing: A review. *Materials and Manufacturing Processes* **2018,** *33* (5), 479-498.https://doi.org/10.1080/10426914.2017.1388523

64. Agarwal, S.; Greiner, A.; Wendorff, J. H., Electrospinning of Manmade and Biopolymer Nanofibers-Progress in Techniques, Materials, and Applications. *Advanced Functional Materials* **2009,** *19* (18), 2863-2879.https://doi.org/10.1002/adfm.200900591

65. Dror, Y.; Kuhn, J.; Avrahami, R.; Zussman, E., Encapsulation of enzymes in biodegradable tubular structures. *Macromolecules* **2008,** *41* (12), 4187-4192.https://doi.org/10.1021/ma071599r

66. Klein, S.; Kuhn, J.; Avrahami, R.; Tarre, S.; Beliavski, M.; Green, M.; Zussman, E., Encapsulation of Bacterial Cells in Electrospun Microtubes. *Biomacromolecules* **2009,** *10* (7), 1751-1756.https://doi.org/10.1021/bm900168v

67. Korehei, R.; Kadla, J. F., Encapsulation of T4 bacteriophage in electrospun poly(ethylene oxide)/cellulose diacetate fibers. *Carbohydrate Polymers* **2014,** *100*, 150-157.https://doi.org/10.1016/j.carbpol.2013.03.079

68. Lagerwall, J. P. F.; McCann, J. T.; Formo, E.; Scalia, G.; Xia, Y. N., Coaxial electrospinning of microfibres with liquid crystal in the core. *Chemical Communications* **2008,** (42), 5420-5422.https://doi.org/10.1039/b810450f

69. Li, D.; Xia, Y. N., Direct fabrication of composite and ceramic hollow nanofibers by electrospinning. *Nano Letters* **2004,** *4* (5), 933-938.https://doi.org/10.1021/nl049590f

70. Zhu, M. M.; Han, J. Q.; Wang, F.; Shao, W.; Xiong, R. H.; Zhang, Q. L.; Pan, H.; Yang, Y.; Samal, S. K.; Zhang, F.; Huang, C. B., Electrospun Nanofibers Membranes for Effective Air Filtration. *Macromolecular Materials and Engineering* **2017,** *302* (1).https://doi.org/10.1002/mame.201600353

71. Xue, J.; Xie, J.; Liu, W.; Xia, Y., Electrospun Nanofibers: New Concepts, Materials, and Applications. *Accounts of Chemical Research* **2017,** *50* (8), 1976-1987.https://doi.org/10.1021/acs.accounts.7b00218

72. Molinie, P.; Boudia, S., Mastering picocoulombs in the 1890s: The Curies' quartz-electrometer instrumentation, and how it shaped early radioactivity history. *Journal of Electrostatics* **2009,** *67* (2-3), 524-530.https://doi.org/10.1016/j.elstat.2009.01.031

73. Wainer, E., HIGH TITANIA DIELECTRICS. *Transactions of the Electrochemical Society* **1946,** *89*, 331-

356.https://doi.org/10.1149/1.3071718

74. T., O., On barium titanate ceramics. *Busseiron Kenkyu* **1947,** *6* (1–27),

75. VulBM., Highand ultrahighdielectric constantmaterials. *Elektrichestvo* **1946,** *3*,

76. Sawaguchi, E.; Shirane, G.; Takagi, Y., PHASE TRANSITION IN LEAD ZIRCONATE. *Journal of the Physical Society of Japan* **1951,** *6* (5), 333-339.https://doi.org/10.1143/jpsj.6.333

77. Sawaguchi, E., FERROELECTRICITY VERSUS ANTIFERROELECTRICITY IN THE SOLID SOLUTIONS OF $PbZrO_3$ AND $PbTiO_3$. *Journal of the Physical Society of Japan* **1953,** *8* (5), 615-629.https://doi.org/10.1143/jpsj.8.615

78. Fu, Y. Q.; Luo, J. K.; Nguyen, N. T.; Walton, A. J.; Flewitt, A. J.; Zu, X. T.; Li, Y.; McHale, G.; Matthews, A.; Iborra, E.; Du, H.; Milne, W. I., Advances in piezoelectric thin films for acoustic biosensors, acoustofluidics and lab-on-chip applications. *Progress in Materials Science* **2017,** *89*, 31-91.https://doi.org/10.1016/j.pmatsci.2017.04.006

79. Que, M. L.; Zhou, R. R.; Wang, X. D.; Yuan, Z. Q.; Hu, G. F.; Pan, C. F., Progress in piezo-phototronic effect modulated photovoltaics. *Journal of Physics-Condensed Matter* **2016,** *28* (43).https://doi.org/10.1088/0953-8984/28/43/433001

80. Y. Qi, T. D. N., P. K. Purohit, M. C. McAlpine,, *Stretchable Electronics (Ed: T. Someya)*. Wiley-VCH: 2012; p p. 111.

81. Chorsi, M. T.; Curry, E. J.; Chorsi, H. T.; Das, R.; Baroody, J.; Purohit, P. K.; Ilies, H.; Nguyen, T. D., Piezoelectric Biomaterials for Sensors and Actuators. *Advanced Materials* **2019,** *31* (1).https://doi.org/10.1002/adma.201802084

82. Jacob, J.; More, N.; Kalia, K.; Kapusetti, G., Piezoelectric smart biomaterials for bone and cartilage tissue engineering. *Inflammation and Regeneration* **2018,** *38*.https://doi.org/10.1186/s41232-018-0059-8

83. Li, Q.; Wang, Q., Ferroelectric Polymers and Their Energy-Related Applications. *Macromolecular Chemistry and Physics* **2016,** *217* (11), 1228-1244.https://doi.org/10.1002/macp.201500503

84. Wan, C. Y.; Bowen, C. R., Multiscale-structuring of polyvinylidene fluoride for energy harvesting: the impact of molecular-, micro- and macro-structure. *Journal of Materials Chemistry A* **2017,** *5* (7), 3091-3128.https://doi.org/10.1039/c6ta09590a

85. Bystrov, V. S.; Paramonova, E. V.; Bdikin, I. K.; Bystrova, A. V.; Pullar, R. C.; Kholkin, A. L., Molecular modeling of the piezoelectric effect in the ferroelectric polymer poly(vinylidene fluoride) (PVDF). *Journal of Molecular Modeling* **2013,** *19* (9), 3591-3602.https://doi.org/10.1007/s00894-013-1891-z

86. Smith, M.; Calahorra, Y.; Jing, Q. S.; Kar-Narayan, S., Direct observation of shear piezoelectricity in poly-L-lactic acid nanowires. *Apl Materials* **2017,** *5* (7).https://doi.org/10.1063/1.4979547

87. Ochiai, T.; Fukada, E., Electromechanical properties of poly-L-lactic acid. *Japanese Journal of Applied Physics Part 1-Regular Papers Short Notes & Review Papers* **1998,** *37* (6A), 3374-3376.https://doi.org/10.1143/jjap.37.3374

88. Fukada, E., ON THE PIEZOELECTRIC EFFECT OF SILK FIBERS. *Journal of the Physical Society of Japan* **1956,** *11* (12), 1301-1301

89. Kapat, K.; Shubhra, Q. T. H.; Zhou, M.; Leeuwenburgh, S., Piezoelectric Nano-Biomaterials for Biomedicine and Tissue Regeneration. *Advanced Functional Materials*. **2020**, 30 (44), https://doi.org/10.1002/adfm.201909045

90. Harvey, E. N., THE LUMINESCENCE OF ADHESIVE TAPE. *Science* **1939,** *89* (2316), 460-461.https://doi.org/10.1126/science.89.2316.460

91. Yucel, T.; Cebe, P.; Kaplan, D. L., Structural Origins of Silk Piezoelectricity. *Advanced Functional Materials* **2011,** *21* (4), 779-785.https://doi.org/10.1002/adfm.201002077

92. Koh, L. D.; Cheng, Y.; Teng, C. P.; Khin, Y. W.; Loh, X. J.; Tee, S. Y.; Low, M.; Ye, E. Y.; Yu, H. D.; Zhang, Y. W.; Han, M. Y., Structures, mechanical properties and applications of silk fibroin materials. *Progress in Polymer Science* **2015,** *46*, 86-110.https://doi.org/10.1016/j.progpolymsci.2015.02.001

93. Ding, J. X.; Zhang, J.; Li, J. N.; Li, D.; Xiao, C. S.; Xiao, H. H.; Yang, H. H.; Zhuang, X. L.; Chen, X. S., Electrospun polymer biomaterials. *Progress in Polymer Science* **2019,** *90*, 1-34.https://doi.org/10.1016/j.progpolymsci.2019.01.002

94. Theocharis, A. D.; Skandalis, S. S.; Gialeli, C.; Karamanos, N. K., Extracellular matrix structure. *Advanced Drug Delivery Reviews* **2016,** *97*, 4-27.https://doi.org/10.1016/j.addr.2015.11.001

95. Gu, X. S.; Ding, F.; Williams, D. F., Neural tissue engineering options for peripheral nerve

regeneration. *Biomaterials* **2014,** *35* (24), 6143-6156.https://doi.org/10.1016/j.biomaterials.2014.04.064

96. Chen, Q. S.; Chen, D.; Wu, J.; Lin, J. M., Flexible control of cellular encapsulation, permeability, and release in a droplet-templated bifunctional copolymer scaffold. *Biomicrofluidics* **2016,** *10* (6).https://doi.org/10.1063/1.4972107

97. Faghihi, F.; Mirzaei, E.; Ai, J.; Lotfi, A.; Sayahpour, F. A.; Ebrahimi-Barough, S.; Joghataei, M. T., Differentiation Potential of Human Chorion-Derived Mesenchymal Stem Cells into Motor Neuron-Like Cells in Two- and Three-Dimensional Culture Systems (vol 53, pg 1862, 2016). *Molecular Neurobiology* **2016,** *53* (3), 1873-1873.https://doi.org/10.1007/s12035-015-9172-8

98. Guo, J. H.; Liu, Y.; Lv, Z. J.; Wei, W. J.; Guan, X.; Guan, Q. L.; Leng, Z. Q.; Zhao, J. Y.; Miao, H.; Liu, J., Potential Neurogenesis of Human Adipose-Derived Stem Cells on Electrospun Catalpol-Loaded Composite Nanofibrous Scaffolds. *Annals of Biomedical Engineering* **2015,** *43* (10), 2597-2608.https://doi.org/10.1007/s10439-015-1311-x

99. Kuppan, P.; Sethuraman, S.; Krishnan, U. M., Interaction of human smooth muscle cells with nanofibrous scaffolds: Effect of fiber orientation on cell adhesion, proliferation, and functional gene expression. *Journal of Biomedical Materials Research Part A* **2015,** *103* (7), 2236-2250.https://doi.org/10.1002/jbm.a.35360

100. Loo, Y.; Zhang, S. G.; Hauser, C. A. E., From short peptides to nanofibers to macromolecular assemblies in biomedicine. *Biotechnology Advances* **2012,** *30* (3), 593-603.https://doi.org/10.1016/j.biotechadv.2011.10.004

101. Costa, F. S., R.; Boccaccini,, *7 - Fibrous protein-based biomaterials (silk, keratin, elastin, and resilin proteins) for tissue regeneration and repair*. Woodhead Publishing: Cambridge, UK, **2018**; 175–204.

102. Gulati, K.; Meher, M. K.; Poluri, K. M., Glycosaminoglycan-based resorbable polymer composites in tissue refurbishment. *Regenerative Medicine* **2017,** *12* (4), 431-457.https://doi.org/10.2217/rme-2017-0012

103. Venugopal, J.; Low, S.; Choon, A. T.; Kumar, T. S. S.; Ramakrishna, S., Mineralization of osteoblasts with electrospun collagen/hydroxyapatite nanofibers. *Journal of Materials Science-Materials in Medicine* **2008,** *19* (5), 2039-2046.https://doi.org/10.1007/s10856-007-3289-x

104. Kim, H. J.; Kim, U. J.; Vunjak-Novakovic, G.; Min, B. H.; Kaplan, D. L., Influence of macroporous protein scaffolds on bone tissue engineering from bone marrow stem cells. *Biomaterials* **2005,** *26* (21), 4442-4452.https://doi.org/10.1016/j.biomaterials.2004.11.013

105. Li, C. M.; Jin, H. J.; Botsaris, G. D.; Kaplan, D. L., Silk apatite composites from electrospun fibers. *Journal of Materials Research* **2005,** *20* (12), 3374-3384.https://doi.org/10.1557/jmr.2005.0425

106. Phromviyo, N.; Lert-itthiporn, A.; Swatsitang, E.; Chompoosor, A., Biodegradable poly(vinyl alcohol)/polyoxalate electrospun nanofibers for hydrogen peroxide-triggered drug release. *Journal of Biomaterials Science-Polymer Edition* **2015,** *26* (14), 975-987.https://doi.org/10.1080/09205063.2015.1069781

107. Kim, H. W.; Lee, H. H.; Knowles, J. C., Electrospinning biomedical nanocomposite fibers of hydroxyapaite/poly(lactic acid) for bone regeneration. *Journal of Biomedical Materials Research Part A* **2006,** *79A* (3), 643-649.https://doi.org/10.1002/jbm.a.30866

108. Tiwari, A. P.; Joshi, M. K.; Lee, J.; Maharjan, B.; Ko, S. W.; Park, C. H.; Kim, C. S., Heterogeneous electrospun polycaprolactone/polyethylene glycol membranes with improved wettability, biocompatibility, and mineralization. *Colloids and Surfaces a-Physicochemical and Engineering Aspects* **2017,** *520*, 105-113.https://doi.org/10.1016/j.colsurfa.2017.01.054

109. Braghirolli, D. I.; Steffens, D.; Pranke, P., Electrospinning for regenerative medicine: a review of the main topics. *Drug Discovery Today* **2014,** *19* (6), 743-753.https://doi.org/10.1016/j.drudis.2014.03.024

110. Bhardwaj, N.; Kundu, S. C., Electrospinning: A fascinating fiber fabrication technique. *Biotechnology Advances* **2010,** *28* (3), 325-347.https://doi.org/10.1016/j.biotechadv.2010.01.004

111. Zhang, Y. Z.; Venugopal, J.; Huang, Z. M.; Lim, C. T.; Ramakrishna, S., Crosslinking of the electrospun gelatin nanofibers. *Polymer* **2006,** *47* (8), 2911-2917.https://doi.org/10.1016/j.polymer.2006.02.046

112. Zhong, S. P.; Zhang, Y. Z.; Lim, C. T., Tissue scaffolds for skin wound healing and dermal reconstruction. *Wiley Interdisciplinary Reviews-Nanomedicine and Nanobiotechnology* **2010,** *2* (5), 510-525.https://doi.org/10.1002/wnan.100

113. Kumbar, S. G.; James, R.; Nukavarapu, S. P.; Laurencin, C. T., Electrospun nanofiber scaffolds:

engineering soft tissues. *Biomedical Materials* **2008,** *3* (3).https://doi.org/10.1088/1748-6041/3/3/034002

114. Miguel, S. P.; Figueira, D. R.; Simoes, D.; Ribeiro, M. P.; Coutinho, P.; Ferreira, P.; Correia, I. J., Electrospun polymeric nanofibres as wound dressings: A review. *Colloids and Surfaces B-Biointerfaces* **2018,** *169*, 60-71.https://doi.org/10.1016/j.colsurfb.2018.05.011

115. Khil, M. S.; Cha, D. I.; Kim, H. Y.; Kim, I. S.; Bhattarai, N., Electrospun nanofibrous polyurethane membrane as wound dressing. *Journal of Biomedical Materials Research Part B-Applied Biomaterials* **2003,** *67B* (2), 675-679.https://doi.org/10.1002/jbm.b.10058

116. Saber-Samandari, S.; Saber-Samandari, S.; Kiyazar, S.; Aghazadeh, J.; Sadeghi, A., In vitro evaluation for apatite-forming ability of cellulose-based nanocomposite scaffolds for bone tissue engineering. *International Journal of Biological Macromolecules* **2016,** *86*, 434-442.https://doi.org/10.1016/j.ijbiomac.2016.01.102

117. Lin, J. T.; Li, C. H.; Zhao, Y.; Hu, J. C.; Zhang, L. M., Co-electrospun Nanofibrous Membranes of Collagen and Zein for Wound Healing. *Acs Applied Materials & Interfaces* **2012,** *4* (2), 1050-1057.https://doi.org/10.1021/am201669z

118. Venugopal, J. R.; Zhang, Y. Z.; Ramakrishna, S., In vitro culture of human dermal fibroblasts on electrospun polycaprolactone collagen nanofibrous membrane. *Artificial Organs* **2006,** *30* (6), 440-446.https://doi.org/10.1111/j.1525-1594.2006.00239.x

119. Tran, S.; DeGiovanni, P.-J.; Piel, B.; Rai, P., Cancer nanomedicine: a review of recent success in drug delivery. *Clinical and Translational Medicine* **2017,** *6*.https://doi.org/10.1186/s40169-017-0175-0

120. Bhattarai, R. S.; Bachu, R. D.; Boddu, S. H. S.; Bhaduri, S., Biomedical Applications of Electrospun Nanofibers: Drug and Nanoparticle Delivery. *Pharmaceutics* **2019,** *11* (1).https://doi.org/10.3390/pharmaceutics11010005

121. Jose Torres-Martinez, E.; Cornejo Bravo, J. M.; Serrano Medina, A.; Perez Gonzalez, G. L.; Villarreal Gomez, L. J., A Summary of Electrospun Nanofibers as Drug Delivery System: Drugs Loaded and Biopolymers Used as Matrices. *Current Drug Delivery* **2018,** *15* (10), 1360-1374.https://doi.org/10.2174/1567201815666180723114326

122. Qi, R. L.; Guo, R.; Zheng, F. Y.; Liu, H.; Yu, J. Y.; Shi, X. Y., Controlled release and antibacterial

activity of antibiotic-loaded electrospun halloysite/poly(lactic-co-glycolic acid) composite nanofibers. *Colloids and Surfaces B-Biointerfaces* **2013,** *110*, 148-155.https://doi.org/10.1016/j.colsurfb.2013.04.036

123. Wang, S. G.; Zheng, F. Y.; Huang, Y. P.; Fang, Y. T.; Shen, M. W.; Zhu, M. F.; Shi, X. Y., Encapsulation of Amoxicillin within Laponite-Doped Poly(lactic-co-glycolic acid) Nanofibers: Preparation, Characterization, and Antibacterial Activity. *ACS Applied Materials & Interfaces* **2012,** *4* (11), 6393-6401.https://doi.org/10.1021/am302130b

124. Wibroe, P. P.; Ahmadvand, D.; Oghabian, M. A.; Yaghmur, A.; Moghimi, S. M., An integrated assessment of morphology, size, and complement activation of the PEGylated liposomal doxorubicin products Doxil (R), Caelyx (R), DOXOrubicin, and SinaDoxosome. *Journal of Controlled Release* **2016,** *221*, 1-8.https://doi.org/10.1016/j.jconrel.2015.11.021

125. Zheng, F. Y.; Wang, S. G.; Shen, M. W.; Zhu, M. F.; Shi, X. Y., Antitumor efficacy of doxorubicin-loaded electrospun nano-hydroxyapatite-poly(lactic-co-glycolic acid) composite nanofibers. *Polymer Chemistry* **2013,** *4* (4), 933-941.https://doi.org/10.1039/c2py20779f

126. Qi, R. L.; Tian, X. J.; Guo, R.; Luo, Y.; Shen, M. W.; Yu, J. Y.; Shi, X. Y., Controlled release of doxorubicin from electrospun MWCNTs/PLGA hybrid nanofibers. *Chinese Journal of Polymer Science* **2016,** *34* (9), 1047-1059.https://doi.org/10.1007/s10118-016-1827-z

127. Shamos, M. H.; Lavine, L. S., PIEZOELECTRICITY AS A FUNDAMENTAL PROPERTY OF BIOLOGICAL TISSUES. *Nature* **1967,** *213* (5073), 267-&.https://doi.org/10.1038/213267a0

128. Guzelsu, N.; Demiray, H., Electromechanical properties and related models of bone tissues: A review. *International Journal of Engineering Science* **1979,** *17* (7), 813-851.https://doi.org/https://doi.org/10.1016/0020-7225(79)90013-2

129. Aksel, E.; Jones, J. L., Advances in Lead-Free Piezoelectric Materials for Sensors and Actuators. *Sensors* **2010,** *10* (3), 1935-1954.https://doi.org/10.3390/s100301935

130. Liu, W. F.; Ren, X. B., Large Piezoelectric Effect in Pb-Free Ceramics. *Physical Review Letters* **2009,** *103* (25).https://doi.org/10.1103/PhysRevLett.103.257602

131. Zhan, S. H.; Yu, H. B.; Li, Y.; Jiang, B.; Zhang, X.; Yan, C. H.; Ma, S. Q., Co-Electrospun BaTiO3 Hollow Fibers Combined with Sol-Gel Method. *Journal of Dispersion Science and Technology*

2008, *29* (9), 1345-1348.https://doi.org/10.1080/01932690701866930

132. Jalalian, A.; Grishin, A. M.; Wang, X. L.; Cheng, Z. X.; Dou, S. X., Large piezoelectric coefficient and ferroelectric nanodomain switching in Ba(Ti0.80Zr0.20)O3-0.5(Ba0.70Ca0.30)TiO3 nanofibers and thin films. *Applied Physics Letters* **2014,** *104* (10), 103112.https://doi.org/10.1063/1.4867013

133. Shoichet, M. S., Polymer Scaffolds for Biomaterials Applications. *Macromolecules* **2010,** *43* (2), 581-591.https://doi.org/10.1021/ma901530r

134. Damaraju, S. M.; Shen, Y. Y.; Elele, E.; Khusid, B.; Eshghinejad, A.; Li, J. Y.; Jaffe, M.; Arinzeh, T. L., Three-dimensional piezoelectric fibrous scaffolds selectively promote mesenchymal stem cell differentiation. *Biomaterials* **2017,** *149*, 51-62.https://doi.org/10.1016/j.biomaterials.2017.09.024

135. Wang, A. C.; Hu, M.; Zhou, L. W.; Qiang, X. Y., Self-Powered Well-Aligned P(VDF-TrFE) Piezoelectric Nanofiber Nanogenerator for Modulating an Exact Electrical Stimulation and Enhancing the Proliferation of Preosteoblasts. *Nanomaterials* **2019,** *9* (3).https://doi.org/10.3390/nano9030349

136. Lee, Y. S.; Collins, G.; Arinzeh, T. L., Neurite extension of primary neurons on electrospun piezoelectric scaffolds. *Acta Biomaterialia* **2011,** *7* (11), 3877-3886.https://doi.org/10.1016/j.actbio.2011.07.013

137. Lee, Y. S.; Arinzeh, T. L., The Influence of Piezoelectric Scaffolds on Neural Differentiation of Human Neural Stem/Progenitor Cells. *Tissue Engineering Part A* **2012,** *18* (19-20), 2063-2072.https://doi.org/10.1089/ten.tea.2011.0540

138. Motamedi, A. S.; Mirzadeh, H.; Hajiesmaeilbaigi, F.; Bagheri-Khoulenjani, S.; Shokrgozar, M. A., Piezoelectric electrospun nanocomposite comprising Au NPs/PVDF for nerve tissue engineering. *Journal of Biomedical Materials Research Part A* **2017,** *105* (7), 1984-1993.https://doi.org/10.1002/jbm.a.36050

139. Hoop, M.; Chen, X. Z.; Ferrari, A.; Mushtaq, F.; Ghazaryan, G.; Tervoort, T.; Poulikakos, D.; Nelson, B.; Pane, S., Ultrasound-mediated piezoelectric differentiation of neuron-like PC12 cells on PVDF membranes. *Scientific Reports* **2017,** *7*.https://doi.org/10.1038/s41598-017-03992-3

140. Hsieh, C. L.; Grange, R.; Pu, Y.; Psaltis, D., Three-dimensional harmonic holographic microcopy using nanoparticles as probes for cell imaging. *Optics Express* **2009,** *17* (4), 2880-2891.https://doi.org/10.1364/oe.17.002880

141. Weber, N.; Lee, Y. S.; Shanmugasundaram, S.; Jaffe, M.; Arinzeh, T. L., Characterization and in vitro cytocompatibility of piezoelectric electrospun scaffolds. *Acta Biomaterialia* **2010,** *6* (9), 3550-3556.https://doi.org/10.1016/j.actbio.2010.03.035

142. Wang, A. C.; Liu, Z.; Hu, M.; Wang, C. C.; Zhang, X. D.; Shi, B. J.; Fan, Y. B.; Cui, Y. G.; Li, Z.; Ren, K. L., Piezoelectric nanofibrous scaffolds as in vivo energy harvesters for modifying fibroblast alignment and proliferation in wound healing. *Nano Energy* **2018,** *43*, 63-71.https://doi.org/10.1016/j.nanoen.2017.11.023

143. Guo, H. F.; Li, Z. S.; Dong, S. W.; Chen, W. J.; Deng, L.; Wang, Y. F.; Ying, D. J., Piezoelectric PU/PVDF electrospun scaffolds for wound healing applications. *Colloids and Surfaces B-Biointerfaces* **2012,** *96*, 29-36.https://doi.org/10.1016/j.colsurfb.2012.03.014

144. Persano, L.; Dagdeviren, C.; Su, Y. W.; Zhang, Y. H.; Girardo, S.; Pisignano, D.; Huang, Y. G.; Rogers, J. A., High performance piezoelectric devices based on aligned arrays of nanofibers of poly(vinylidenefluoride-co-trifluoroethylene). *Nature Communications* **2013,** *4*.https://doi.org/10.1038/ncomms2639

145. Beringer, L. T.; Xu, X.; Shih, W.; Shih, W. H.; Habas, R.; Schauer, C. L., An electrospun PVDF-TrFe fiber sensor platform for biological applications. *Sensors and Actuators a-Physical* **2015,** *222*, 293-300.https://doi.org/10.1016/j.sna.2014.11.012

146. Liu, Z.; Zhang, S.; Jin, Y. M.; Ouyang, H.; Zou, Y.; Wang, X. X.; Xie, L. X.; Li, Z., Flexible piezoelectric nanogenerator in wearable self-powered active sensor for respiration and healthcare monitoring. *Semiconductor Science and Technology* **2017,** *32* (6).https://doi.org/10.1088/1361-6641/aa68d1

147. Park, S.-H.; Lee, H. B.; Yeon, S. M.; Park, J.; Lee, N. K., Flexible and Stretchable Piezoelectric Sensor with Thickness-Tunable Configuration of Electrospun Nanofiber Mat and Elastomeric Substrates. *ACS Applied Materials & Interfaces* **2016,** *8* (37), 24773-24781.https://doi.org/10.1021/acsami.6b07833

148. Fang, J.; Niu, H. T.; Wang, H. X.; Wang, X. G.; Lin, T., Enhanced mechanical energy harvesting using needleless electrospun poly(vinylidene fluoride) nanofibre webs. *Energy & Environmental Science* **2013,** *6* (7), 2196-2202.https://doi.org/10.1039/c3ee24230g

149. Ishida, K.; Huang, T. C.; Honda, K.; Shinozuka, Y.; Sakurai, T., Insole Pedometer With

Piezoelectric Energy Harvester and 2 V Organic Circuits. *Ieee Journal of Solid-State Circuits* **2013,** *48* (1), 255-264.https://doi.org/10.1109/jssc.2012.2221253

150. Liu, X.; Zhao, H.; Lu, Y. X.; Li, S.; Wang, X. H., In vitro cardiomyocyte-driven biogenerator based on aligned piezoelectric nanofibers. *Nanoscale* **2016,** *8* (13), 7278-7286.https://doi.org/10.1039/c5nr08430j

Chapter 2

1 Introduction

Owing to their excellent flexibility, piezoelectric polymers are good alternatives for applications similar to the ones described above. Among the known piezoelectric polymer classes, PVDF is the only commercial product used as a piezoelectric membrane, due to its high piezoelectric activity[1, 2]. Considering the high electrostatic field and polymer jet characteristics of the electrospinning process, electrospinning is ideally suited for producing piezoelectric nanofibers with the β phase formation through in situ electric poling and mechanical stretching. Additionally, electrospinning is a very convenient way of preparing ultra-thin, flexible and ultra-light piezoelectric membranes, making them more applicable in certain specific areas. Recent literature surveys show the exploitation of the piezoelectric properties of either single electrospun PVDF nanofibers[3, 4] or nanofiber mats for energy conversion, power generation, and biomedical applications[5-7].

However, one of the problems associated with chapter 2 is that the β phase content of pure PVDF electrospun nanofibers is still at a low level, which leads to a small output power and weak piezoelectricity. Therefore, we attempted to increase the β phase content by the addition of a suitable amount of MWCNTs to the spinning solution, and simultaneously raise the alignment of PVDF nanofibers by using a high speed rotating drum collecting system.

In this chapter, we aim to systematically study the PVDF/MWCNTs nanofibers parameters including: morphology, alignment, crystal structure, mechanical properties, output voltage and cytotoxicity.

2 Materials and methods

2.1 Materials

Tissue culture plates (TCPs) was purchased from Thomas scientific.

Polyvinylidene Fluoride (PVDF) Mw=600,000 was bought from Shanghai 3F New Material Co., Ltd. Multiwalled carbon nanotubes (MWCNTs) was purchased from Beijing Deke Daojin Science And Technology Co., Ltd.

Polycaprolactone (PCL), Dimethylformamide (DMF), Tetrahydrofuran (THF), 3-[4,5-dimethyl-2-thiazolyl]-2,5-diphenyl-2H-tetrazolium bromide (MTT), Acetone, Ethanol were obtained from Sigma Aldrich (USA).

Dulbecco's Modified Eagle's Medium (DMEM), Fetal bovine serum (FBS), antibiotic-antimycotic (AA) and L929cells Hangzhou Jinuo Biomedical Technology (Hangzhou, China)

2.2 Methods

2.2.1 Fibers fabrication (PVDF, PVDF/MWCNTs, PCL)

PVDF:

To prepare electrospun PVDF nanofibers, solvent mixtures were prepared, composed of DMF and acetone in two different volume ratios of 8:2 and 6:4, respectively. Then, PVDF powder was dissolved in the solvent mixture and the concentration of PVDF solution (8%, 10%, 12%, 14% w/v), expressed as mass of polymer (g)/solvent volume (ml), was stirred overnight at room temperature. 10 milliliters from the solution were then transferred into a plastic syringe with a metallic orthogonally cut-ended needle (tip diameter of 0.6 mm) and the PVDF fibers were spun under different electric field (10 kV, 15 kV, 20 kV) with a flowing rate of 1 ml/h. In order to collect random and aligned fibers, a rotating drum collector was used at various speeds (50, 300. 2000 rpm). The distance between the tip of the syringe needle and the drum collector was 15 cm. The thickness of PVDF fiber meshes was controlled by the deposition time which was 0.5, 1 and 2 hours. The whole electrospinning processing was conducted at constant

temperature of 25 ℃ degrees and the range of humidity between 50% and 70%. All the electrospun PVDF nanofiber meshes were dried in an oven at 40 ℃ overnight, to evaporate the residual solvent, and after that all nanofiber meshes were removed gently from the surface of the aluminum foil with tweezers; these nanofiber mesh samples were classified and labeled carefully for next steps.

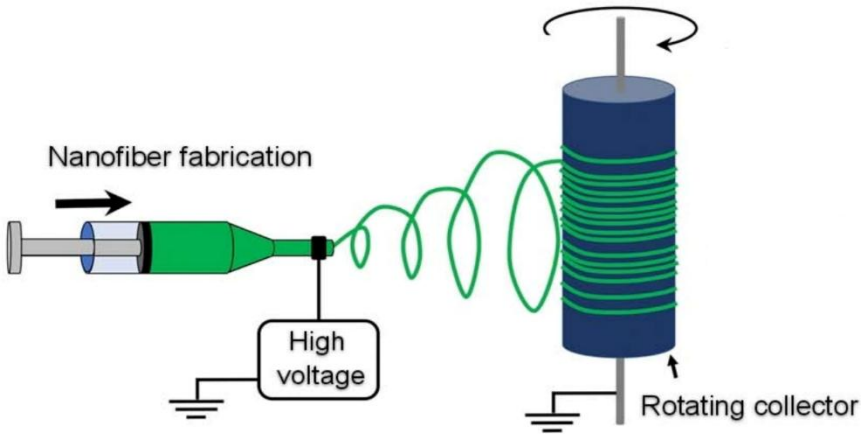

Fig. 10. electrospinning process

PVDF/MWCNTs:

PVDF was dissolved in a DMF/acetone mixture (DMF/acetone ratio 6:4) at the concentration of 10%, 12% respectively. The MWCNTs were dispersed in the PVDF solution via 2 hours sonication followed by continuous stirring for 3 days. The concentrations of MWCNTs in the final working solutions were 0.1%, 0.5%, 1%, 2%, respectively, related to the polymer mass. The PVDF/MWCNTs solution was then placed in a plastic syringe for electrospinning. The electrospinning conditions as follows: collecting distance was 15 cm; deposition time was 2 hours; rotating drum speed was 50 and 2000 rpm. The whole electrospinning processing was conducted at constant temperature of 25 ℃ and the range of humidity between 50% and 70%. PVDF/MWCNTs nanofiber meshes were removed and kept safely as with previous methods.

PCL:

PCL was dissolved in 1:1 THF/DMF (w/w) at a concentration of 15% w/v. The electrospinning process was conducted as follows: the polymer solution was transferred into a 5 ml glass syringe with an orthogonally cut-ended needle. A syringe driver was used to control the solution flow rate at 1 ml/h. To produce PCL fibers, a voltage of 10 kV was applied between the syringe needle and the collector. Fibers were collected on a grounded piece of aluminum foil which was placed on the drum collector plate 10 cm from the needle-end.

2.2.2 Characterization methods

Scanning electron microscope

After electrospinning all the nanofiber mesh samples, small cuts were separated for scanning electron microscopy testing. The small cuts were stacked on the surface of carbon conductive paste, then coated with gold powder by JFC 1600 auto fine coater to increase conductivity so that electrons can impinge samples easily. Using the scanning electron microscope (S-4800, Hitachi, Japan), the fibers' morphology was observed. The acceleration voltage of the SEM system was 15 KV. Fiber diameter was measured through image processing software (ImageJ).

Fourier Transform Infrared Spectroscopy

FTIR was used to confirm the PVDF composition and also to estimate the α/β phase ratio. Spectra were acquired in a Fourier transform infrared spectrometer using both the transmittance and ATR (Attenuated Total. Reflectance) techniques. The α, β crystal phase peaks and the α/β phase ratios were investigated in PVDF fibers prepared under different conditions. FTIR-ATR apparatus revealed to be suitable for fibrous samples, sample preparation is simple and easy to operate, test process is fast and results are reliable.

X-ray diffraction

X-ray diffraction (XRD) patterns were recorded on an X-ray diffractometer (D/Max-2550, Rigaku, Japan). The samples were irradiated using a monochromatized Cu Kα (1.54056 Å) X-ray source with a step size (2θ) of 0.01 °and a scan step time of 1.0 s. The operating voltage and current used were 36 kV and 30 mA, respectively, and the scanning range was 5–40 °(2θ).

Fast Fourier transform

According to a previous procedure[8], a two-dimensional fast Fourier transform (2D FFT) approach is applied to measure the alignment rates of the nanofibers. In brief, a square region was captured from SEM images and then analyzed with Image-J software to create corresponding frequency plots and 2D FFT alignment plots.

Mechanical testing

Electrospinning fiber scaffolds for mechanical analysis were cut with scissors into 3 x 0.5 cm rectangular samples, following a cardboard pattern of the same dimensions. Then, the tensile behavior of pure PVDF and PVDF/MWCNTs fibers were tested on an Instron model 5969 at stretching speed of 10 mm/min at room temperature. Up to five specimens were tested for each sample.

Output voltage

The measured electrical output of the PVDF nanofiber meshes were used to characterize the piezoelectric response for our electrospun nanofibers. We selected two different ways to determine the piezoelectric capacity of our samples, which include the pure nanofiber meshes and the nanofibers assembled on our interdigitate electrodes.

Pure nanofibers meshes

The samples were prepared simply by sandwiching the as-spun PVDF nanofiber meshes between two copper foils. The samples were placed on a test bench and

submitted to a periodic bending movement. An oscilloscope (Wavesurfer 104MXs-B, LeCroy) was used to measure the electrical signals generated between the electrodes.

Nanofibers based on interdigitated electrode

The different samples of fibers were fixed on the electrode with insulating tape, then the encapsulated nanofibers with electrode were fixed on the sound vibration exciter (B&K type 4808). An oscilloscope connected to the electrodes was used to measure the electrical signals under mechanical excitation by the sound vibrator.

In vitro cell cytotoxicity

Nanofibers meshes preparation

Different samples of PVDF/MWCNTs nanofibers and PCL nanofibers meshes were first placed in a 24 well tissue culture plate and fixed with stainless steel rings. Then they were all sterilized with ethanol for 2 hours and soaked with medium overnight before cell seeding.

MTT:

Fibroblasts (L929) were seeded onto nanofiber membranes (n=4) at a density of 1×10^4 cells/well for 1, 3, 5, and 7 days. At the appointed time the culture media were removed, and then washed three times with PBS to remove the residual culture media. Each sample was added with 360 μL serum-free DMEM medium and 40 μL MTT solution (5 mg/mL MTT stock solution in PBS), and incubated at 37 ℃ for 3 hours to allow the formation of MTT formazan. Thereafter, the culture media were extracted and 400 μL dimethylsulfoxide (DMSO) was added. When the formazan crystals were sufficiently resolved, 100 μL of each sample was poured into a 96-well plate and tested by an BioTek Synergy 2 plate reader, at 570 nm.

REMA:

For REMA, the cell seeding density was still set at 1×10^4 cells per well. L929 cells were seeded in 4 parallel 24-well TCPs, cultured for 1, 3, 5, and 7 days and washed with phosphate buffered saline (PBS), respectively. At each time point, resazurin working solution (40 mL resazurin solution and 360 mL medium) was added to each well, followed by incubating for another 3 hours at 37 ℃. After that, the resazurin-containing medium (100 mL) of each sample was transferred into individual well of a Corning™ 96-well solid black polystyrene microplate and the fluorescence intensity value at 530/590 nm excitation/emission wavelength was measured using a BioTek Synergy 2 plate reader.

3 Results and Discussion

3.1 Fiber morphology

3.1.1 The effect of solvent composition on PVDF fiber morphology

Many organic solvents can be used to prepare PVDF electrospinning working solution, such as N, N-dimethylformamide (DMF), N-methylpyrrolidone (NMP), and dimethyl sulfoxide (DMSO). Both of DMSO and NMP have low volatility and high boiling point, which is not conducive to electrospinning process[9, 10]. In general, DMF has good solubility, moderate boiling point and good volatility, which is suitable for fabricating PVDF electrospun nanofibers[11]. In addition, the presence of organic solvents in PVDF solution having high conductivity such as DMF leads to the formation of thinner fibers with a uniform shape, that is, bead-free[12]. These results are due to the good electrical conductivity of the polymer solution leading to a higher stretching of the polymer solution during the electrospinning process. The polymer solutions are being stretched owing to the repulsion of charges present on their surface and more charges can be created due to the high conductivity of the solution[13]. Several studies showed that PVDF electrospun with DMF could result in fiber with excellent

piezoelectric properties. Therefore, the mixture of DMF and acetone was selected as the solvent of PVDF.

The solution forms a jet during the spinning process and is stretched by the electric force. The polymer molecular chain is reoriented and aligned[13]. As the solvent evaporates, the jet solidifies into fibers deposit on the collection device. For the study of solvent ratios, the volume ratios of 8:2 and 6:4 were selected. When discussing the influence of the solvent ratio, the applied voltage was set to 15 kV, the flow rate was 1 ml/h, the collecting distance was 15 cm, and the electrospinning was performed under the same conditions of PVDF solution concentration.

DMF has a higher boiling point, higher viscosity, and lower volatility, while acetone has a lower boiling point, lower viscosity, and better volatility. Therefore, changing the proportion of the solvent will change the viscosity and volatility of the solvent.

Fig. 11 shows SEM images of samples with different ratios of DMF and acetone. It can be seen that the ratio of the solvent has a great influence on the morphology of the fibers. The 8:2 solvent had low volatility during the electrospinning process, the fiber was not sufficiently stretched, and the morphology of the deposited fiber was uneven. With the increase of acetone content, the viscosity of the solution decreases, the volatility of the solvent accelerates, and the fiber morphology tends to be clear and uniform.

Therefore, different volume ratios of DMF / acetone solvents have a great effect on the morphology and diameter of electrospun PVDF fiber membranes. When the volume ratio of DMF and acetone is 6:4, the solvent is volatile and the electrospinning process is stable. At the same time, the electrospun fiber meshes have good morphology and uniform diameter distribution. We chose a volume ratio of DMF / acetone of 6:4 as the optimal parameter of the electrospinning polymer solvent.

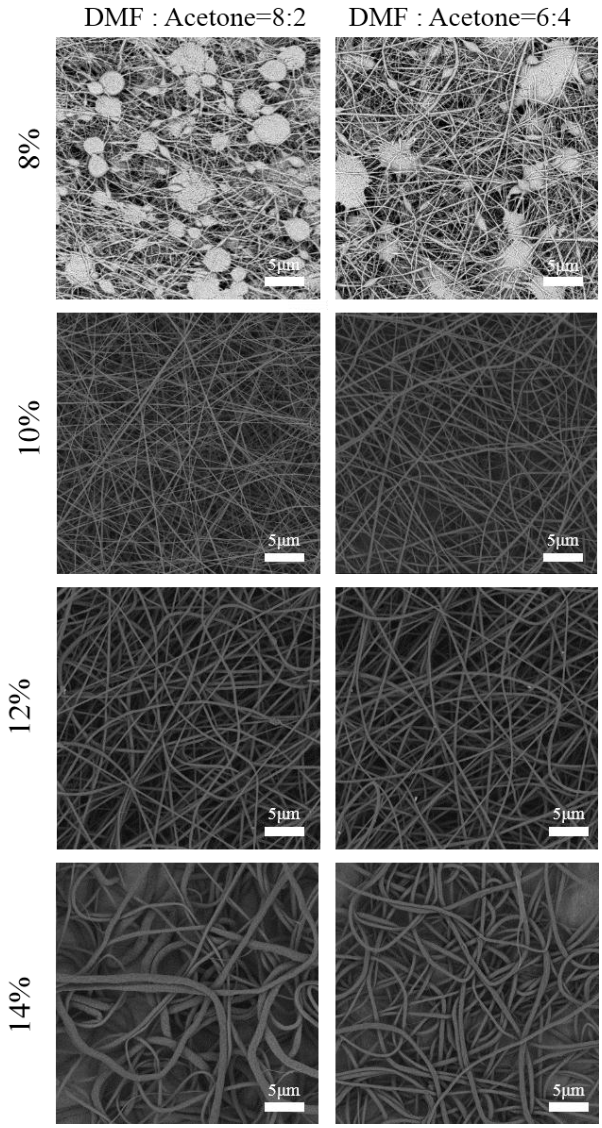

Fig. 11. SEM images of PVDF fibers fabricated with different solvent volume ratios of DMF and acetone, and different concentration of polymer solution**.**

3.1.2 The effect of polymer concentration on PVDF fiber morphology

The concentration of the spinning solution is one of the most important factors in the electrospinning process, which determines the viscosity and surface tension of the spinning solution and has a great influence on the morphology of the fibers. To study the concentration of PVDF spinning solution, a solvent with a volume ratio of 6:4 between DMF and acetone was selected. The spinning solution concentrations were 8%,

10%, 12%, and 14%, respectively. At an applied voltage of 15 kV, the flow rate was 1 ml/h and the collecting distance was 15 cm.

Figure 11 shows the SEM images of the samples at different concentrations of PVDF electrospinning solution. We could observe that the concentration of spinning solution has a great effect on the fiber morphology. When the concentration of spinning solution was 8%, the solution had low viscosity and weak surface tension, and the jet could not be stretched completely under the electric field. So, we obtain neither fibers nor beads.

As the concentration of the spinning solution increased, the viscosity and surface tension of the polymer solution also increased. The beads on the fiber meshes started to disappear, and the fiber morphology was improved. Therefore, when the polymer concentration was above 10%, the viscosity and surface tension allow the polymer jet to stretch under the electric field. Nevertheless, semi-entangled state still allowed some bead formation.

When the polymer solution was 12%, we can see that the SEM images show uniform nanofibers without any beads. These are the optimal conditions for PVDF electrospinning, providing the viscosity does not become too high.

When the concentration was increased to 14%, the viscosity of the solution became too high, which resulted in difficulty for the fluid to flow through the needle. The fibers morphology observed from the SEM images shown that the diameter of the fibers was distributed over a wide micrometers range.

Therefore, we could conclude that the optimal range of polymer solution concentration is between 10% and 12%, not only avoiding the formation of beads, but also regarding to the distribution of nanofiber diameter.

3.1.3 The effect of applied voltage on PVDF fiber morphology

In order to study the effect of the apply voltage on the PVDF fibers morphology, we set up three different voltage values (10 kV, 15 kV, 20 kV), selected two different solution concentrations (10% ,12%) and kept all the other conditions constant, like 1 ml/h of flow rate, 15 cm of collecting distance. When the applied voltage was lower than 10 kV, the Taylor cone was unstable and the small droplets from the needle tip deposited on the collecting device directly. When the applied voltage was higher than 20 kV, the electrostatic force accelerated the jet too much, causing the flight duration to be too short and thus preventing the appropriate stretching of the fibers[14]. Therefore, the SEM images of different voltage and concentrations shown that the uniform morphology and diameter distribution of PVDF fibers came from the sample which is 15 kV and 12% (Fig. 12).

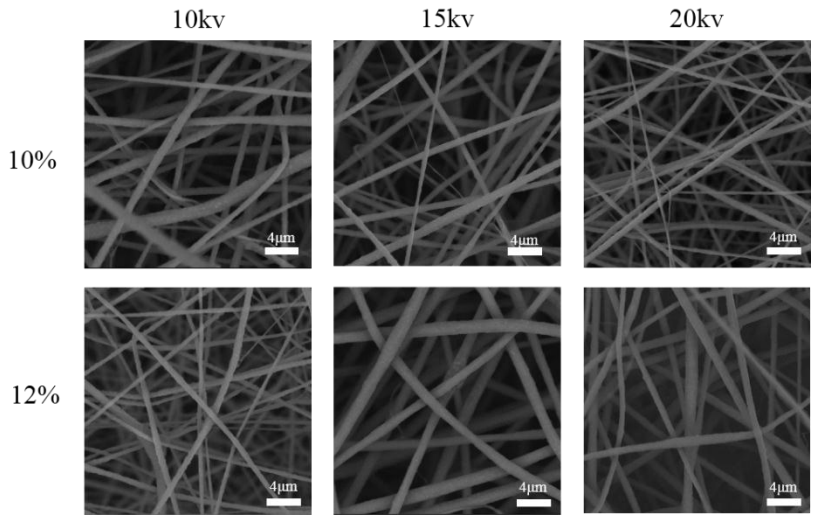

Fig. 12. SEM images of PVDF fibers at two different concentration (10%, 12%) and three different supply voltage (10 kV, 15 kV and 20 kV).

3.1.4 Aligned and anisotropy morphology analysis

The influence of the rotational speed of the collector on the resulting morphology was studied by SEM. Micrographs of the PVDF fibers prepared by electrospinning are

presented in Fig. 13. Thus, nonaligned and aligned scaffolds can be produced with a prevailing fiber orientation by focusing their deposit onto a rotating drum collector at different speeds (50, 300, and 2000 rpm).

The SEM images shown that the fibers processed with a low speed (50 and 300 rpm) are not aligned in the rotation direction. In the opposite direction, the use of higher rotation speeds (2000 rpm) leads to a unidirectional alignment of PVDF fibers, that is, in the rolling direction. In fact, at higher speeds, the centrifugal force generated around the rotating drum combined to the sustained shear forces by the jet during electrospinning process contributes to the fibers' alignment in one uniaxial direction.

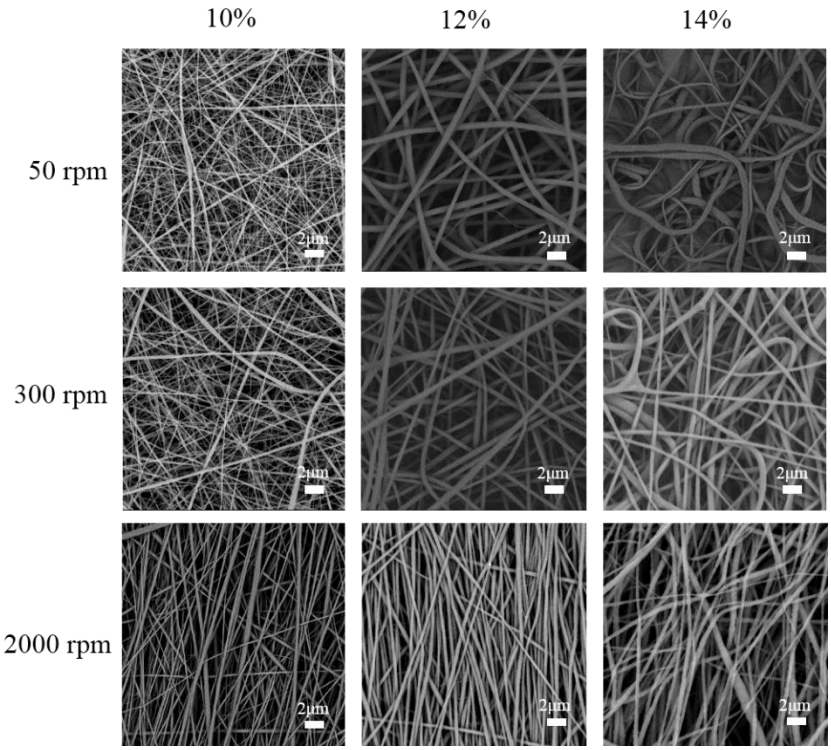

Fig. 13. SEM images of PVDF fibers at three different speed on drum collector (50, 300, and 2000 rpm) and different concentrations (10%, 12% and 14%).

For further confirmation, Fig. 14 shows the diameter distribution of each sample. It is easy to see that depending on the rotation speed of the drum collector, the average fiber diameters of the nonaligned, and high-aligned scaffolds change significantly at

the three different concentrations. A decrease of the fibers' diameter is caused by the higher speeds of the collector rotation (2000 rpm), where the centrifugal force has contributed to the elongation of the fibers before being collected on the drum. For example, we pick the samples (12% concentration of PVDF) which have average diameters of 304.8±181.6 nm, 282.4±153.7 nm, and 170.1±63.4 nm, obtained for rotation speeds of 50, 300, and 2000 rpm, respectively.

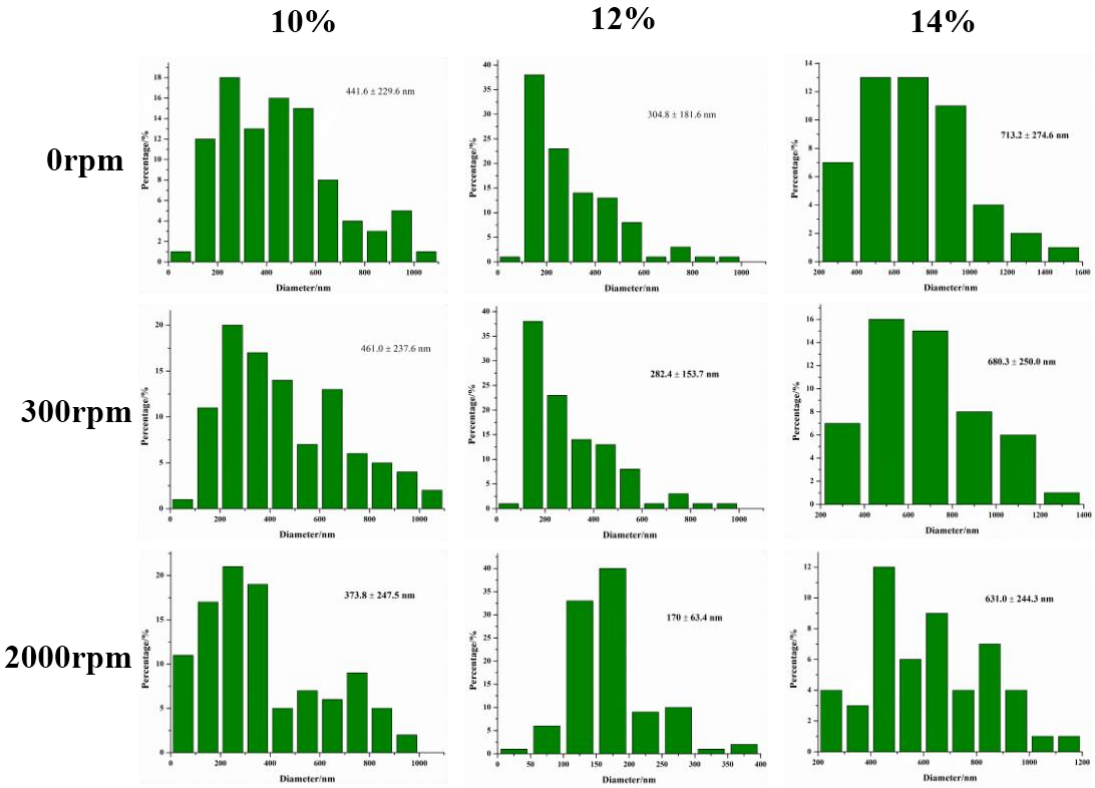

Fig. 14. The diameter distribution of PVDF nanofibers at different at three different speed on drum collector (50, 300, and 2000 rpm) and different concentrations (10%, 12% and 14%).

In addition, the FFT analysis of the SEM images of the nanofiber samples were used to characterize the anisotropy of the scaffolds and measure the alignment level of the nanofibers. Patterned, grayscale pixels are distributed in the output image of the FFT analysis to reflect the degree of fiber alignment of the original data image. A representative FFT analysis of randomly oriented and aligned nanofiber mats, are

presented in Figure 15. A significant difference appears between the FFT images of the aligned nanofibers and randomly oriented nanofibers. The representative FFT of the original data image of the random fibers (Fig. 15a) generates an output image with symmetrically and circularly distributed pixels. On the other hand, the FFT data of the image with aligned fibers results in an output image with non-randomly and elliptically distributed pixels (Fig. 15b).

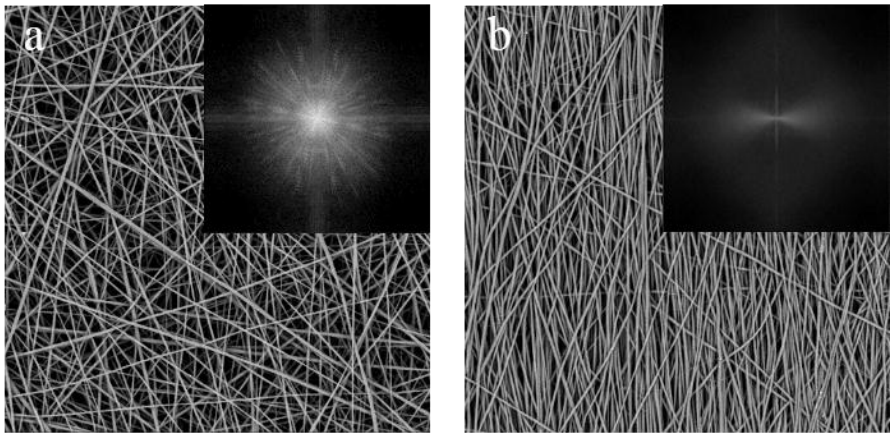

Fig. 15. SEM images of random and aligned nanofibers morphology and frequency plots of FFT analysis.

3.1.5 The comparison of morphology between PCL, PVDF and PVDF/MWCNTs fibers

Polycaprolactone (PCL), a non-piezoelectric control, was used since PVDF cannot be processed into a nonpiezoelectric form due to its piezoelectric β-phase content. Although PCL has a different surface chemistry from PVDF, PCL was chosen primarily due to its slow degradation rate and ease in fabricating fibrous scaffolds similar in morphology and size to PVDF scaffolds. Additionally, PCL is well known for its biocompatibility with many cell types and is in clinical use.

Thus, the SEM images (Fig. 16.) show us that the morphology of PCL and PVDF nanofibers are similar. Especially, PCL nanofibers also exhibit high alinement when the rotation drum speed is 2000 rpm. We can confirm that the electrospun PCL nanofiber is a suitable nonpiezoelectric materials as control group.

We also obtained SEM images of PVDF and PVDF doped with different amounts of MWCNTs fibers. These images show that smooth and bead-free solid fibers were obtained for all samples, although small changes in the fiber distribution were noted. These were due to the higher charge density of the electrified jet forming more uniform and much thinner fibers, from the polymer solution containing suitable and well dispersed MWCNTs. At the higher MWCNTs concentration, above 1% and 2%, PVDF/MWCNTs nanofibers diameter distribution becomes more disperse due to aggregation.

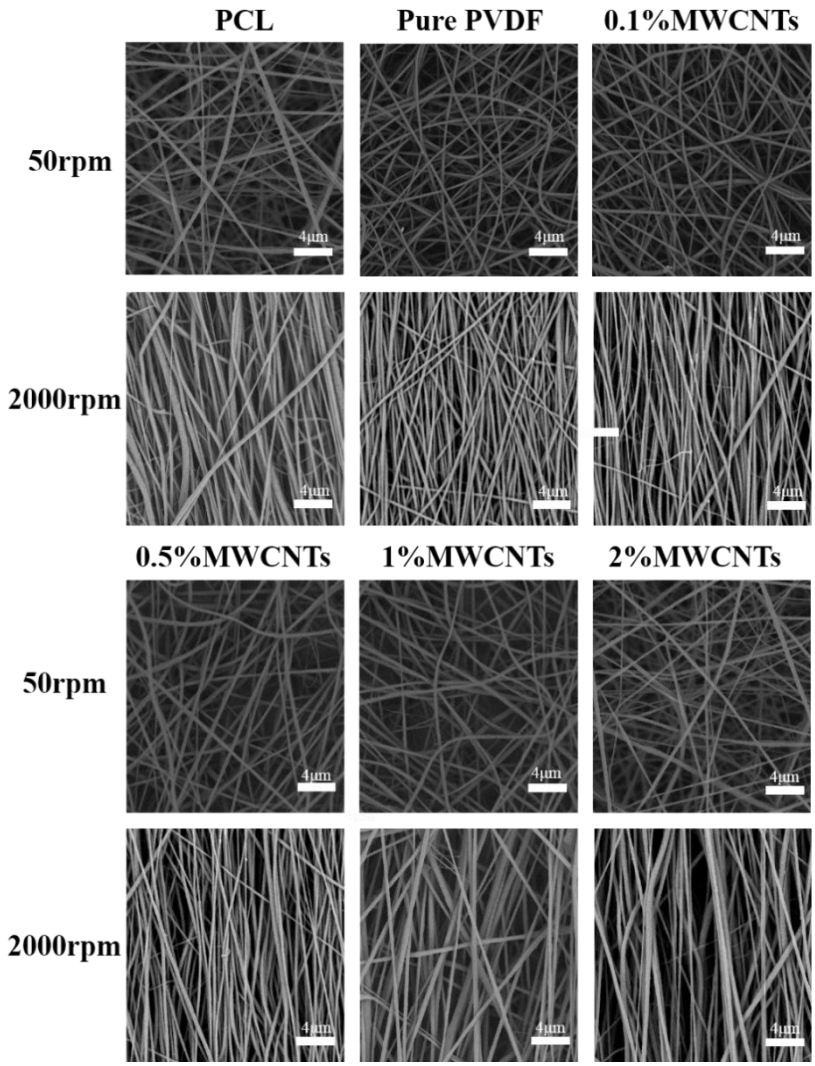

Fig. 16. The SEM images of PCL, PVDF, PVDF/MWCNTs nanofibers at two different speed of drum collector (50 and 2000rpm).

3.2 Piezoelectric response characterization

3.2.1 Crystal phase structure

It is well known that PVDF exists in five different crystal forms. The α phase consists of TGTG conformations, while the β phase consists of the TTTT conformation[15-18]. Among the five structures, the β phase is a polar structure, plays an important role in

the piezo-, pyro- and ferroelectric properties of the polymer. Therefore, samples with higher β phase were expected to display a stronger piezoelectric response [19].

XRD

Fig. 17 shows the XRD patterns of the nanofibers obtained with different MWCNTs weight ratios. The PVDF powder exhibited prominent peaks at 2θ=18.8 °, 20.2 °, and 26.6 °, corresponding to the (020), (110), and (021) reflections of α phase, respectively. In the case of pure PVDF nanofiber sample, these peaks were sharply decreased, while a new peak appeared at 2θ=20.6 °, corresponding to the (110) reflections of the β phase formation[20]. This was due to elongation forces, stretching, and simultaneous poling during the electrospinning process, promoting the formation of the polar β phase. Interestingly, the peaks at 18.8 °and 20.2 ° almost disappeared as the mass fraction of MWCNTs increased to 0.1% and 0.5%, and a stronger β peak at 2θ=20.6 ° became dominant compared with the pure PVDF nanofibers mats. It was also found that both crystallinity and β phase proportion decreased upon a further increase of the MWCNTs concentration to 1% and 2%.

This was further confirmed by the data shown in Table 4, the crystallinity of the PVDF powder was 47.2%, and the powder were completely in the α phase. Although the crystallinity of the electrospun PVDF fibers decreased to 30.9%, 55% of the material was β phase. When the percentage of MWCNTs was 0.5%, the crystallinity and the proportion of the β phase increased to 38.6% and 69%, respectively.

Table 4. Crystallinity and β phase content of PVDF/MWCNTs fiber meshes with different concentration of WMCNTs

PVDF/wt%	MWCNTs/wt%	Crystallinity/%	β phase/%
powder	0	47.2	0
12	0	30.9	55

12	0.1	37.1	57
12	0.5	38.6	69
12	1	33.2	49
12	2	24.9	48

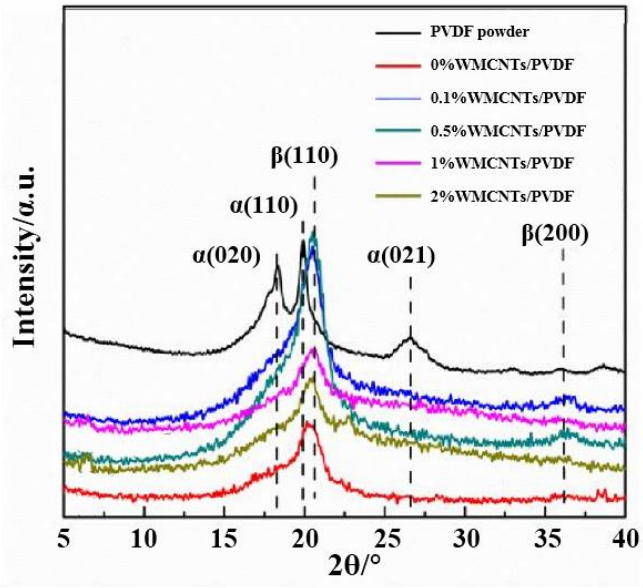

Fig. 17. The XRD patterns of PVDF powder and PVDF nanofibers doped with different concentration of MWCNTs.

The mechanism of the change to the β crystalline phase during the PVDF/MWCNTs composites electrospinning process is clear. For pure PVDF nanofibers, the PVDF chain can be partially crystallized in the β phase under the electric field, but localized amorphous microstructures still exist[21, 22]. The situation was changed when a small percentage of MWCNTs (0.1% and 0.5%) is added into PVDF nanofibers. Under the external electric field, the conductive of the CNTs can produce inductive charges on the surface, thus leading to a larger Coulomb force during the electrospinning. This

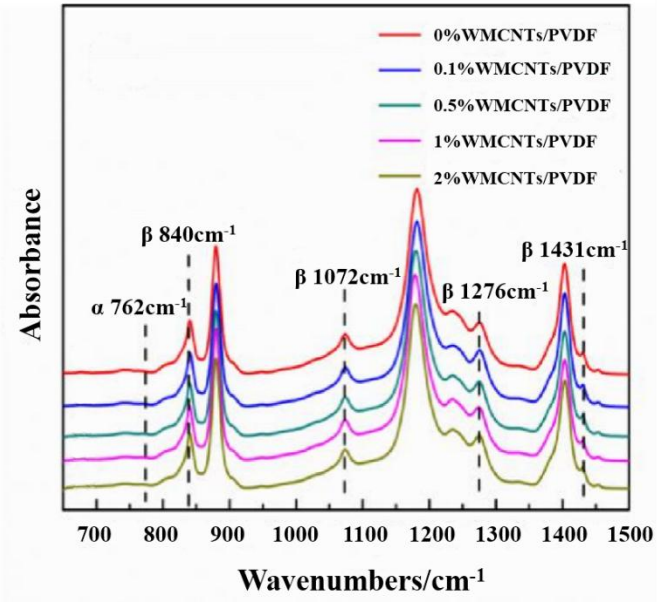

Fig. 18. The FTIR spectra in the ATR mode for nanofibers of pure PVDF and PVDF

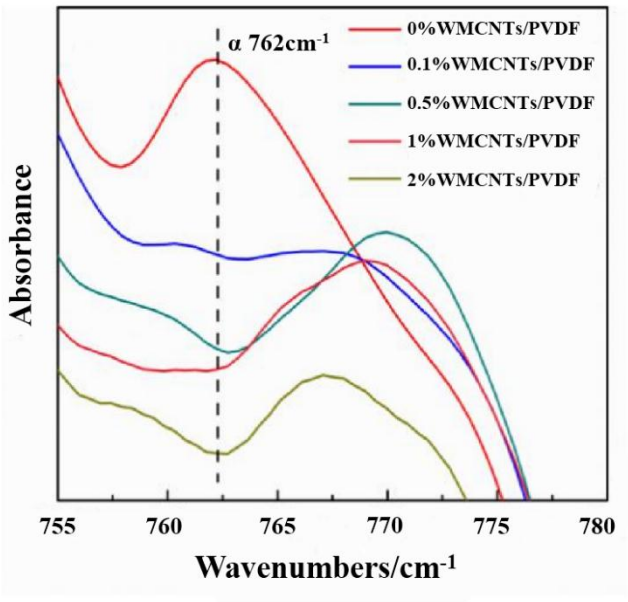

Fig. 19. The FITR spectra and magnification of the α phase at 762 cm^{-1} of pure PVDF and PVDF blended with different concentrations of MWCNTs.

attracts PVDF chains to crystallize on the MWCNTs surface in the β form, which then act as nucleating agents that promote the transformation of local amorphous regions

into the β crystalline phase. As a result, the amount of β crystalline phase was enhanced compared with that achieved in the pure PVDF nanofibers. However, over-addition of MWCNTs promotes aggregations, allowing electric charges to disperse over the aggregate and resulting in a lower charge density, consequently reducing the polarizability of PVDF nanofibers as well as their crystallinity.

FTIR

Vibrational spectroscopy has made significant contributions towards the studies of the structure and crystalline polymorphs of polymers[23-25]. Fig. 18 shows FTIR spectra in the ATR mode for nanofibers of bare PVDF and PVDF with different MWCNT concentrations. The characteristic absorption bands at 840 cm^{-1} (CH_2 rocking), 1074 cm^{-1} (C-C stretching band), 1275 cm^{-1} (trans band), and 1430 cm^{-1} (CH_2 bending) are attributed to the ferroelectric all-trans β phase[26, 27]. The peak at 762 cm^{-1}, attributed to α phase (in-plane bending or rocking), was clearly seen in the spectrum of the bare PVDF fibers but was sharply decreased in the samples doped with MWCNTs (Fig. 19). This further confirmed that the addition of MWCNTs suppressed the amount of α phase present in the electrospun PVDF nanofibers, enhancing the β phase, in accordance with the XRD results. Also, we confirm that over-addition of MWCNTs cancels the enhancement effect.

In addition, we can still determine the relative fraction of β phase present in each sample from the FTIR spectra. Using the characteristic absorption bands of α and β phases at 762 cm^{-1} and 846 cm^{-1}, respectively, and assuming these absorption bands follow Beer-Lambert Law with absorption coefficients of $K_\alpha = 6.1 \times 10^4$ and $K_\beta = 7.7 \times 10^4$ cm^2/mol, the fraction of β phase can be calculated using the following equation[28]:

$$F(\beta) = {X_\beta}/{X_\alpha + X_\beta} = {A_\beta}/{1.26A_\alpha + A_\beta}$$

Where X_α and X_β are the crystalline mass fractions of the α and β phases and A_α and A_β correspond to absorption bands at 762 cm^{-1} and 846 cm^{-1}.

Table 5. β phase content of PVDF/MWCNTs fiber meshes with different concentration of MWCNTs

PVDF/wt%	MWCNTs/wt%	βphase/%
12	0	55
12	0.1	61
12	0.5	76
12	1	59
12	2	56

Comparing the results between FTIR and XRD, we can clearly confirm the percentages of β phase show the same trend for all samples, which for different MWCNTs content (Table 6). Meanwhile, the value obtained from FTIR is always higher than XRD.

In general, infrared spectrum peaks at 762 cm^{-1} and 846 cm^{-1} with high intensity were previously used to characterize the crystal phase in most of the published studies. However, in recent years, some researchers have shown that the peaks around 840 cm^{-1} are characteristic from both β and γ phases [29]. Thus, the β phase characterization from the wavenumber of 846 cm^{-1} includes both the β and γ phase, and this might be the reason why the FTIR results are always slightly higher than XRD. Since the γ phase also exhibits piezoelectric behavior, the FTIR characterization gives us the overall composition on piezoelectric phases. Anyway, no matter XRD or FTIR results, 0.5% of MWCNTs blended with PVDF nanofibers always exhibit the highest value of the β

phase percentage. These results will be confirmed by the output voltage characterization.

Table 6. β phase content of PVDF/MWCNTs fiber meshes

with different concentration of MWCNTs between FTIR and XRD difference

PVDF/wt%	MWCNTs/wt%	FTIR	XRD
12	0	55	55
12	0.1	61	57
12	0.5	76	69
12	1	59	49
12	2	56	48

3.2.2 Mechanical testing of PVDF nanofiber meshes

Fig. 20 shows the typical stress/strain curves of all PVDF nanofiber meshes. The Young ś moduli (the slope of the curves) of the all PVDF/MWCNTs nanofibers were much higher than that of the pure PVDF nanofibers, especially for the 0.5% and 1% PVDF/MWCNTs samples. A slight decline in mechanical properties for the 2% sample may have been due to its low crystallinity, as confirmed by the XRD results. Therefore, we have to point out that the mechanical properties of the 1% PVDF/MWCNTs nanofibers were the best of all the samples, but the most interesting conclusion is that by changing the MWCNTs content in the fibers, it is possible to modulate the mechanical properties in order to prepare scaffolds with different characteristics for specific applications.

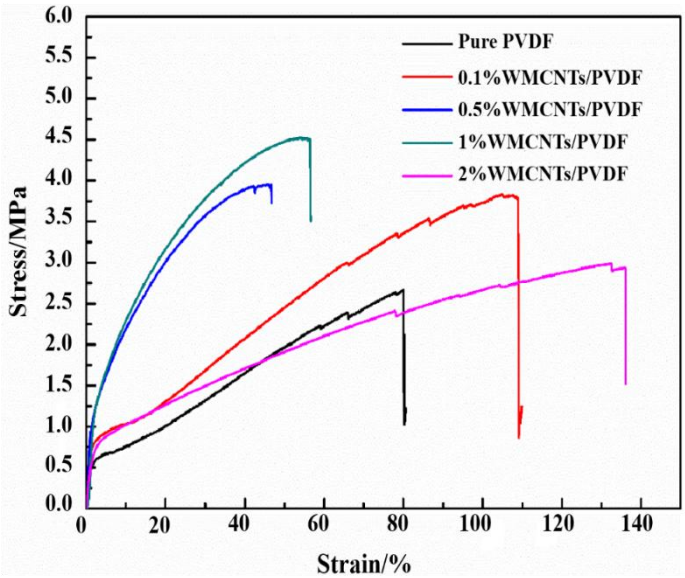

Fig. 20. The stress/strain curves of PVDF/MWCNTs nanofiber meshes for different concentrations of MWCNTs.

3.2.3 Output voltage

Output voltage of pure nanofiber meshes

The measured output voltage corresponded to the three stages of the illustration in Fig. 21, the initial state, the bending state, and the release state. A pulse voltage signal accompanied by an opposite pulse output voltage was recorded when the nanofiber meshes was subjected to a bending and release strain. Under continual bending and unbending cycles, the pure PVDF nanofiber meshes repeatedly generated, an open-circuit voltage of 0.2V (Fig. 22). The phenomenon can be explained as follows: the mechanical strain produced during the bending state can induce piezoelectric charges, which results in the potential difference across the two sides of the nanofiber meshes. In response, external free electrons are driven to the nanofibers to balance this potential created by the dipoles. As the external pressure on the nanofiber meshes was removed by the unbending motion, the piezoelectric potential between the two sides of the device

disappeared, and the free electrons that have accumulated at both sides of meshes generate an opposing potential.

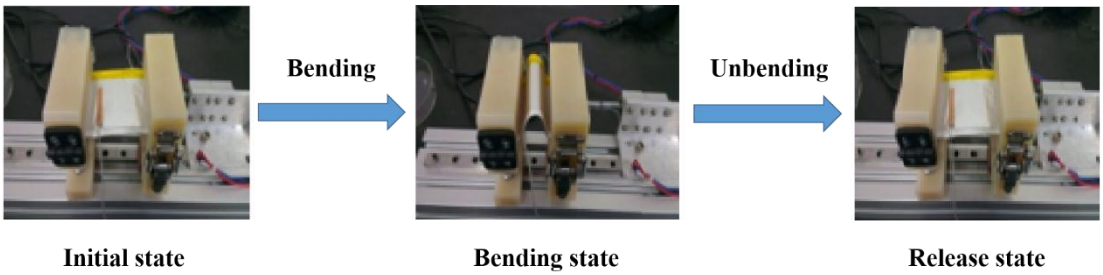

Fig. 21. Schematic of the output voltage testing process.

In addition, the output voltage rose sharply in the samples of PVDF/MWCNTs nanofibers with MWCNTs weight ratios of 0.1% and 0.5%. The output voltage of 0.1% PVDF/MWCNTs nanofibers is about 1.7V, and the peak voltage reached about 2V for 0.5%PVDF/MWCNTs nanofibers. Interestingly, a higher MWCNTs concentration than 0.5% (1% and 2%) led to decrease in the piezoelectric voltage (Fig. 22).

We noticed a nonlinear dependence of the output voltage on the proportion of the β phase in the electrospun PVDF/MWCNTs nanofiber meshes. That is, while the β phase content of the 0.1%MWCNTs and 0.5%MWCNTs were slightly increased, the output voltages were raised to a much greater extent (Fig. 22). Therefore, we believe that the change in surface and volume conductivity of PVDF/MWCNTs nanofiber meshes played an important role in the output voltage.

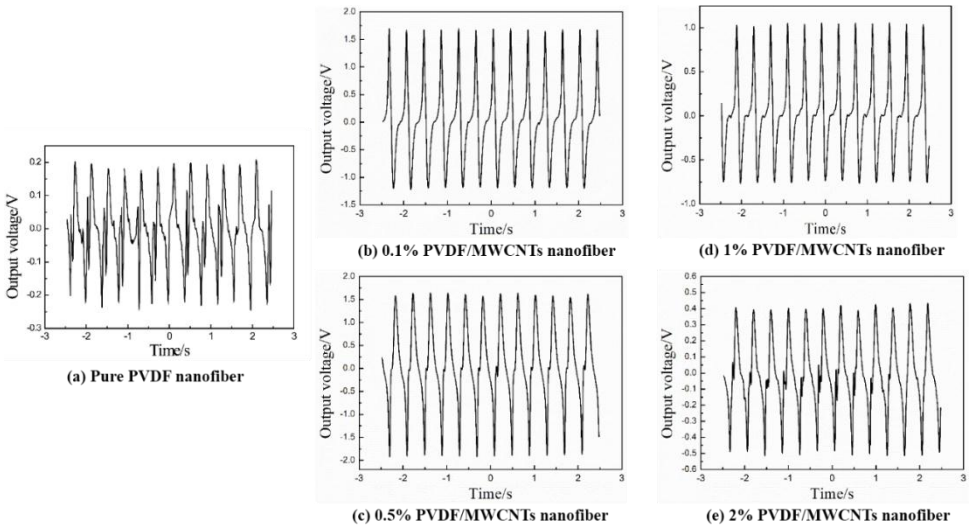

Fig. 22. The measured output voltage for different concentrations of PVDF/MWCNTs nanofibers.

Output voltage of nanofibers assembled on interdigitated electrodes

The measurement of the output voltage of nanofibers assembled on interdigitated electrodes undergoing the mechanical stimulation are shown in Figure 23. The pulse voltage signal was recorded when the nanofibers on electrodes were subjected to a vibration from the sound vibrator equipment. Under the continual mechanical stimulation, the different electrode assembled nanofibers, repeatedly generated different results.

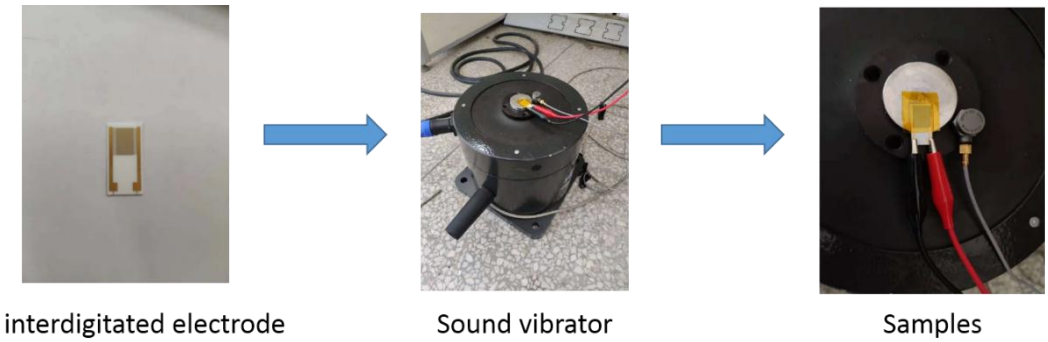

Fig. 23 Schematic of output voltage of nanofibers based on electrode testing processing

In Fig. 24, the highest output voltage among all samples is PVDF/MWCNTs nanofibers with MWCNTs weight ratios of 0.5%, which is 0.15 V, it is also the sample with the highest signal-to-noise ratio. Compared with all of PVDF/MWCNTs nanofibers, the pure PVDF nanofiber samples still exhibit the lowest output voltage. It means the MWCNTs blended with PVDF nanofibers also shown strong piezoelectric effect based on our interdigitated electrode. Comparing all the PVDF nanofibers with MWCNTs, it is clear that 1% and 2% PVDF/MWCNTs nanofibers exhibit similar output voltage around 0.08V. The 0.1% PVDF/MWCNTs nanofibers present the lowest output voltage among all the PVDF/MWCNTs fiber samples, which is 0.04V.

The output voltage from the different samples shows a similar trend of the piezoelectric effect, between the bending of sandwiched nanofiber meshes and vibration test of the interdigitated electrode-assembled nanofibers. Thus, we can clearly confirm, the piezoelectric effect of our nanofibers meshes based on interdigitated electrode is strong enough and we can assume that the inverse piezoelectric effect should also be strong enough for our objectives. Thus, this device is suitable to undergo the experiments of testing the inverse piezoelectric stimulation in cells culture.

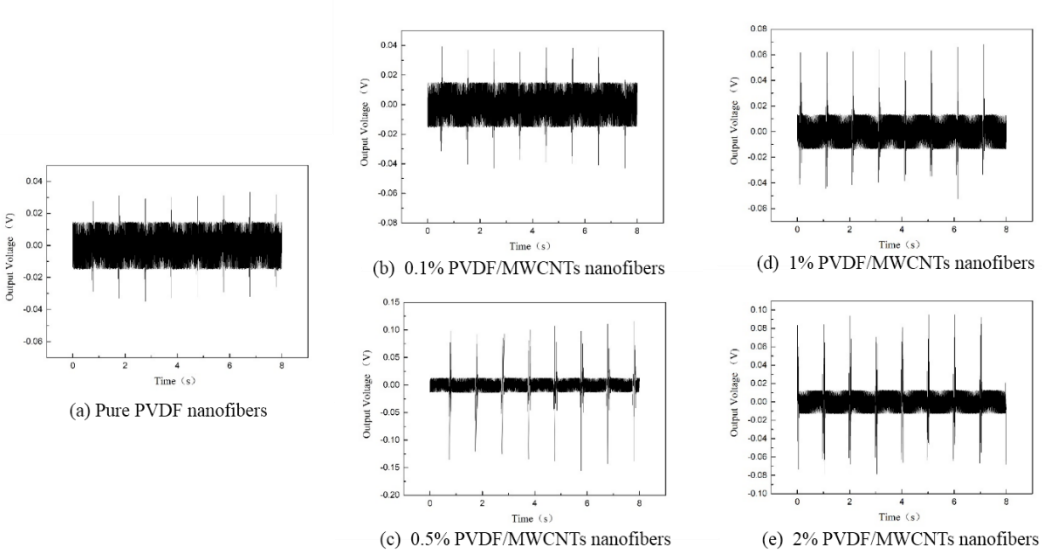

Fig. 24. The measured output voltage for different concentrations of PVDF/MWCNTs nanofibers based on interdigitated electrode.

3.3 In vitro cytocompatibility

To test the cytocompatibility of the PVDF and PVDF/MWCNTs nanofiber meshes, 3-(4,5-dimethylthiazol-2-yl)-2,5-diphenyltetrazolium bromide (MTT) assay of cell viability has been proven to be a popular method. Although MTT assay has been extensively used to evaluate the metabolic activity of live cells, some researchers have shown that MTT formazan can be physically adsorbed onto electrospun nanofibrous mats with a high specific surface area to volume ratio, leading to a false negative result of the cell viability assay[29]

Resazurin microtiter assay (REMA, also named Alamar Blue assay) has also been widely used for determining the cytocompatibility of biomaterials. In this method, the added resazurin can be reduced by the intracellular enzymes of live cells to form a water-soluble pink fluorescent compound, resorufin, whose fluorescence emission can be quantitatively monitored to directly reflect the cell viability. Compared with the MTT colorimetric method, the resazurin assay shows distinctive merits since it does not use harmful solvents and does not require the cells to be killed before analysis. Thus, in our case, the cytocompatibility of nanofibers was studied by REMA and MTT assays.

The results of cell viability from both MTT and REMA show us the same trend for all samples. However, the comparison of cell viability between different fiber composition was complex and interesting.

First of all, as shown in Figure 21, the cell viability has no clear distinction between PCL and pure PVDF nanofibers for which the percentage of live cells is a little bit lower than for TCP and don’t differ significantly from the control TCP. This demonstrated that all of these electrospun nanofibers are biocompatible.

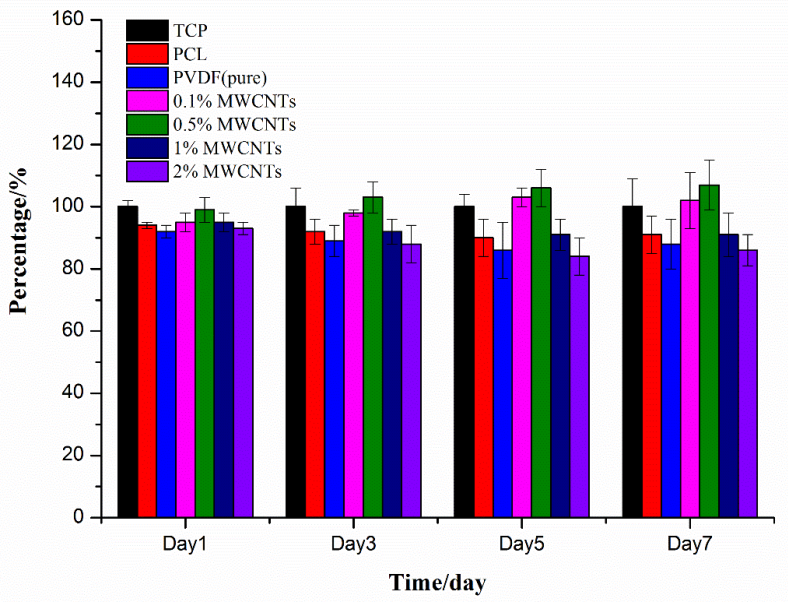

Fig. 25. MTT results of L929 cells cultivated on nanofiber meshes for 1, 3, 5 and 7days

The results from different PVDF/MWCNTs/ MWCNTs fibers show us two different trend (figure 25 and 26). The cell viability of cells cultured on the sample of 0.1% and 0.5% PVDF/MWCNTs fibers is higher than TCP. It means these two samples are not just biocompatible, they show an increase in the proliferation of L929 cells. Interestingly, cell viability of the other two samples (1% and 2% PVDF/MWCNTs) is lower than TCP which means that when the percentage of carbon nanotubes was increased beyond 1%, the cells proliferation on PVDF/MWCNTs hybrid nanofibers is lower than at the low concentrations of MWCNTs.

In order to evaluate the difference between the MTT and REMA assays, for the same samples, we picked up the 0.5%PVDF/MWCNTs nanofibers. Figure 27 shows that the viability of cells measured with REMA is higher than with the MTT assay, which is consistent with the possible adsorption of MTT formazan onto the electrospun nanofibers. Therefore, we believe REMA to be more accurate than MTT and chose REMA as the first method to analyze the cytocompatibility of our samples during subsequent experiments.

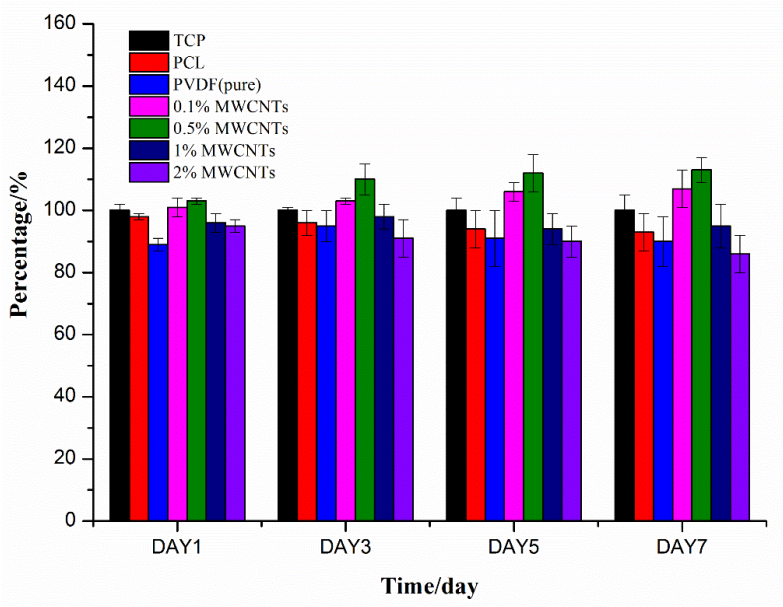

Fig. 26. REMA results of L929 cells cultivated on nanofiber meshes for 1, 3 , 5 and 7days

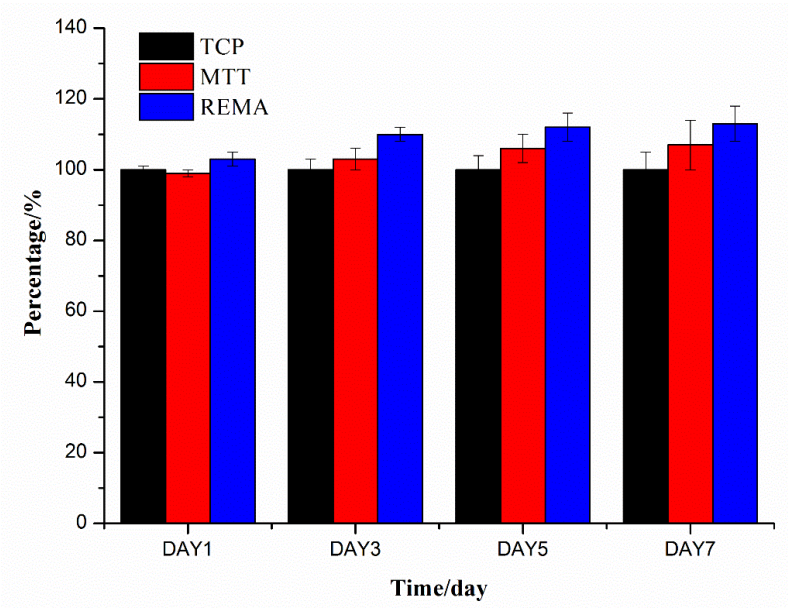

Fig. 27. The comparison of MTT and REMA of L929 cells cultivated on 0.5% PVDF/MWCNTs/ MWCNTs nanofiber meshes for 1, 3, 5 and 7days.

4 Conclusion

We have demonstrated that PVDF/MWCNTs piezoelectric nanofibers can be directly prepared via electrospinning, without any post-processing poling treatment. The effect of the addition of MWCNTs on the fiber diameter, mechanical properties, β phase composition, output voltage and cytotoxicity were investigated. With the increasing concentration of MWCNTs and high speed rotating drum collector system, the average fiber diameter and distribution of PVDF/MWCNTs nanofibers are decreased and improved. Appropriate amount of MWCNTs are helpful to the crystallization process and β phase formation which are confirmed by XRD and FTIR. The maximum output voltage exhibited by PVDF nanofibers in the presence of 0.5 wt% WMCNTs is as high as 2V, while the average diameter is 170.1±63.4 nm, compared with the pure PVDF nanofibers.

References

1. Xin, Y.; Zhu, J. F.; Sun, H. S.; Xu, Y.; Liu, T.; Qian, C. H., A brief review on piezoelectric PVDF nanofibers prepared by electrospinning. *Ferroelectrics* **2018,** *526* (1), 140-151.https://doi.org/10.1080/00150193.2018.1456304

2. Mokhtari, F.; Latifi, M.; Shamshirsaz, M., Electrospinning/electrospray of polyvinylidene fluoride (PVDF): piezoelectric nanofibers. *Journal of the Textile Institute* **2016,** *107* (8), 1037-1055.https://doi.org/10.1080/00405000.2015.1083300

3. Liu, X.; Kuang, X. L.; Xu, S. X.; Wang, X. H., High-sensitivity piezoresponse force microscopy studies of single polyvinylidene fluoride nanofibers. *Materials Letters* **2017,** *191*, 189-192.https://doi.org/10.1016/j.matlet.2016.12.066

4. Sengupta, D.; Kottapalli, A. G. P.; Chen, S. H.; Miao, J. M.; Kwok, C. Y.; Triantafyllou, M. S.; Warkiani, M. E.; Asadnia, M., Characterization of single polyvinylidene fluoride (PVDF) nanofiber for flow sensing applications. *Aip Advances* **2017,** *7* (10).https://doi.org/10.1063/1.4994968

5. Ali, F.; Raza, W.; Li, X. L.; Gul, H.; Kim, K. H., Piezoelectric energy harvesters for biomedical applications. *Nano Energy* **2019,** *57*, 879-902.https://doi.org/10.1016/j.nanoen.2019.01.012

6. Tandon, B.; Blaker, J. J.; Cartmell, S. H., Piezoelectric materials as stimulatory biomedical materials and scaffolds for bone repair. *Acta Biomaterialia* **2018,** *73*, 1-20.https://doi.org/10.1016/j.actbio.2018.04.026

7. Haider, A.; Haider, S.; Kang, I. K., A comprehensive review summarizing the effect of electrospinning parameters and potential applications of nanofibers in biomedical and biotechnology. *Arabian Journal of Chemistry* **2018,** *11* (8), 1165-1188.https://doi.org/10.1016/j.arabjc.2015.11.015

8. Ayres, C.; Bowlin, G. L.; Henderson, S. C.; Taylor, L.; Shultz, J.; Alexander, J.; Telemeco, T. A.; Simpson, D. G., Modulation of anisotropy in electrospun tissue-engineering scaffolds: Analysis of fiber alignment by the fast Fourier transform. *Biomaterials* **2006,** *27* (32), 5524-5534.https://doi.org/10.1016/j.biomaterials.2006.06.014

9. Kim, Y. W.; Lee, D. K.; Lee, K. J.; Kim, J. H., Single-step synthesis of proton conducting poly(vinylidene fluoride) (PVDF) graft copolymer electrolytes. *European Polymer Journal* **2008,** *44* (3), 932-939.https://doi.org/10.1016/j.eurpolymj.2007.12.020

10. Lin, D. J.; Chang, C. L.; Lee, C. K.; Cheng, L. P., Preparation and characterization of microporous PVDF/PMMA composite membranes by phase inversion in water/DMSO solutions. *European Polymer Journal* **2006,** *42* (10), 2407-2418.https://doi.org/10.1016/j.eurpolymj.2006.05.008

11. Cheng, L. P., Effect of temperature on the formation of microporous PVDF membranes by precipitation from 1-octanol/DMF/PVDF and water/DMF/PVDF systems. *Macromolecules* **1999,** *32* (20), 6668-6674.https://doi.org/10.1021/ma990418l

12. Yee, W. A.; Kotaki, M.; Liu, Y.; Lu, X. H., Morphology, polymorphism behavior and molecular orientation of electrospun poly(vinylidene fluoride) fibers. *Polymer* **2007,** *48* (2), 512-521.https://doi.org/10.1016/j.polymer.2006.11.036

13. Kong, C. S.; Yoo, W. S.; Jo, N. G.; Kim, H. S., Electrospinning Mechanism for Producing Nanoscale Polymer Fibers. *Journal of Macromolecular Science Part B-Physics* **2010,** *49* (1), 122-131.https://doi.org/10.1080/00222340903344390

14. Li, D.; Xia, Y. N., Electrospinning of nanofibers: Reinventing the wheel? *Advanced Materials* **2004,** *16* (14), 1151-1170.https://doi.org/10.1002/adma.200400719

15. Mohammadi, B.; Yousefi, A. A.; Bellah, S. M., Effect of tensile strain rate and elongation on crystalline structure and piezoelectric properties of PVDF thin films. *Polymer Testing* **2007,** *26* (1), 42-50.https://doi.org/10.1016/j.polymertesting.2006.08.003

16. Lovinger, A. J., FERROELECTRIC POLYMERS. *Science* **1983,** *220* (4602), 1115-1121.https://doi.org/10.1126/science.220.4602.1115

17. Davis, G. T.; McKinney, J. E.; Broadhurst, M. G.; Roth, S. C., ELECTRIC-FIELD-INDUCED PHASE-CHANGES IN POLY(VINYLIDENE FLUORIDE). *Journal of Applied Physics* **1978,** *49* (10), 4998-5002.https://doi.org/10.1063/1.324446

18. Briber, R. M.; Khoury, F., THE MORPHOLOGY OF POLY(VINYLIDENE FLUORIDE) CRYSTALLIZED FROM BLENDS OF POLY(VINYLIDENE FLUORIDE) AND POLY(ETHYL ACRYLATE). *Journal of Polymer Science Part B-Polymer Physics* **1993,** *31* (10), 1253-1272.https://doi.org/10.1002/polb.1993.090311001

19. Cauda, V.; Stassi, S.; Bejtka, K.; Canayese, G., Nanoconfinement: an Effective Way to Enhance PVDF Piezoelectric Properties. *Acs Applied Materials & Interfaces* **2013,** *5* (13), 6430-6437.https://doi.org/10.1021/am4016878

20. Li, L.; Zhang, M. Q.; Rong, M. Z.; Ruan, W. H., Studies on the transformation process of PVDF from alpha to beta phase by stretching. *Rsc Advances* **2014,** *4* (8), 3938-3943.https://doi.org/10.1039/c3ra45134h

21. Ahn, Y.; Lim, J. Y.; Hong, S. M.; Lee, J.; Ha, J.; Choi, H. J.; Seo, Y., Enhanced Piezoelectric Properties of Electrospun Poly(vinylidene fluoride)/Multiwalled Carbon Nanotube Composites Due to High beta-Phase Formation in Poly(vinylidene fluoride). *Journal of Physical Chemistry C* **2013,** *117* (22), 11791-11799.https://doi.org/10.1021/jp4011026

22. Huang, S.; Yee, W. A.; Tjiu, W. C.; Liu, Y.; Kotaki, M.; Boey, Y. C. F.; Ma, J.; Liu, T. X.; Lu, X. H., Electrospinning of Polyvinylidene Difluoride with Carbon Nanotubes: Synergistic Effects of Extensional Force and Interfacial Interaction on Crystalline Structures. *Langmuir* **2008,** *24* (23), 13621-13626.https://doi.org/10.1021/la8024183

23. Erdtman, E.; Satyanarayana, K. C.; Bolton, K., Simulation of alpha- and beta-PVDF melting mechanisms. *Polymer* **2012,** *53* (14), 2919-2926.https://doi.org/10.1016/j.polymer.2012.04.045

24. Zhang, H. P.; Zhang, P.; Li, Z. H.; Sun, M.; Wu, Y. P.; Wu, H. Q., A novel sandwiched membrane as polymer electrolyte for lithium ion battery. *Electrochemistry Communications* **2007,** *9* (7), 1700-1703.https://doi.org/10.1016/j.elecom.2007.03.021

25. Nallasamy, P.; Mohan, S., Vibrational spectroscopic characterization of form II poly(vinylidene fluoride). *Indian Journal of Pure & Applied Physics* **2005,** *43* (11), 821-827

26. Andrew, J. S.; Clarke, D. R., Effect of electrospinning on the ferroelectric phase content of polyvinylidene difluoride fibers. *Langmuir* **2008,** *24* (3), 670-672.https://doi.org/10.1021/la7035407

27. Lanceros-Mendez, S.; Mano, J. F.; Costa, A. M.; Schmidt, V. H., FTIR and DSC studies of mechanically deformed beta-PVDF films. *Journal of Macromolecular Science-Physics* **2001,** *B40* (3-4), 517-527.https://doi.org/10.1081/mb-100106174

28. Gregorio, R.; Cestari, M., EFFECT OF CRYSTALLIZATION TEMPERATURE ON THE CRYSTALLINE PHASE CONTENT AND MORPHOLOGY OF POLY(VINYLIDENE FLUORIDE). *Journal of Polymer Science Part B-Polymer Physics* **1994,** *32* (5), 859-870

29. Zheng, F. Y.; Wang, S. G.; Hou, W. X.; Xiao, Y. C.; Liu, P. C.; Shi, X. Y.; Shen, M. W., Comparative study of resazurin reduction and MTT assays for cytocompatibility evaluation of

nanofibrous materials. *Analytical Methods* **2019,** *11* (4), 483-489.https://doi.org/10.1039/c8ay02310g

Chapter 3

1 Effect of inverse piezoelectric stimulation on the behavior of fibroblasts

1.1 Introduction

Electrical stimulation is known to influence cell behavior such as proliferation, differentiation and regeneration. Furthermore a number of previous studies have shown that piezoelectric materials generate electrically charged surfaces[1-3]. Electrospinning has been recently introduced as the most promising technique to manufacture scaffolds for tissue engineering applications, including materials that exhibit piezoelectric properties. These scaffolds should partially mimic the structure and function of natural extracellular matrices (ECM), thereby enhancing cell adhesion via (1) the interconnectivity of voids favorable for cell in-growth and (2) the high surface area to volume ratio, which enlarges cell-scaffold interface. Thus far, a number of natural and synthetic polymers have been electrospun into bioactive scaffolds for different applications[4].

A recent study has reported the preparation and in vitro cytocompatibility of PVDF electrospun scaffolds and argued that there is tremendous potential of the scaffolds for tissue engineering applications. Guo *et al.* have investigated the electrospun PVDF/PU membrane as a scaffold for wound healing applications[1]. In another work, Wang *et al.* have reported the piezoelectric nanofibrous scaffold as *in vivo* energy harvesters and for modifying fibroblast alignment and proliferation in wound healing[2].

However, the mechanism through which inverse piezoelectricity influences cell behavior is unclear. Thus, in this part, we aim to investigate how piezoelectric and non-piezoelectric materials affect the cells' morphology, proliferation and migration.

1.2 Materials and methods

1.2.1 Materials

Interdigitate electrode was purchased from Suzhou Zhongtong Sensor Technology Co., Ltd.

Cell counting Kit-8 (CCK8), Alamar blue Cell viability Kit and CytoSelect™ 24-Well Wound Healing Assay kit were bought from Shanghai Yuchun Biological Technology Co., Ltd.

4',6-diamidino-2-phenylindole (DAPI), Triton X-100, Phalloidin and Bovine Serum Albumin (BSA) were obtained from Sigma Aldrich. NIH3T3 cells offer from Shanghai Institute of Biology, Chinese Academy of Sciences.

1.2.2 Methods

Cell culture

Device preparation and sterilization

The size of the interdigitated electrode is 4 cm x 4 cm and the thickness of the Au electrodes is 200 nm, and the gap between the two parallel electrode is 0.1 mm. Each sample of electrospun nanofibers of was cut into 4 cm x 4 cm, and fixed on the interdigitated electrode with medical glue on the edge of electrode plate. After the nanofibers mesh fixation, a 3D printed polylactic acid (PLA) hollow cylinder with an inside diameter of 16 mm, a geometry similar to standard 24 well plates (well diameter of 15.6 mm) was fixed on the surface of the fibers with medical glue. The whole assembly allows the insertion of a liquid medium inside the cylinder and therefore is suitable for cells incubation. The schematic diagram of the device is shown in Fig. 28.

After the preparation of the cell culture device, the lead wires from the electrodes were connected to a signal generator and the fibers were submitted to an electric driving signal of 10 V, 5 Hz square wave with 50% duty cycle. Just for comparison, the 10 V amplitude driving signal, across the 0.1 mm electrode gap, corresponds to an electric field intensity of 100 kV/m, which is the same order of magnitude of the electrospinning electrostatic field (67 to 133 kV/m). This electric field is in the range typically used to drive PVDF membranes and should be strong enough to drive the inverse piezoelectric effect on our device.

The whole inverse piezoelectric stimulation device (IPSD) was sterilized under the UV light overnight, then soaked in the 75% ethanol for 4 hours and washed 3 times with PBS. Before cell culture, the device was further soaked in the cell culture medium overnight in the incubator.

The other electrospun nanofibers meshes were cut into a round piece with a diameter of 15 mm, which were then fixed at the bottom of each well, in the 24 well plates with stainless steel rings. The well plates with fibers were sterilized with ethanol for 1 hour, then rinsed 3 times with PBS for 15 minutes. Before the cell culture, the well plates with nanofibers were soaked in the cell culture medium overnight in the incubator.

The interdigitated electrode with PVDF/MWCNTs nanofibers were fixed on the bottom of the cell culture petri dishes. After the nanofiber meshes fixation, then the hollow cylinders with the inside diameter of 16 mm similar to 24 well plates (diameter=15.6 mm) printed by 3D printer were fixed on the surface of fibers by medical glue. The whole device was sterilized under the UV light overnight, and then soaked in the 75% ethanol for 4 hours and washed with 3 times PBS. Before cell culture, the device was further soaked in the cell culture medium overnight in the incubator.

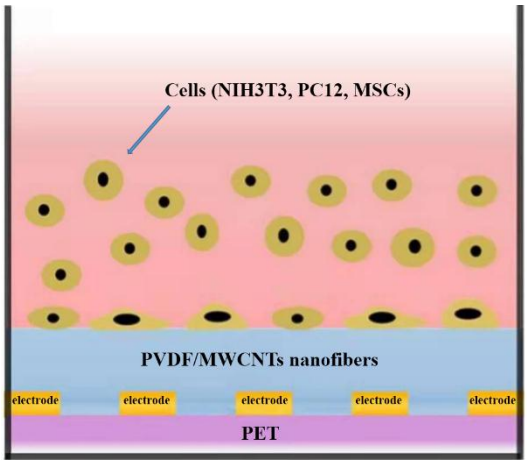

Fig. 28. Schematic diagram of cell culture device

The other electrospun nanofibers meshes were cut into a round piece with a diameter of 15 mm, which were then fixed at the bottom of each well, in the 24 well plates with stainless steel rings. The well plates with fibers were sterilized with ethanol for 1 hour, then rinsed 3 times with PBS for 15 mintues. Before the cell culture, the well plates with nanofibers were soaked in the cell culture medium overnight in the incubator.

Cell culture and inverse piezoelectric stimulation

NIH3T3 cells were selected for fibroblasts modeling, the initial cells seeded in the IPSD and electrospun fiber filled well plates prepared earlier. The cells were cultured in Dulbecco's Modified Eagle's Medium (DMEM) supplemented with 10% fetal bovine calf serum (FBS) and 1% penicillin-streptomycin (PS) in a humidified atmosphere with 5% CO_2 in air at 37 ℃. The culture medium was refreshed every 2 days.

After the cells were seeded in the IPS, the electric signal generator was connected to the interdigitated electrode as shown in Fig. 29. The inverse piezoelectric stimulation was applied 24 hours after seeding, and the cells were stimulated for 30mins with 5Hz square wave frequency and 10V per day. All of the samples without the IPS treatment served as control groups.

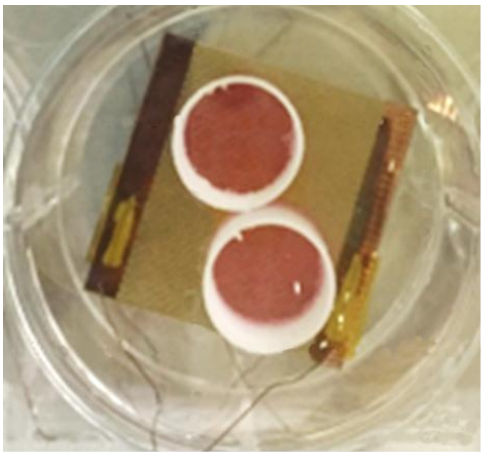

Fig.29 Cells culture device with hollow cylinders on the nanofiber meshes and interdigitated electrode.

Cell morphology and proliferation （SEM LCSM CCK8）

To verify the cell morphologies of the cells cultured on the nanofiber scaffolds, both the stimulated and non-stimulated experiments, we used SEM and LCSM. Briefly, 2×10^4 cells were seed on the nanofibers in the IPSD and 24 well plates.

SEM,

Cell morphology on the all fibers was examined from samples taken after 1, 3, 5 days post-seeding. The cells cultured on the nanofibers were fixed by 4% paraformaldehyde for 30 minutes, then dehydrated with increasing concentration of ethanol and followed by drying at room temperature overnight. Before the SEM observation,nanofibers were sputter-coated with gold and viewed using an accelerating voltage of 15 kV and a working distance of 18–20 mm.

LSCM

For the LSCM observation, samples were taken with the same periodicity as for SEM (1, 3, 5 days post-seeding). The cells were fixed with 100 μL of 4% paraformaldehyde for 15 mins, followed by rinse with PBS. Then, the cells on the nanofiber meshes were

soaked and permeabilized with PBS solution containing 0.1% Triton X-100 for 15 min at room temperature. Secondly, the cytoskeleton was stained with phalloidin. The phalloidin working solution was prepared in PBS containing 3% BSA. During the staining process the samples were kept in a dark environment at room temperature for 30 min. After rinsing with PBS, the cells nuclei were stained with DAPI for 10 min, followed by rinsing with PBS. The stained cells were saved in dark environment at 4 ℃ for further fluorescence microscopy investigation.

Cell proliferation

The proliferation of the cultured NIH3T3 cells was measured using the cell count alamar blue. Briefly, 2×10^4 cells were seed on the nanofibers in 24-well culture plates and IPSD. After 1, 3, 5 days post-seeding, the culture medium was replaced with 1 mL DMEM medium including 10% alamar blue. After 3 hours incubation at 37 ℃, the alamar blue solution was removed to 96well plates and the fluorescence at 560nm/590nm was read. Cells seeded directly on the bottom of the 24-well culture plates were used as controls.

Cell migration

To investigate the migration of NIH3T3 cells based on all nanofiber samples we used the *in vitro* cell migration assay, the Cytoselect^{TM} 24 well wound healing assay kit. Before the cell culture, a stainless steel ring with a bridge (1mm) in the middle was fixed on the top of nanofiber meshes. Briefly, $5\ x10^4$ cells were seeded onto the surfaces of each fiber sample. After 1 day incubation, the stainless steel rings were removed to generate a consistent 1mm gap in the middle of the fiber mesh surface. NIH3T3 cells were allowed to migrate into the gap on various nanofiber meshes for 1 and 2 days respectively. After fixation, cells were stained with methylene blue and microscopy images of the gap were taken to analyze the migration distance of NIH3T3 cells. At least 5 representative points along the gap of each sample were used for evaluating the migration rate from the three samples for each time point.

Statistical analysis

Each experiment was repeated at least 3 times on different days and data were expressed as the mean ±SD. All the proliferation and cell migration measurements were collected in triplicate for each group. Statistical analysis was carried out by the one-way analysis of variance (one-way ANOVA) using Origin software. The statistical difference between two sets of data was considered when $p < 0.05$and $p < 0.01$.

1.3 Results and discussion

1.3.1 Cell proliferation

Carbon nanotubes are novel materials that have unique properties and potential to be developed into useful products. In the past decade, various studies have been conducted on the application of CNTs in the biomedical field[5]. However, the interaction between the CNTs and the biological environment is very complex and unpredictable. Numerous studies have found that CNTs can show different levels of toxicity depending on their manufacturing method, surface-to-volume ratio, shape, concentration etc.[6] For instance, they reported cell viability and adhesion was improved on multi-wall carbon nanotube films7-9. Other studies report that CNTs could reduce the cell viability[10, 11]. Thus, the cell viability and proliferation of NIH3T3 based on different nanofibers with and without MWCNTs need to be evaluated.

The proliferation of NIH3T3 based on samples without inverse piezoelectric stimulation.

The Figure 30 LSCM and Figure 31 proliferation results clearly shown that the cell numbers of day 1 has no apparent difference between all the samples. On day 3, it was found that the proliferation of NIH3T3 cells on the well plates was little higher than the random PCL and PVDF nanofibers. The numbers of cells based on PCL and PVDF was slightly different. Interestingly, the cell numbers on both random and aligned

PVDF/MWCNTs is similar with TCPs. The number of cells on the electrode is the lowest value. As compared to day 3, the proliferation rate of the cells on the PVDF/MWCNTs after 5 days were the highest in all samples. This means 0.5% MWCNTs blended with PVDF fibers increase the proliferation of NIH3T3 cells However, the proliferation rate of cells based on the random and aligned PVDF/MWCNTs was similar since the day 1. It shows that the alignment of PVDF/MWCNTs does not affect the NIH3T3 cells proliferation. In comparison, between the number of cells on TCPs and random PVDF and PCL nanofibers, the results are similar to those at day3. Thus, it shown that the random PVDF and PCL electrospun nanofibers is biocompatible, but they do not really improve the cells proliferation. In this 5 days proliferation assay, the cells on the electrode are the lowest from day 3 and day 5. It means our interdigitate electrode material (Au and PET) is not a suitable material for cells culture. However, the proliferation rate of day 5 is still around of 80% of TCPs. Thus it means the naked interdigitate is not toxic and could be used in cells culture for a negative control group.

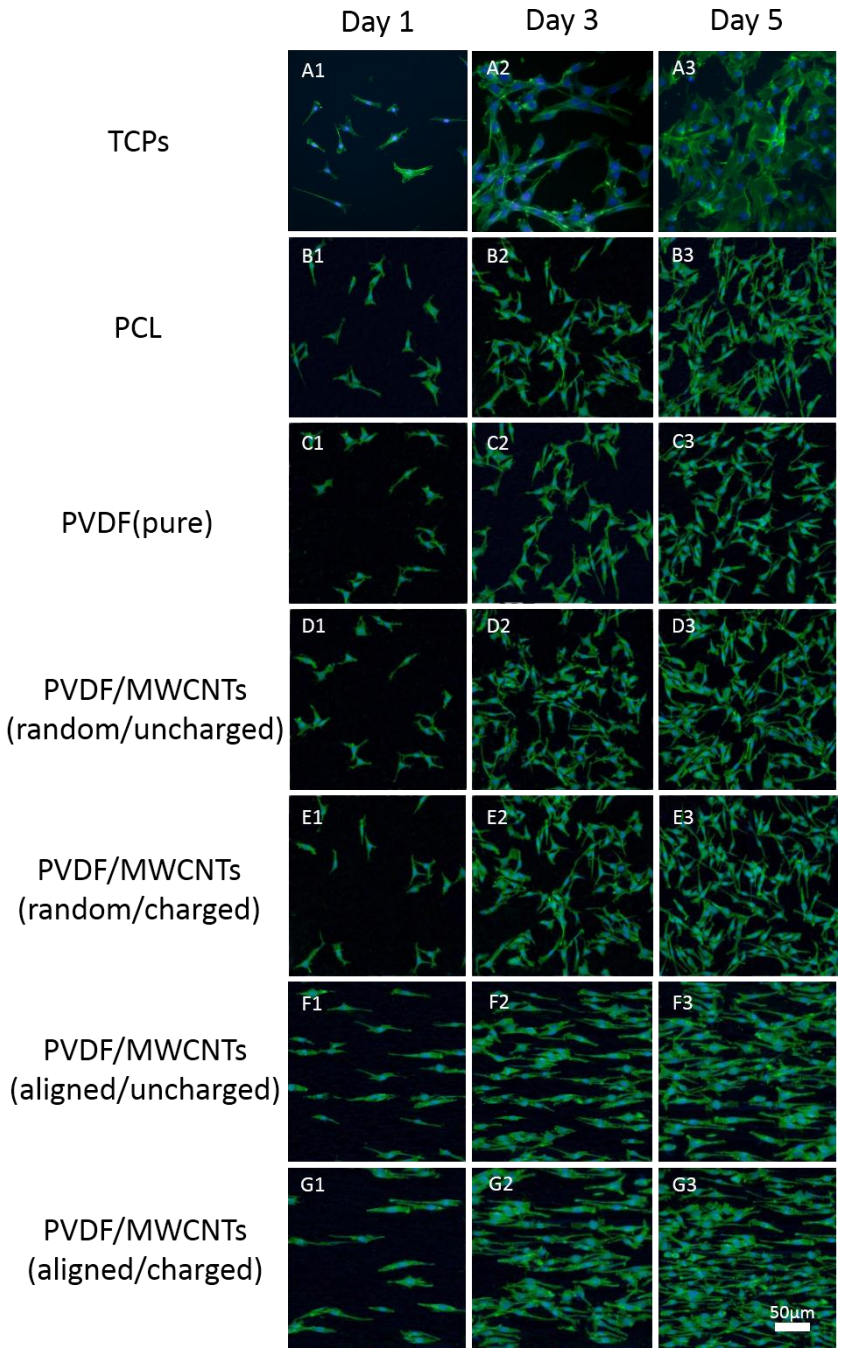

Fig. 30 The confocal images of NIH3T3 cells on different samples after 1 day, 3 days and 5 days of growth. Sample A123 are cells on cover slips, sample B123 are cells on the PCL nanofibers, sample C123 are cells on pure PVDF nanofibers, sample DEFG are cells on the PVDF/MWCNTs aligned and random nanofibers with and without stimulated.

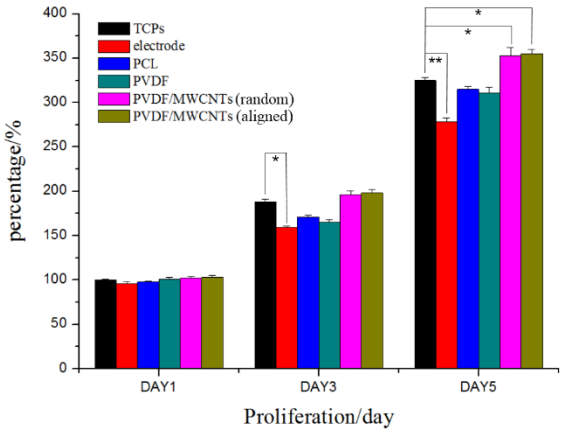

Fig. 31 The proliferation of NIH3T3 cells based on all samples without IPS at 1, 3, 5 days including TCPs, interdigital electrode, PCL, PVDF, PVDF/MWCNTs (random), PVDF/MWCNTs (aligned).

The proliferation of NIH3T3 based on samples with inverse piezoelectric stimulation.

It is well known that bioelectric signals can be observed *in vitro* and *in vivo*, for example, in epithelial wound sites or the surface of tumor cells[12]. Also, bioelectric fields play an important role in biological morphogenesis and growth. Furthermore, endogenous and exogenous electric fields also participate in the process of wound healing, tissue regeneration and so on[13]. Thus, in past decades, effort has been put on understanding the effect of various applications, based on electric stimulation, on cells behavior. In the 1960s, it has been shown that treating with DC current a skin defect in rabbit ears, increased the wound healing efficiency[14]. Since then, the potential of electrical charges to stimulate cell proliferation have been reported. Such as, Chao *et al* reported the effect of applied DC electric field on ligament fibroblast migration and wound healing[15]. Recently, studies have demonstrated that piezoelectric materials can be applied to produce surface charge and stimulate a variety of cell functions[16]. However, all of the research on piezoelectric stimulation of cells behavior make use of the direct piezoelectric effect. For example, Guo *et al* reported that PU/PVDF

electrospun scaffolds improved the proliferation of fibroblasts[1]. In our device, it is possible to investigate the effect of inverse piezoelectric effect on the fibroblasts. Especially, the capacity of improved PVDF/MWCNTs aligned nanofibers to adjust the proliferation of fibroblasts.

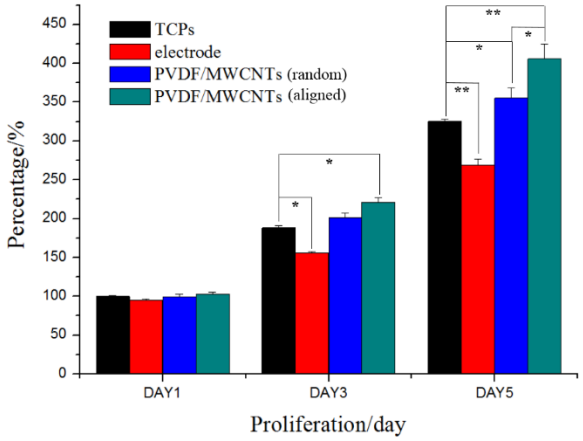

Fig. 32 The proliferation of NIH3T3 cells cultured on the nanofiber scaffolds and submitted to piezoelectric stimulation, at 1, 3, 5 days. Experiments were performed on bare electrode, PVDF/MWCNTs (random), PVDF/MWCNTs (aligned).

According to the results of the proliferation assay, the LSCM images (Fig. 30) clearly show the number of cells based on the stimulated aligned PVDF/MWCNTs nanofibers is higher than any other samples since day 3 and day 5, especially in day 5. It shows that proliferation of NIH3T3 cells could be improved by inverse piezoelectric stimulation. However, the number of cells on random PVDF/MWCNTs fibers with stimulated was lower and quite similar to PVDF/MWCNTs without stimulated, although a bit higher than TCP. These interesting results indicates that random PVDF/MWCNTs may not be able to generate enough inverse piezoelectric effect to distinguish from non-stimulated samples.

On Fig. 33, at day 1 all samples show similar numbers of live cells. Increasing the cell culture time, the amount of cells based on stimulated scaffolds begins to increase.

Fig. 33 compares all samples tested, with and without stimulation, aligned and non-aligned. In comparison to the TCPs and PVDF/MWCNTs samples, the cells based on the bare electrode (with or without stimulation) always show the lowest cell viability and proliferation rate and without meaningful difference between stimulated and non-stimulated experiments. It means the weak electric field generated by the bare interdigitate electrodes in the liquid medium has no effect on the proliferation of NIH3T3 cells.

In conclusion, the results of the proliferation assay on the various samples, it is clear that the stimulation provided by the assembly of PVDF/MWCNTs aligned nanofibers on interdigitate electrodes can improve the proliferation of NIH3T3 cells and since the electric field is very weak, the improvement must come from the mechanical stimulation generated through the inverse piezoelectric effect. Meanwhile, the PCL and PVDF electrospun nanofibers also show good biocompatibility at the same level of TCP. Also, the alignment of the fibers doesn't seem to lead to an improvement over the random fibers. Comparing the different fiber composition is it clear that improved proliferation over the pure PVDF comes from two sources: the first is the addition of MWCNTs to PVDF; the second is from the inverse piezoelectric stimulation.

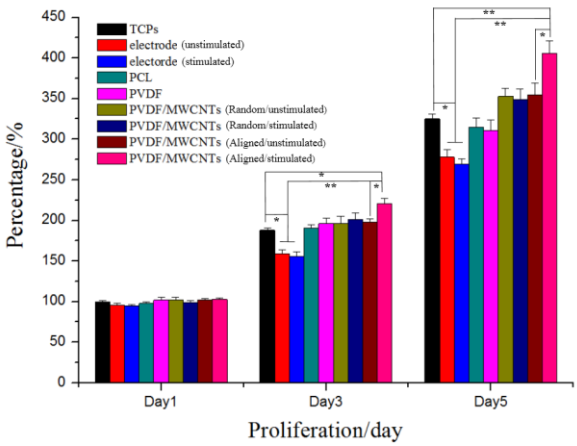

Fig. 33 The proliferation of NIH3T3 cells based on all samples at 1, 3, 5 days.

1.3.2 Cell morphology

Cellular colonization is a key issue in tissue engineering. To understand cell behavior, it is important to study the fibroblasts morphology when attached to different nanofiber scaffold topography. Thus, NIH3T3 cells morphology was studied by LSCM after 1, 3 and 5 days incubation, as depicted on Fig. 30, which shows the confocal images of NIH3T3 cells stained with cytoskeleton and nuclei.

From the observation of SEM images of Fig. 34, on the day 1, the cells just grow up on the surface of the nanofibers meshes on the all of samples. After day 5, many cells grow attached to the fiber's body, or bridged in the void space between the fibers and even in the three-dimensional structure between different nanofiber layers, which mimics the three-dimensional nature of the extra cellular matrix. Furthermore, the LSCM images from the cover slips shown the shape of NIH3T3 cells had a larger spreading area. Whereas the size of single cells grown on the simple two-dimensional surface is larger than the cells grown on the fibers, also cells growing on nanofibers would tend to spread along one fiber, forming a long axis and a narrow shape, or interact with more fibers and follow the three-dimensional structure, spreading in more directions.

Comparing the images on Fig. 30, between aligned and random fibers, the NIH3T3 cells stained cytoskeleton and nuclei show that the morphology on the different alignment of nanofibers at days 1, 3, 5 is also different. It is clearly illustrated that the cells grow along the aligned fibers and are elongated along the direction of the long axis. Furthermore, the size of NIH3T3 on the aligned fibers is smaller and the shape is narrower than the cells on the random fibers. Since the aligned nanofibers' topography is more densely packed, reducing the space between individual fibers, that small space allowed the cells to attach and spread. This topographic effect on the cells proliferation could play an important role in some tissue engineering applications, such as neural regeneration.

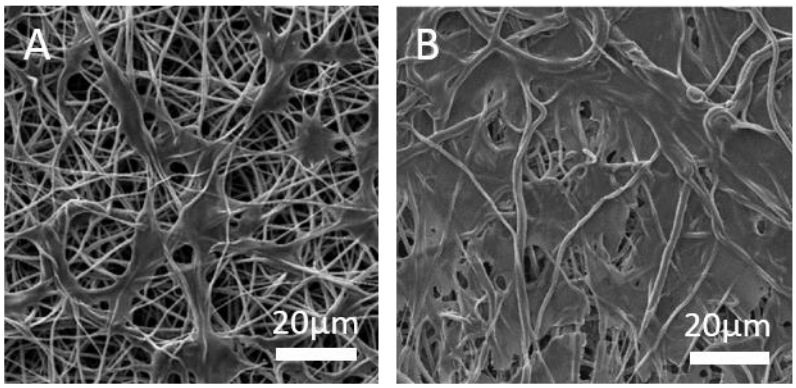

Fig. 34 The SEM images of NIH3T3 cells based on random PVDF/MWCNTs fibers. A is cell morphology based on the nanofibers on day 1, B is cell morphology on day 5.

1.3.3 Cell migration

Cell migration, which involves a multi-step cyclic process, is necessary for wound repair. The basic migration pattern requires: extension of a protrusion; stable attachment of the leading edge of the protrusion to a nearby point of the ECM; forward movement of the cell body; release of adhesions and retraction at the cell rear[17]. Fibroblasts are the most important cell line involved in producing the ECM, therefore, the migration of fibroblasts plays a key role in the formation of granulation tissue and further wound repairing[18]. Thus, effect of our inverse piezoelectric device on cells migration is important and meaningful for the potential application on wound healing.

In order to investigate the effect of fibers orientation and inverse piezoelectric stimulation on the NIH3T3 cells migration, an *in vitro* wound healing assay was performed by culturing the cells on the "wound gap" created by the steel rings. The culture stained with the methylene blue after 1 and 2 days shown that the migration of NIH3T3 cells was significantly regulated by the alignment fiber scaffold and the inverse piezoelectric stimulation. In the Fig. 35, it is clear that the wound gap distance

was smaller for aligned PVDF/MWCNTs nanofibers with inverse piezoelectric stimulation than for the other samples and it even closes completely after 2 days. The gap on the aligned PVDF/MWCNTs nanofibers without stimulation is also smaller than the TCPs and electrode on day 1 and day 2 but not as small as for the stimulated experiments. These results reveal that the migration of NIH3T3 cells can be improved not just by the scaffold's structure but also by the inverse piezoelectric stimulation.

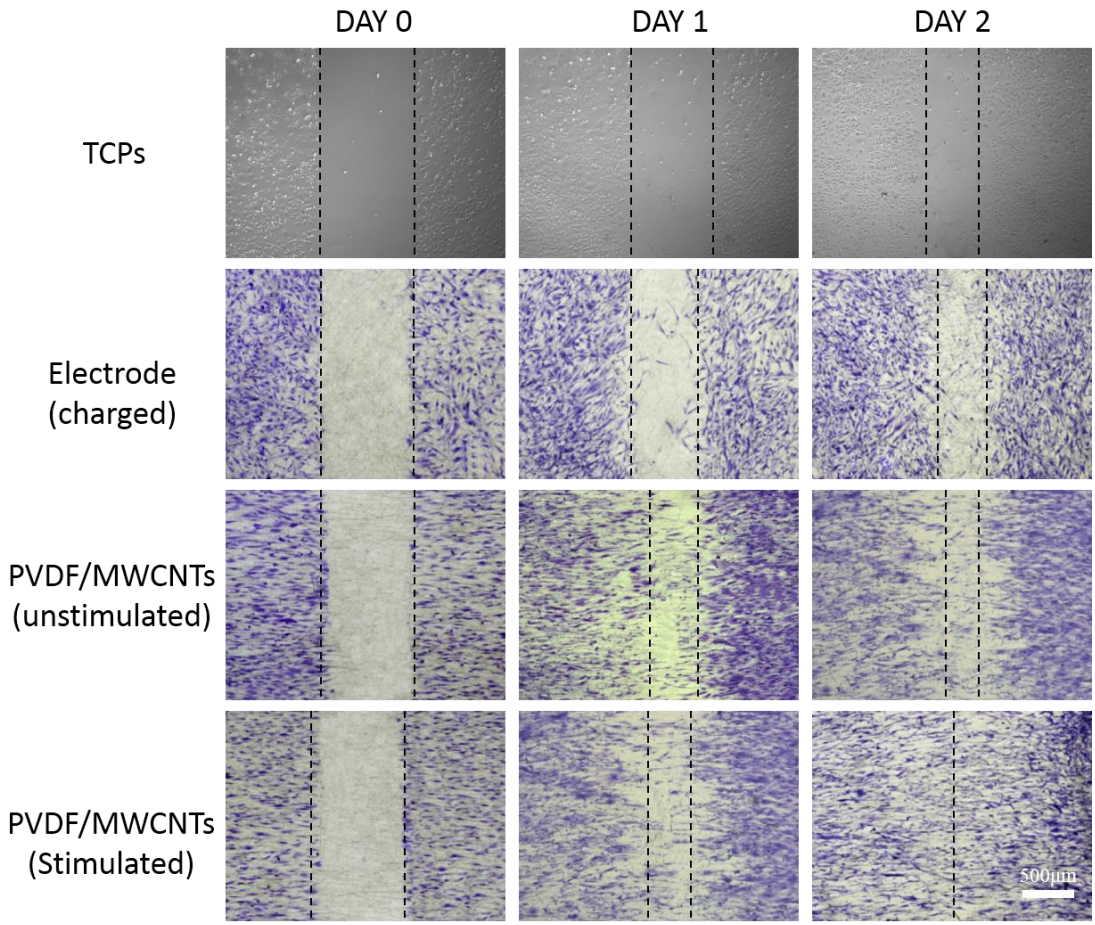

Fig.35 The migration of NIH3T3 cells based on different samples at day 0, day 1, day 2, including TCPs, Electrode (charged), aligned PVDF/MWCNTs stimulated and without stimulated.

1.4 Conclusion

In this part of the project,we made a systematic investigation of the fibroblasts cell viability, proliferation and migration on different electrospun nanofibers and also the cells' response to the inverse piezoelectric stimulation. From all of the nanofiber samples, the aligned PVDF/MWCNTs electrospun nanofibers assembled on the interdigitate electrodes with inverse piezoelectric stimulation, exhibited the highest bioactivity. With the inverse piezoelectric stimulation for 30 minutes per day, PVDF/MWCNTs not just improved the proliferation of NIH3T3 cells but also guided the cells migration more efficiently. This meaningful result reveals that the inverse piezoelectricity stimulation holds a great potential for applications on wound healing and other tissue engineering.

2 The effect of PVDF/MWCNTs inverse piezoelectric stimulation on nerve tissue engineering.

2.1 Introduction

Nowadays, an increasing number of people suffer with neurodegenerative diseases at worldwide level[19]. Thus, the tissue engineering for neural regeneration received a lot of attention from researchers. Replenishing neurons seems to be the ultimate therapy to cure these diseases[20]. Experiments with electrical stimulation have revealed that it can enhance proliferation and also the differentiation of various cell types, including cardiomyocytes and neural cells[21, 22]. The use of electricity to direct the *in vitro* development of axons and neurites of neural cells has been widely reported[23]. On the other hand, electrospun nanofibers scaffolds using natural or synthetic polymers with structure similar to natural extra cellular matrix have been applied for nerve regeneration. Especially, the aligned electrospun nanofibers provide guidance for directional cell migration and proliferation as well as neurite growth[24-26]. In particular, Silantyeva *et al* reported that aligned functionalized nanofibers can accelerate neural differentiation of mouse embryonic stem cells [27]. Furthermore, carbon nanotubes has been evaluated for the neural regeneration due to the surface topography and their intrinsic conductivity[28]. In recent years, the impact of both single walled carbon nanotubes and multi walled carbon nanotubes on neuronal behaviors was reported, especially for their ability to promote neurite extension[29].

Therefore, our device which uses aligned PVDF/MWCNTs assembled on electrodes, should hold some potential for applications in neural tissue engineering, due to the to the good topography of aligned fibers, the improvement of conductivity from MWCNTs and perhaps the inverse piezoelectric stimulation. In addition, PC12 cells were selected as a neuronal cell model, widely used in neurobiology and neurovirology due to their subculture ability[30, 31]. Thus, in this part of the project, we chose PC12 cells

as a modeling cell to evaluate the effect of PVDF/MWCNTs inverse piezoelectric stimulation on the proliferation and differentiation.

2.2 Materials and Methods

2.2.1 Materials

Hams F 12 nutrient medium (F12), Horse serum (HS), Neural growth factor (NGF) and Alamar Blue Kit were purchased from Shanghai Yuchun Biological Technology Co., Ltd.

Anti-rabbit NF200 and Anti-rabbit IgG-FITC were bought from Sigma Aldrich.

PC12 cells offer from Shanghai Institute of Biology, Chinese Academy of Sciences.

2.2.2 Methods

Cell culture

As the previous cells culture of NIH3T3 cells, PC12 cells were cultured in a similar process on IPSD and well plates. The medium of PC12 cells included 84% DMEM/F12, 10% Horse Serum, 5% FBS, and 1% antibiotic/antimycotic solution. Before the cells culture, all culture materials sterilized with the same process as for NIH3T3 cells.

Cell adhesion assay

The PC12 cells adhesion efficiency was evaluated by counting the number of cells attached on the different nanofibers, while the cell number was measured with Alamar blue assay, as specified by the manufacturer. 12 hours after seeding the nanofibers with $5x10^4$ cells, the medium was removed and the nanofibers with PC12 cells were rinsed with PBS three times. Alamar blue solution was added to each well followed by incubation at 37 ℃ for 4 hours. Then, the alamar blue solution was removed to 96 well

plates and the fluorescence at 560nm/590nm was read. The number of cells was calculated from the fluorescence intensity.

Cell proliferation assay

PC12 cells were seeded at the density of $2x10^4$ per well and IPSD, cultured for 1, 3, 5 and 7 days. The inverse piezoelectric stimulation (5Hz, 10V, 30 minutes per day) was started on the day after the cells were seeded on fibers and the daily sampling for the proliferation assay was done 8 hours later. Then, alamar blue was added to each sample, followed by incubation for 3 hours at 37 ℃. After that, the medium of each sample was transferred to 96 well plates and measured using a plate reader.

Cell differentiation assay

In the differentiation of PC12 cells assay, the medium was switched to a differential medium composed of DMEM/F12 supplemented with 1% HS, 0.5% FBS, 1% antibiotic/antimitotic solution and 100 ng/ml Nerve growth factor (NGF). The random PVDF nanofibers were selected to be a negative control, which was cultured in a medium without NGF. 2×10^4 PC12 cells were seeded on each sample, the medium was refreshed every day after the inverse piezoelectric stimulation.

Cell morphology

The morphology of PC12 cells after culture in medium with and without NGF, after 7 days, was evaluated by scanning electron microscopy at 15 kV, after coating with a gold layer. The preparation of all fiber samples followed the same procedure as described for the NIH3T3 cells morphology characterization.

Immunostaining

After 7 days of cell culture in differentiation medium on different nanofibers, immunofluorescence staining of nerve specific protein NF200 was performed for further evaluation of the neural differentiation of PC12 cells. The nanofiber meshes

were rinsed 3 times with PBS and then fixed with 4% formaldehyde for 30 minutes at room temperature. After the fixation of cells on the nanofibers, all samples were permeabilized with 0.1% Triton X-100 for 5 minutes followed by incubation with 1% BSA solution for 90 minutes. Subsequently, the cells with nanofibers were stained with anti-NF200 produced in rabbit as the primary antibody for 2 hours. The anti rabbit IgG-FITC antibody was used as the secondary antibody to combine with the primary for 1 hour. Then the samples were stained with DAPI and observed under laser scanning confocal microscope.

Statistical analysis

Each experiment was repeated at least 3 times on different days and data were expressed as the mean ± SD. All the proliferation measurements were collected in triplicate for each group. Statistical analysis was carried out by the one-way analysis of variance (one-way ANOVA) using Origin software. The statistical difference between two sets of data was considered when $p < 0.05$and $p < 0.01$.

2.3 Results and discussion

2.3.1 Cells adhesion efficiency

The cell adhesion efficiency is one of most important cell behaviors in the early period after the cells have been seeded on the scaffolds. The materials with high adhesion efficiency of cells can improve the cell proliferation, migration and other cell functions. Thus, we aim to evaluate the PC12 cells adhesion on TCPs, random PVDF nanofibers, random PVDF/MWCNTs and aligned PVDF/MWCNTs nanofibers.

As can be seen in Fig. 36 we found that PVDF/MWCNTs fibers (both random and aligned) show the highest number of cells. This interesting result revealed that the alignment of PVDF nanofibers does not change the PC12 cell adhesion. According to previous work, due to higher specific surface area, the scaffolds containing CNTs

exhibit higher protein adsorption rate [4], which may account for higher cell adhesion on the fibers with MWCNTs. However, the number of cells on the random pure PVDF nanofibers was the lowest, even lower than TCPs. This result matched the proliferation assay of NIH3T3 cells and L929 cells. The lower adhesion efficiency of cells on scaffolds always comes with lower proliferation rate.

The higher adhesion efficiency of the aligned and random PVDF/MWCNTs nanofibers for the PC12 cells hints, at this system's great potential for cell proliferation and differentiation.

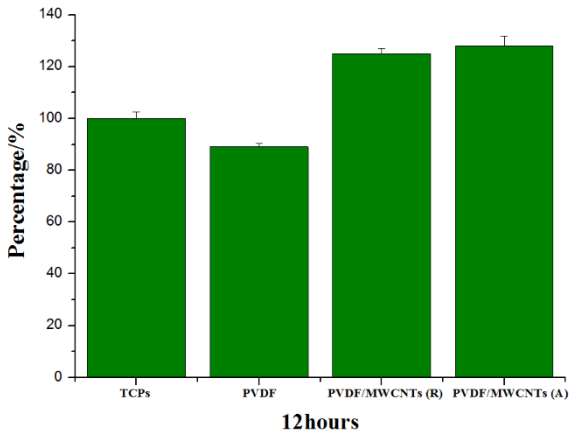

Fig. 36 PC12 cells adhesion efficiency based on TCPs, random PVDF nanofibers, PVDF/MWCNTs (random) nanofibers, PVDF/MWCNTs (aligned) nanofibers.

2.3.2 Cells proliferation under inverse piezoelectric stimulation.

Piezoelectric materials can induce transient change of surface charge without extra energy sources and have been shown to a high level of neuronal differentiation and neurite outgrowth in mouse neuroblastoma cells as compared to non-piezoelectric controls [3]. In addition, the ability of a tissue scaffold to support the proliferation of

cells is one of the major criteria to determine its application in target tissue regeneration. Thus, in order to further investigate the effect of inverse piezoelectric nanofibers stimulation on cells response, TCPs, pure random PVDF, aligned PVDF/MWCNTs with and without inverse piezoelectric stimulation were tested for the proliferation study.

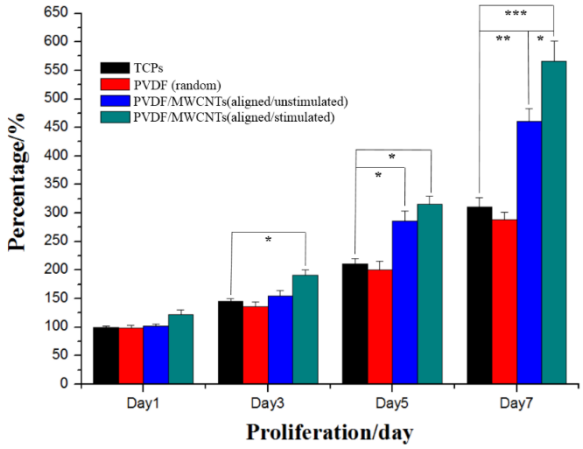

Fig. 37 The proliferation rate of PC12 cells based on TCPs, PVDF (random), PVDF/MWCNTs (aligned/unstimulated), PVDF/MWCNTs (aligned/stimulated)

As shown in Fig. 37, PC12 cells proliferated gradually on all electrospun nanofibers from day 1 to day 7. However, the cell proliferation showed significant behavior on different nanofiber composition. On day 1, cells cultured on aligned PVDF/MWCNTs with IPS already shown slightly better growth than other samples, while all other samples show similar numbers of alive cells. At day 3, day 5 and day 7, the piezoelectric stimulated PVDF/MWCNTs aligned fibers show much greater proliferation rate. Also, since the day 3 until day 7, the aligned PVDF/MWCNTs nanofibers without piezoelectric stimulation, show higher growth rates than TCPs and random PVDF nanofibers. It means the MWCNTs associated with PVDF fibers can increase the proliferation of PC12 cells. This result matched the adhesion assay, the MWCNTs not

just improved the PC12 cells attachment also improved the proliferation. In addition, the number of cells on TCPs is always higher than for random pure PVDF nanofibers, which corresponds to TCP's optimized ability to make most cells grow efficiently and healthy.

Because of the enhanced proliferation of PC12 cells on aligned PVDF/MWCNTs nanofibers, undergoing the inverse piezoelectric stimulation, we believe that stimulation can play an important role in neural tissue engineering.

2.3.3 Cell differentiation under inverse piezoelectric stimulation

The morphology of PC12 cells by SEM

As known, the morphology of PC12 cells is sphere shaped. Before culturing with NGF, the consistent and uniform morphology of PC12 cells grown on the random PVDF(-NGF) fibers could be observed, as shown by the spherical shape of cells in SEM images of Fig. 38A. In Fig. 38B, the elongated shape exhibited by the cells cultured on PVDF(+NGF) fibers, shows the characteristic result of incubation with NGF. Meanwhile, the PC12 cells grown with NGF on aligned PVDF/MWCNTs nanofibers exhibit more projected neurites, especially, the cells submitted to the inverse piezoelectric stimulation, which exhibit longer neurites and well aligned morphology, following the fibers' alignment. The observation of the changes on the PC12 cells morphology reveals the possibility of the aligned fibers and the stimulation to trigger the differentiation. To confirm this hypothesis, we performed the NF200 expression in the fluorescence analysis.

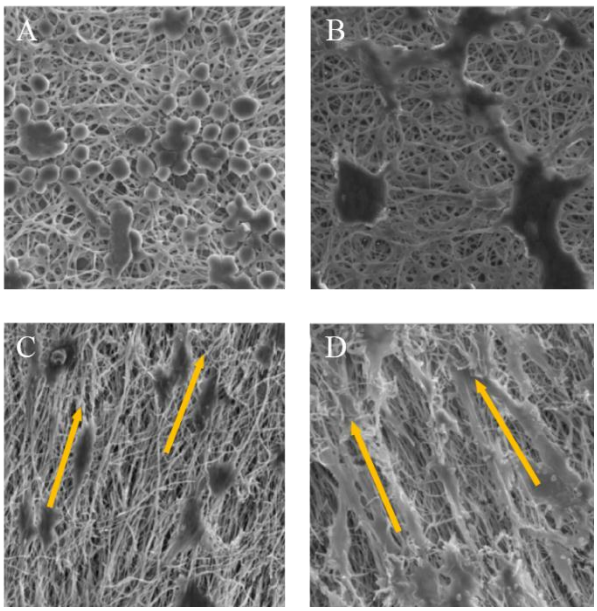

Fig. 38 the morphology of PC12 cells observed by SEM. A is random PVDF (-NGF) nanofibers, B is random PVDF (+NGF) nanofibers, C is aligned PVDF/MWCNTs (+NGF) uncharged nanofibers, D is aligned PVDF/MWCNTs (+NGF) charged nanofibers.

Immunofluorescence analysis

After stimulated by NGF, PC12 cells stop proliferating and start to differentiate into neuron cells. The appearance of one or more neurites on PC12 cells, is generally considered to be the result of differentiation induced by the NGF. The neurofilament protein 200 (NF200) is an important cytoskeletal component unique to neurons. It consists of three neurofilament subunits with molecular weights of 68 kD, 160 kD and 200 kD. They are not only related to the shape and structure of neurons, but also play an important role in axonal transport. Therefore, the expression of NF200 was evaluated to confirm the differentiation of PC12 cells on different nanofibers. The immunofluorescence staining of NF200 can also compare the cell phenotype and neurite outgrowth on different nanofibers.

Fig. 39 shows confocal fluorescence images of PC12 cells based on random PVDF(+NGF)(-NGF) nanofibers, and aligned PVDF/MWCNTs(+NGF) nanofibers with and without inverse piezoelectric stimulation. It shows that NF200 is expressed on the all PC12 cells cultured with differentiation inducing medium (+NGF). However, the PVDF/MWCNTs nanofibers showed more support for NF200 expression compared to pure random PVDF nanofibers and TCPs. Especially, the morphology of PC12 cells on aligned PVDF/MWCNTs show more neuron-like appearance with extended neurites.

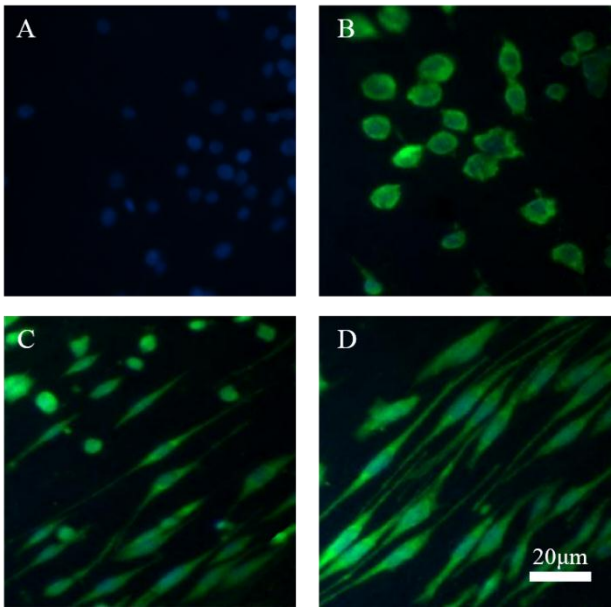

Fig. 39 The fluorescence images of PC12 cells morphology based on different nanofibers, A is random PVDF (-NGF) nanofibers, B is random PVDF (+NGF) nanofibers, C is aligned PVDF/MWCNTs (+NGF) nanofibers, D is aligned PVDF/MWCNTs (+NGF) nanofibers with inverse piezoelectric stimulation.

Meanwhile, in comparison between the cells' morphology based on the two experiments with aligned PVDF/MWCNTs nanofibers, the cells that were submitted to the inverse piezoelectric stimulation shown the extended neurites and elongated shape following the direction of the fibers' orientation. These results confirmed that the inverse piezoelectric stimulation enhances the differentiation of PC12 cells and

therefore, we believe the mechanical stimulation provided by the inverse piezoelectric effect improved the extended neurites growth.

2.4 Conclusion

In this part, it was demonstrated that the adhesion, proliferation and differentiation of PC12 cells can be significantly enhanced by the MWCNTs and inverse piezoelectric stimulation. The MWCNTs blended with PVDF nanofibers shown the highest adhesion efficiency of PC12 cells, more than pure PVDF and TCPs. The results of 7 days proliferation assay confirm the MWCNTs not just improved the adhesion but also improved the proliferation. Moreover, the inverse piezoelectric PVDF/MWCNTs fibers shown highest bioactivities in all samples. The 7 days differentiation results clearly revealed that the PC12 cells undergoing the inverse piezoelectric stimulation could express high NF200 and more neuron-like growth with extended neurites. Therefore, in the early stage of PC12 cells culture, inverse piezoelectric PVDF/MWCNTs holds a great potential for nerve regeneration applications.

3 The effect of inverse piezoelectric stimulation by PVDF/MWCNTs nanofibers, on the behavior of mesenchymal stem cells

3.1 Introduction

Mesenchymal stem cells (MSCs) have attracted wide attention in the area of tissue engineering in the past few years due to their differentiation potential towards different cell lines such as osteoblasts, adipocytes and chondrocytes[32]. Usually, their differentiation could be induced by soluble chemical factors[33]. Nowadays, with the development of biomaterials, it has been reported the interaction between the materials and the cells has a considerable influence on MSCs function and differentiation[34]. As already mentioned, the electrospun nanofibers have been widely regarded as ideal substrates for tissue engineering due to their similar structure to natural extra cellular matrix. Especially, the topography of nanofiber networks can guide the alignment of specific types of cells that lead to the deposition of an organized anisotropic ECM [35]. Such as Barker demonstrated, MSCs align with and deposit fibrocartilaginous ECM in the predominant nanofiber direction[36]. In addition, carbon nanotubes are becoming increasingly attractive materials as they can be modified by functionalization and used as scaffold materials for promoting tissue regeneration and stem cell therapy due to their remarkable mechanical, optical and electrical properties[37-40]. Such as Kinsuk reported COOH-functionalized CNTs represent a promising scaffold component for future use in the selective differentiation of canine MSCs in regenerative medicine[41]. Moreover, among the applications of piezoelectric technologies, particularly the piezoelectric nanopattern and nanofibers, those which involve interfaces with biological system represent an exciting area of rapid development. For instance, Zhou investigated the polypyrrole nanocones and dynamic piezoelectric stimulation induced stem cell osteogenic differentiation[42].

Therefore, in this part of the project, we aim to: first, to investigate the isolation and identification of mesenchymal stem cells; secondly, to study the effect of inverse piezoelectric stimulation with our aligned PVDF/MWCNTs nanofibers, on the cells functions, such as, adhesion, proliferation, and differentiation of MSCs.

3.2 Materials and methods

3.2.1 Materials

Alkaline phosphatase assay kit (ALP), Alizarin Red stain kit, Oil red O stain kit were bought from Shanghai Yuchun Biological Technology Co., Ltd.

Dexamethasone, indomethacin and 3-isobutyl-1-methylxanthine were purchased from Sigma Aldrich

3.2.2 Methods of isolation and identification of bone mesenchymal stem cell

Isolation of BMSCs

In general, there are four basic methods for extraction and culture of bone marrow mesenchymal stem cells: whole bone marrow adherence method, cell surface molecular marker sorting method, density gradient centrifugation method and cell screening method[43]. Relatively, the whole bone marrow adherence method is more convenient, so in this part, we choose this method to extract and isolate rat bone marrow mesenchymal stem cells. The main operation methods as follows:

(1) Male rats of about 100 g were dislocated at the neck and immersed in 75% alcohol for 10 minutes.

(2) Cut the skin of both lower limbs with scissors, separate the superficial fascia and muscles in sequence, expose the upper end of the femoral shaft and the lower end of

the tibia, and then remove it completely. Place in a 50 ml centrifuge tube, pour 75% alcohol, and quickly move it to a sterile workbench.

(3) In the sterile workbench, we cut both ends of the bone with scissors and leave it in a Petri dish. Take another Petri dish with DMEM and rinse the bone marrow cavity repeatedly until the bone marrow turns total white. Then, the DMEM containing BMSCs and other cells was transferred to a centrifuge tube.

(4) Centrifuge at 1000 rpm for 5 minutes, discard the supernatant, rinse the cells with low-sugar DMEM medium, and evenly disperse the cells, transfer to a culture bottle, mark them, and place them in a cell incubator.

(5) Change the medium after 24 hours and refresh the medium every three days. After culturing with low-sugar DMEM medium containing 20% FBS and 1% double antibiotic according to the normal cell culture method. BMSCs will grow adherently, and other cells are removed during every refreshing medium step.

Identification of BMSCs

In order to identify the BMSCs, we selected the basic methods such as the observation of cell morphology, characterization of the osteogenic and adipogenic differentiation and expression of certain specific antigens on the surface of cells. The main operation as follows:

Cell morphology observation

After culture of the cells isolated from rat bone marrow for 24 hours, we consider the cells as P0 and observe with inverted microscope.

After medium refresh and adding trypsin 3 times, we consider the cells as P3 and observe the morphology under the inverted microscope.

Flow cytometry analysis

We selected P3 cells as the sample to detect the expression level of surface markers. After trypsin 3 times, the cells were centrifuged for 5 minutes and the suspension removed. Then, added 3% FBS solution and gently pipette until the cells distribute well.

Samples of P3 cells were counted and $1x10^4$ were transferred into EP tubes and stained with antibodies CD34 and CD44, specific for the BMSCs. Labeled cells were acquired with a flow cytometer equipped with the Cellquest program.

Cell differentiation

We also selected P3 cells as the sample to analyze the osteogenic and adipogenic differentiation results.

Osteogenic differentiation of P3 cells

For this experiment, the DMEM was switched to a differentiation medium. The osteogenic differentiation medium was composed of MEM supplemented with 100nM of dexamethasone, 200uM of ascorbic acid and 10 mM of glycerol 2-phosphate, and medium was refreshed every 3 days.

Adipogenic differentiation of P3 cells

In this case, the DMEM was changed to an adipogenic induction medium. The adipogenic medium was composed of DMEM supplemented with 10% PBS, 1% ascorbic acid, 10 μg/L of insulin, 10 μmol/L dexamethasone, 0.5 mmol/L of IBXM and 100 μmol/L indomethacin. The medium was refreshed every 3 days.

ALP staining assay

For ALP staining, cells were covered with a working solution contain 2 mg/ml of Na-α-naphtyl phosphate, 2 mg/mL of fast blue RR salt and 0.1 M Tris buffer (pH=10). After staining in dark for 1 hour, the cells were rinsed with ultrapure water and characterized under the inverted microscope.

Oil red O staining assay

The cells were fixed with 1.5% glutaraldehyde in DPBS for 20 minutes and rinsed with distilled water. About 20 minutes before being used, 0.5% (w/v) Oil Red O solution was prepared in ultrapure water. The cells were covered with this solution for 1 hour at room temperature and washed before being photographed under inverted microscopy.

3.2.3 Method for studying BMSCs behavior under inverse piezoelectric stimulation

Cell adhesion assay

The BMSCs adhesion efficiency was investigated by counting the number of live and attached cells on the nanofibers. After $2x10^4$ cells were seeded on the fibers with DMEM supplemented with 10% FBS and 1% PS for 12 hours, the alamar blue assay was used to count the number of alive cells. The details of this process are similar to the PC12 cells described previously.

Cell proliferation assay

BMSCs cells were seeded at a density of $2x10^4$ on the nanofibers in the well plates and IPSD. The inverse piezoelectric stimulation (5 Hz, 10 V, 30 minutes per day) was started the day after the cells were seeded on the fibers. We consider the day after inverse stimulation as day 1. The cells were incubated for one week and we selected days 1, 3, 5 and 7, for proliferation measurement. The number of cells was counted with the alamar blue assay.

Osteogenic differentiation

Osteogenic differentiation of BMSCs based on TCPs and aligned PVDF/MWCNTs nanofibers without inverse piezoelectric stimulation, was induced as described. For the aligned PVDF/MWCNTs nanofibers based on the electrode, the inverse stimulation (5 Hz, 10 V) was performed for 30 minutes every day. After the stimulation, the inducing

MEM with dexamethasone was refreshed. The whole of osteogenic differentiation assay lasted for 14 days.

Adipogenic differentiation

The process of adipogenic differentiation of BMSCs is similar as our previous work. The inverse piezoelectric stimulation of fibers on BMSCs was also performed by a 10 V and 5 Hz charge to the electrode every 30 minutes per day.

Qualitative and quantitative characterization of Osteogenic and adipogenic differentiation

Other than the ALP staining (previously described), the Alizarin red staining also was used to determine the osteogenic differentiation due to the calcium deposition. Therefore, all samples were fixed with 10% of neutral buffered formalin at 4 ℃ over night. Before staining with 1% Alizarin Red working solution, the samples were washed 3 times with distilled water. The stained samples were examined and photographed using inverted microscope.

For quantitative evaluation of ALP activity, briefly, each sample of cells on nanofibers were rinsed 3 times with Dulbeccos phosphate buffered saline solution (DPBS) and 0.1% (v/v) Triton X-100 (prepared in DPBS) was added to each well. Then, 20 μL of the lysates were transferred into each well and 200 μL of substrates solution were added. The samples were then incubated in the dark at 37 ℃ for 1 hour. Then the reaction was interrupted by adding 100 μL of 0.02M NaOH. The amount of protein in the cell lysates was determined using the bicinchoninic acid (BCA) assay using bovine serum albumin as a standard.

To determine the adipogenic differentiation of BMSCs, we used the previously described Oil red O staining assay. For the quantitative investigation of the adipogenesis process, a 250 μL of isopropanol was added to each well and kept in for

15 minutes. Then, 100 μL were transferred to 96 well plates and the absorbance was read at 490 nm. A standard curve was generated by using serial dilutions of Oil Red O.

3.3 Results and discussion

3.3.1 Isolation and identification of bone mesenchymal stem cell

Cell morphology

To determine the morphology of the isolated rat marrow bone cells, we compared the P0 cells with the P3 on the microscope. From the Fig. 40 , it can be seen that the shape of the P0 cells is round while the P3 cell have a spindle-like shape, typical of MSCs, allowing us to confirm that the P3 bone marrow cells are nearly all BMSCs.

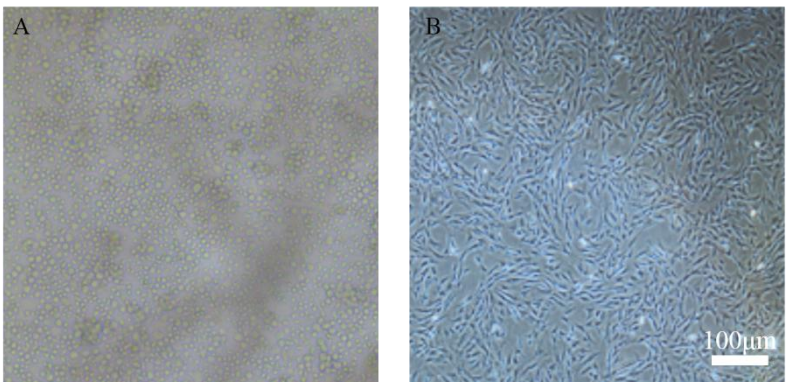

Fig. 40 The morphology of P0 and P3 cells.

Phenotypic characterization of BMSCs

To evaluate the percentages of BMSCs in the P3 cells, we used specific surface markers for detection by flow cytometric analysis. In general, CD34 is a pan-hematopoietic marker and CD44 is the surface marker of MSCs. The results from flow cytometry on Fig. 41, show that most P3 cells (85%) express the CD44 antigen and just

a small number expresses the CD34 antigen. This results was similar to previous research [44] that obtained nearly 90% of BMSCs.

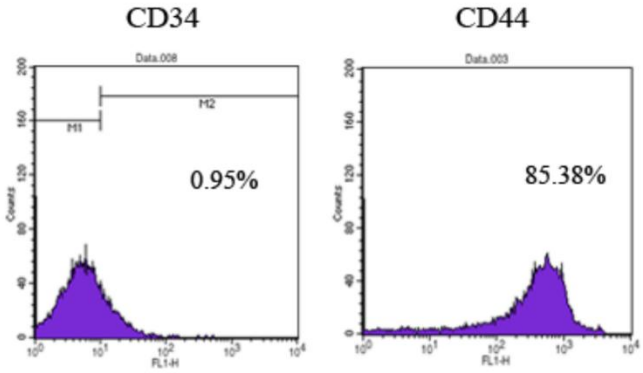

Fig. 41 Flow cytometry analysis of P3 cells with the expression of mesenchymal surface proteins CD 44 and hematopoietic markers CD34.

Osteogenic and adipogenic differentiation

In order to determine the differentiation potential of P3 cells, we induced P3 BMSCs into osteocytes and adipocytes.

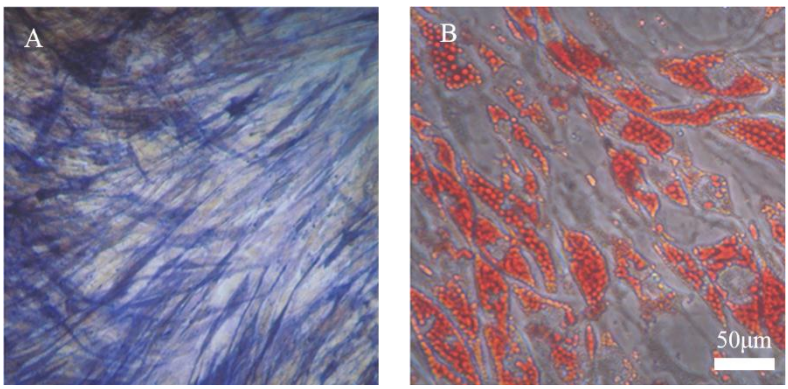

Fig. 42 The images A is ALP staining of P3 cells after two weeks osteogenic induction. The image B is Oil red O staining of P3 cells after two weeks adipogenic induction.

After 2 weeks of incubation in the osteogenic medium, Fig. 42 shows blue mineralized nodules were detected in the cells confirming differentiation to osteocytes. Regarding the adipogenic differentiation potential of BMSCs, it was also confirmed by the accumulation of red lipid droplets in the cytoplasm after 2 weeks of induced incubation.

Conclusion

From the morphology observation, surface marker detection and the results of osteogenic and adipogenic differentiation, we concluded that the isolation process rendered P3 bone marrow cells with at least 85% BMSCs. Therefore, we selected the P3 cells as a model to investigate the effect of our fiber devices on the differentiation potential of BMSCs.

3.3.2 Effect of inverse piezoelectric stimulation on the behavior of BMSCs

According to previous research, carbon nanotubes have exceptional theoretical mechanical properties (such as high strength to weight ratios), as well as possessing nanoscale fiber dimensions similar to crystalline hydroxyapatite found in physiological bone, suggesting strong possibilities for improving the adhesion of osteoblasts, fibroblast, chondrocyte, and smooth muscle cells[45]. Moreover, the random and aligned biomimetic electrospun nanofibers has been widely used in tissue engineering. Unfortunately, current research to direct the fate of stem cells remains limited for the absence of a clear understanding of the mechanism of interfacial interaction between fibers and stem cells. Thus, we aim to evaluate the adhesion results of BMSCs based on random PVDF fibers, random and aligned PVDF/MWCNTs nanofibers.

Cell adhesion efficiency

Fig. 43 shows that after 12 hours of incubation on each nanofiber mesh, the number of live BMSCs on TCPs are the best among all the samples. It reveals that TCPs exhibits

improved adhesion of BMSCs better than any PVDF or PVDF/MWCNTs nanofibers with different orientations. Comparing the adhesion results of BMSCs and PC12 cells, this opposite results shown us that PVDF/MWCNTs only improve the adhesion of PC12 cells and not on BMSCs. In addition, the number of cells on PVDF/MWCNTs fibers is slightly higher than for PVDF fibers, leading to conclude that CNTs slightly improved the adhesion of BMSCs on PVDF nanofibers. The advantageous properties of MWCNTs as were previously described (such as mechanical properties, conductivity etc.) should indeed have a positive effect on BMSCs. Interestingly, the cells viability on random and aligned PVDF/MWCNTs nanofibers are very similar, confirming that the alignment of nanofibers, by itself, does not improve the adhesion of BMSCs in the early period (12 hours), as it happens with the PC12 cells adhesion.

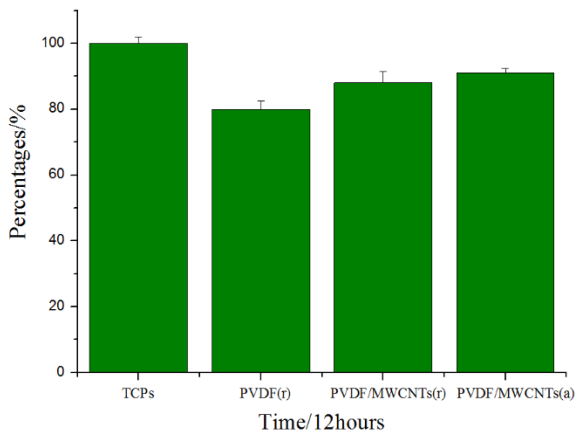

Fig. 43 BMSCs adhesion efficiency on the TCPs, random PVDF nanofibers, random PVDF/MWCNTs, and aligned PVDF/MWCNTs nanofibers.

Cell proliferation

Recently, several studies have applied either electrical or mechanical stimuli to the environments of native skeletal muscle, *in vitro*, to modulate cells behavior[46]. Nevertheless, piezoelectricity, which simultaneously involves both mechanical and

electric stimulations has been rarely reported for stem cells behavior investigation. Jeong-kee *et al* have investigated piezoelectric substrates for generation of myogenic cell sheet fragments from human MSCs[47]. Asuna *et al* have evaluated the cell fate determination of MSCs regulated by a piezo type mechanosensitive ion channel[48]. However, what is the inverse piezoelectricity influence on MSCs proliferation? In this part of the project we aim to evaluate the effect of our inverse piezoelectric PVDF/MWCNTs nanofibers on the proliferation of BMSCs.

From the results of the 7 days proliferation assay depicted in Fig. 44, we can see that TCPs show the best support for proliferation of the BMSCs, when compared to all the fibers, including the inverse piezoelectric stimulated fibers. This result matches the 12 hours adhesion assay meaning that the adhesion efficiency is positively correlated to the proliferation of BMSCs. Compared with the PVDF nanofibers with and without MWCNTs, since day 3 until day 7, the proliferation rate of BMSCs based on PVDF/MWCNTs nanofibers is higher than pure PVDF, confirming that the positive effect of CNTs on cells proliferation is not just valid for PC12 and NIH3T3 cells, but also for BMSCs. However, the results between the stimulated and non-stimulated aligned PVDF/MWCNTs nanofiber experiments don't show any obvious difference. It means the 30 minutes per day inverse piezoelectricity from our device could not influence the BMSCs proliferation.

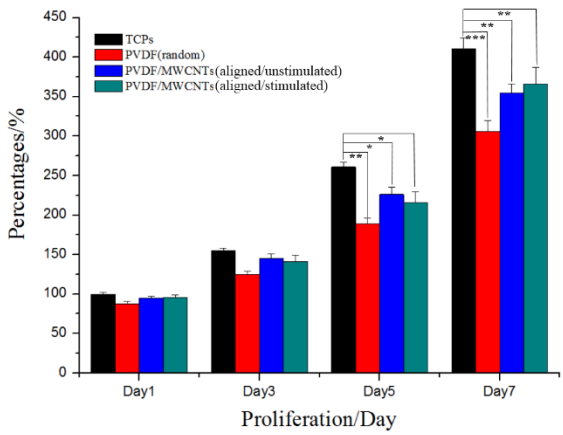

Fig. 44 7 days proliferation assay of BMSCs based on TCPs, random PVDF nanofibers, aligned PVDF/MWCNTs (stimulated) nanofibers.

The effect of inverse piezoelectric stimulation on BMSCs differentiation

Piezoelectric materials have significant applications in tissue engineering as an electroactive scaffold for tissue repair and regeneration. Nowadays, the optimal piezoelectric scaffolds can produce suitable signals, similar to the ECM, which has been observed during remodeling phenomenon in bone and cartilage[49]. For instance, Cijun showed that incorporation of $BaTiO_3$ nanoparticles with PVDF scaffold promoted the cell differentiation more efficiently[50]. Damaraju reported that three-dimensional piezoelectric fibrous scaffolds selectively promoted MSCs cell differentiation. Specifically, they revealed the piezoelectric scaffolds that exhibit low voltage output, or streaming potential, promoted chondrogenic differentiation and piezoelectric scaffolds with a high voltage output promoted osteogenic differentiation[51].

Therefore, after the characterization of PC12 cells differentiation on our inverse piezoelectric device, we aim to test the differentiation efficiency of BMSCs, especially their osteogenic and adipogenic direction. According to the results of cells adhesion and proliferation assay of BMSCs on PVDF/MWCNTs aligned and random fibers, we selected the random and aligned PVDF/MWCNTs nanofibers with and without inverse piezoelectric stimulation for the experiments. We used the incubation of BMSCs on TCPs with inducing medium for positive control and cells culturing without the induced medium on PVDF/MWCNTs with inverse piezoelectric stimulation for negative control.

Qualitative and quantitate characterization of osteogenic and adipogenic differentiation.

Alkaline phosphatase（ALP） is a general term used to describe non-specific phosphomonoesterase, which hydrolyzes phosphate esters, optimally at alkaline pH. It is one of the most widely used biochemical marker of osteoblasts. Alizarin Red stain (ARS) is usually performed to detect calcium deposition on the early period of osteoblasts. Oil red O is a dye that strongly stains lipids, and widely used for identification adipocytes.

Fig. 45 shows the results of the ALP staining, Alizarin red staining and Oil red O staining microscopy images of BMSCs based on random and aligned PVDF/MWCNTs with inverse piezoelectric stimulation, after incubation for 2 weeks in the inducing medium. From Fig. 45 A-D, the random and aligned fibers with stimulation and cultured in the medium without inducing factors. All images shown no staining color on the fibers. We can see that the 30 minutes per day inverse piezoelectric stimulation with PVDF/MWCNTs nanofibers did not promote BMSCs differentiation.

For the osteogenic differentiation.

The results of incubation cultured with inducing medium, on random and aligned PVDF/MWCNTs under the inverse piezoelectric stimulation, for 2 weeks, are shown on the images from Fig. 45 E-L, with the staining colors from ALP and Alizarin red staining. The staining patterns of ALP and ARS show calcium deposition evenly distributed along the orientation of aligned PVDF/MWCNTs fibers. On the random PVDF/MWCNTs fibers, the staining pattern was randomly distributed and tends to gather at the intersection of fibers. It shown that with induced culturing, the BMSCs can differentiated to osteoblasts on both random and aligned PVDF/MWCNTs fibers. Qualitatively we can notice important differences between the two types of fibers, the aligned ones showing a higher staining pattern intensity. Nevertheless, we used the quantitative analysis with ALP staining shown in Fig. 46A, to clarify this matter, showing that the BMSCs based on the aligned PVDF/MWCNTs nanofibers turn out as higher number of osteoblasts, when compared with TCPs and random fibers. As we

know, the random PVDF/MWCNTs fibers do not exhibit strong piezoelectricity in the cell medium environment. Thus, we conclude that the aligned PVDF/MWCNTs fibers with inverse piezoelectric stimulation promote more osteoblasts from BMSCs in 14 days. It means that although the inverse piezoelectric stimulation from aligned PVDF/MWCNTs fibers cannot improve the proliferation of BMSCs, it still shows great bioactivity to improve the efficiency of osteogenic differentiation.

For the adipogenic differentiation

From the Fig. 40 M-P, the staining pattern of oil red O shows similar results to ALP and ARS. The lipid droplets generated by the adipocytes are evenly distributed and arranged along the direction of charged PVDF/MWCNTs nanofibers. On the random PVDF/MWCNTs nanofibers, the lipid droplets gather at the intersection of fibers. The images show that the adipogenic differentiation of BMSCs was successful on both the random and aligned fibers. From the results of Oil red O quantification (Fig. 46B), the TCPs shows slightly higher value than random and aligned PVDF/MWCNTs nanofibers. It means in the adipogenic differentiation process, no significant differences were observed from the inverse piezoelectricity. The higher adipocytes count on TCPs probably is due to the proliferation of BMSCs. In the 7 days proliferation assay of BMSCs on different fibers, TCPs also shown the higher value than any other fibers. Overall, we confirmed that the inverse piezoelectric stimulation does not have any influence on adipogenic differentiation of BMSCs.

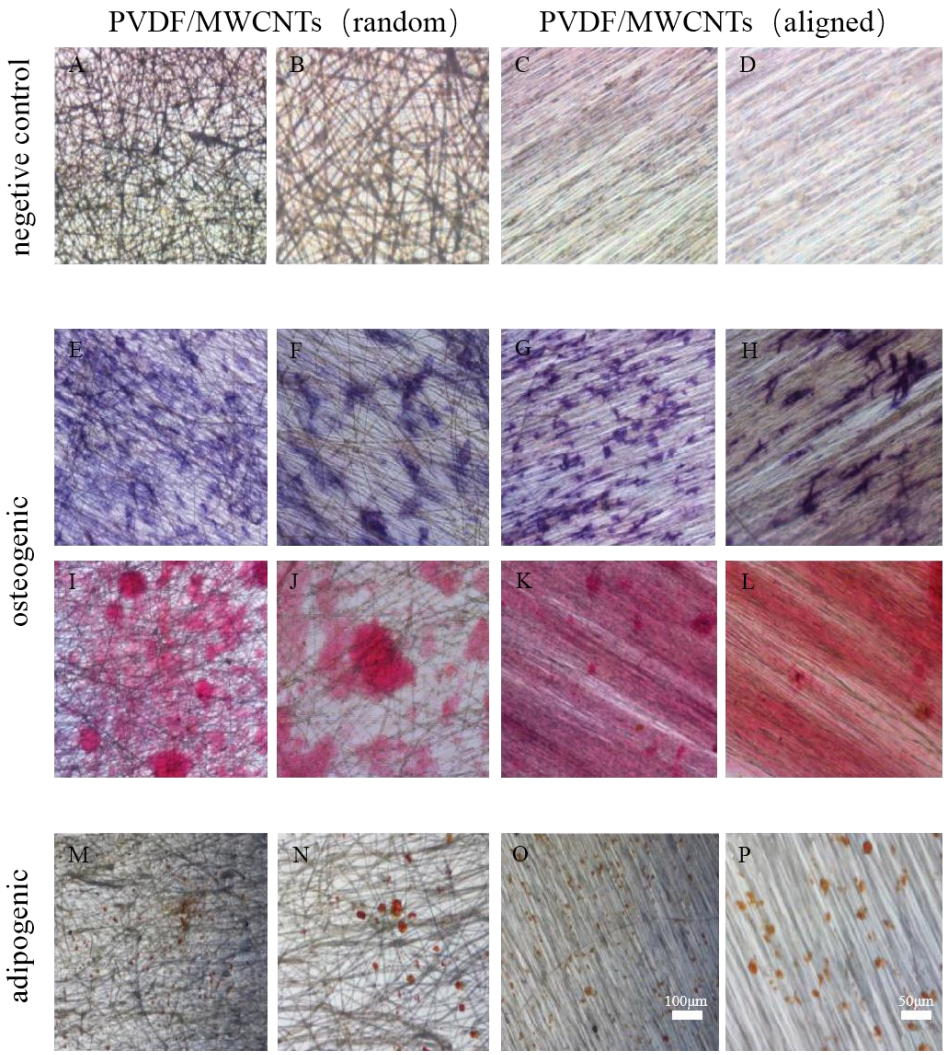

Fig. 45 Images of BMSCs staining on the different random and aligned PVDF/MWCNTs nanofibers. Cells in general cultured medium (A-D), cells with ALP staining (E-H), cells with alizarin red staining (I-L), and cells with oil red O staining (M-P).

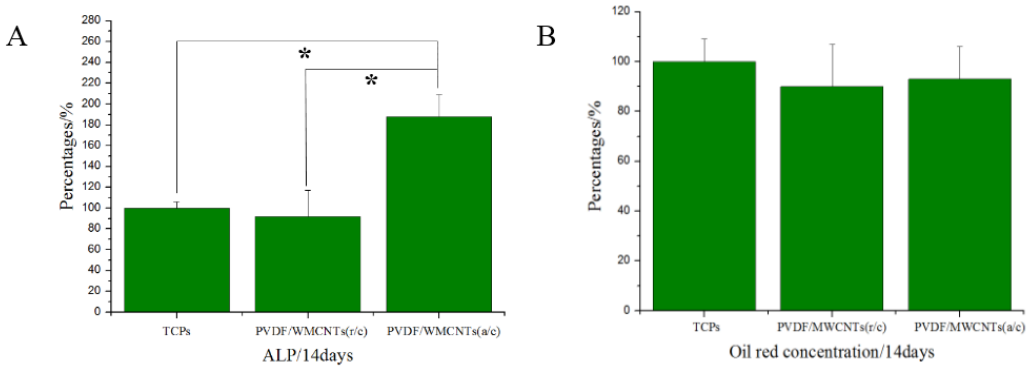

Fig. 46. Quantitation of alkaline phosphatase activity (A) and oil red O activity (B) in solution after staining.

Conclusion

In this part, we investigated how PVDF/MWCNTs nanofibers could affect the BMSCs adhesion, proliferation and differentiation. Although the inverse piezoelectric nanofibers cannot improve the adhesion in the early period and 7 days proliferation of BMSCs, however, it was found that inverse piezoelectric PVDF/MWCNTs nanofibers show great bioactivity for osteogenic differentiation of BMSCs. Due to good cytocompatibility, effective cell elongation, and enhanced osteogenic differentiation, aligned PVDF/MWCNTs nanofibers show excellent potential for tissue engineering and especially in bone regeneration applications.

References

1. Guo, H. F.; Li, Z. S.; Dong, S. W.; Chen, W. J.; Deng, L.; Wang, Y. F.; Ying, D. J., Piezoelectric PU/PVDF electrospun scaffolds for wound healing applications. *Colloids and Surfaces B-Biointerfaces* **2012,** *96*, 29-36.https://doi.org/10.1016/j.colsurfb.2012.03.014

2. Wang, A. C.; Liu, Z.; Hu, M.; Wang, C. C.; Zhang, X. D.; Shi, B. J.; Fan, Y. B.; Cui, Y. G.; Li, Z.; Ren, K. L., Piezoelectric nanofibrous scaffolds as in vivo energy harvesters for modifying fibroblast alignment and proliferation in wound healing. *Nano Energy* **2018,** *43*, 63-71.https://doi.org/10.1016/j.nanoen.2017.11.023

3. Au, H. T. H.; Cheng, I.; Chowdhury, M. F.; Radisic, M., Interactive effects of surface topography and pulsatile electrical field stimulation on orientation and elongation of fibroblasts and cardiomyocytes. *Biomaterials* **2007,** *28* (29), 4277-4293.https://doi.org/10.1016/j.biomaterials.2007.06.001

4. Ameer, J. M.; Kumar, P. R. A.; Kasoju, N., Strategies to Tune Electrospun Scaffold Porosity for Effective Cell Response in Tissue Engineering. *Journal of Functional Biomaterials* **2019,** *10* (3).https://doi.org/10.3390/jfb10030030

5. Kumar, S.; Rani, R.; Dilbaghi, N.; Tankeshwar, K.; Kim, K. H., Carbon nanotubes: a novel material for multifaceted applications in human healthcare. *Chemical Society Reviews* **2017,** *46* (1), 158-196.https://doi.org/10.1039/c6cs00517a

6. Alshehri, R.; Ilyas, A. M.; Hasan, A.; Arnaout, A.; Ahmed, F.; Memic, A., Carbon Nanotubes in Biomedical Applications: Factors, Mechanisms, and Remedies of Toxicity. *Journal of Medicinal Chemistry* **2016,** *59* (18), 8149-8167.https://doi.org/10.1021/acs.jmedchem.5b01770

7. MacDonald, R. A.; Voge, C. M.; Kariolis, M.; Stegemann, J. P., Carbon nanotubes increase the electrical conductivity of fibroblast-seeded collagen hydrogels. *Acta Biomaterialia* **2008,** *4* (6), 1583-1592.https://doi.org/https://doi.org/10.1016/j.actbio.2008.07.005

8. Lobo, A. O.; Antunes, E. F.; Machado, A. H. A.; Pacheco-Soares, C.; Trava-Airoldi, V. J.; Corat, E. J., Cell viability and adhesion on as grown multi-wall carbon nanotube films. *Materials Science & Engineering C-Biomimetic and Supramolecular Systems* **2008,** *28* (2), 264-269.https://doi.org/10.1016/j.msec.2007.01.003

9. Chlopek, J.; Czajkowska, B.; Szaraniec, B.; Frackowiak, E.; Szostak, K.; Beguin, F., In vitro

studies of carbon nanotubes biocompatibility. *Carbon* **2006,** *44* (6), 1106-1111.https://doi.org/10.1016/j.carbon.2005.11.022

10. Ding, L.; Stilwell, J.; Zhang, T.; Elboudwarej, O.; Jiang, H.; Selegue, J. P.; Cooke, P. A.; Gray, J. W.; Chen, F. F., Molecular Characterization of the Cytotoxic Mechanism of Multiwall Carbon Nanotubes and Nano-Onions on Human Skin Fibroblast. *Nano Letters* **2005,** *5* (12), 2448-2464.https://doi.org/10.1021/nl051748o

11. Patlolla, A.; Knighten, B.; Tchounwou, P., MULTI-WALLED CARBON NANOTUBES INDUCE CYTOTOXICITY, GENOTOXICITY AND APOPTOSIS IN NORMAL HUMAN DERMAL FIBROBLAST CELLS. *Ethnicity & Disease* **2010,** *20* (1), 65-72

12. McCaig, C. D.; Song, B.; Rajnicek, A. M., Electrical dimensions in cell science. *Journal of Cell Science* **2009,** *122* (23), 4267-4276.https://doi.org/10.1242/jcs.023564

13. Zhao, M.; Song, B.; Pu, J.; Wada, T.; Reid, B.; Tai, G.; Wang, F.; Guo, A.; Walczysko, P.; Gu, Y.; Sasaki, T.; Suzuki, A.; Forrester, J. V.; Bourne, H. R.; Devreotes, P. N.; McCaig, C. D.; Penninger, J. M., Electrical signals control wound healing through phosphatidylinositol-3-OH kinase-γ and PTEN. *Nature* **2006,** *442* (7101), 457-460.https://doi.org/10.1038/nature04925

14. DeVito, R. V., Healing of Wounds. *Surgical Clinics of North America* **1965,** *45* (2), 441-459.https://doi.org/https://doi.org/10.1016/S0039-6109(16)37542-9

15. Chao, P. H. G.; Lu, H. H.; Hung, C. T.; Nicoll, S. B.; Bulinski, J. C., Effects of applied DC electric field on ligament fibroblast migration and wound healing. *Connective Tissue Research* **2007,** *48* (4), 188-197.https://doi.org/10.1080/03008200701424451

16. Tandon, B.; Blaker, J. J.; Cartmell, S. H., Piezoelectric materials as stimulatory biomedical materials and scaffolds for bone repair. *Acta Biomaterialia* **2018,** *73*, 1-20.https://doi.org/10.1016/j.actbio.2018.04.026

17. Yamada, K. M.; Sixt, M., Mechanisms of 3D cell migration. *Nature Reviews Molecular Cell Biology* **2019,** *20* (12), 738-752.https://doi.org/10.1038/s41580-019-0172-9

18. Werner, S.; Krieg, T.; Smola, H., Keratinocyte-fibroblast interactions in wound healing. *Journal of Investigative Dermatology* **2007,** *127* (5), 998-1008.https://doi.org/10.1038/sj.jid.5700786

19. Ashrafian, H.; Harling, L.; Darzi, A.; Athanasiou, T., Neurodegenerative disease and obesity:

what is the role of weight loss and bariatric interventions? *Metabolic Brain Disease* **2013,** *28* (3), 341-353.https://doi.org/10.1007/s11011-013-9412-4

20. Maragakis, N. J.; Rothstein, J. D., Mechanisms of Disease: astrocytes in neurodegenerative disease. *Nature Clinical Practice Neurology* **2006,** *2* (12), 679-689.https://doi.org/10.1038/ncpneuro0355

21. Chan, Y. C.; Ting, S.; Lee, Y. K.; Ng, K. M.; Zhang, J.; Chen, Z.; Siu, C. W.; Oh, S. K. W.; Tse, H. F., Electrical Stimulation Promotes Maturation of Cardiomyocytes Derived from Human Embryonic Stem Cells. *Journal of Cardiovascular Translational Research* **2013,** *6* (6), 989-999.https://doi.org/10.1007/s12265-013-9510-z

22. Kam, N. W. S.; Jan, E.; Kotov, N. A., Electrical Stimulation of Neural Stem Cells Mediated by Humanized Carbon Nanotube Composite Made with Extracellular Matrix Protein. *Nano Letters* **2009,** *9* (1), 273-278.https://doi.org/10.1021/nl802859a

23. Goldberg, J. L.; Espinosa, J. S.; Xu, Y.; Davidson, N.; Kovacs, G. T. A.; Barres, B. A., Retinal Ganglion Cells Do Not Extend Axons by Default: Promotion by Neurotrophic Signaling and Electrical Activity. *Neuron* **2002,** *33* (5), 689-702.https://doi.org/https://doi.org/10.1016/S0896-6273(02)00602-5

24. Zhang, K.; Zheng, H.; Liang, S.; Gao, C., Aligned PLLA nanofibrous scaffolds coated with graphene oxide for promoting neural cell growth. *Acta Biomaterialia* **2016,** *37*, 131-142.https://doi.org/https://doi.org/10.1016/j.actbio.2016.04.008

25. Schnell, E.; Klinkhammer, K.; Balzer, S.; Brook, G.; Klee, D.; Dalton, P.; Mey, J., Guidance of glial cell migration and axonal growth on electrospun nanofibers of poly-ε-caprolactone and a collagen/poly-ε-caprolactone blend. *Biomaterials* **2007,** *28* (19), 3012-3025.https://doi.org/https://doi.org/10.1016/j.biomaterials.2007.03.009

26. Wang, X.; Ding, B.; Li, B., Biomimetic electrospun nanofibrous structures for tissue engineering. *Materials Today* **2013,** *16* (6), 229-241.https://doi.org/https://doi.org/10.1016/j.mattod.2013.06.005

27. Silantyeva, E. A.; Nasir, W.; Carpenter, J.; Manahan, O.; Becker, M. L.; Willits, R. K., Accelerated neural differentiation of mouse embryonic stem cells on aligned GYIGSR-functionalized nanofibers. *Acta Biomaterialia* **2018,** *75*, 129-139.https://doi.org/https://doi.org/10.1016/j.actbio.2018.05.052

28. Tran, P. A.; Zhang, L. J.; Webster, T. J., Carbon nanofibers and carbon nanotubes in regenerative medicine. *Advanced Drug Delivery Reviews* **2009,** *61* (12), 1097-1114.https://doi.org/10.1016/j.addr.2009.07.010

29. Fabbro, A.; Prato, M.; Ballerini, L., Carbon nanotubes in neuroregeneration and repair. *Advanced Drug Delivery Reviews* **2013,** *65* (15), 2034-2044.https://doi.org/https://doi.org/10.1016/j.addr.2013.07.002

30. FOULDS, I. S.; BARKER, A. T., Human skin battery potentials and their possible role in wound healing. *British Journal of Dermatology* **1983,** *109* (5), 515-522.https://doi.org/10.1111/j.1365-2133.1983.tb07673.x

31. Park, J. S.; Park, K.; Moon, H. T.; Woo, D. G.; Yang, H. N.; Park, K.-H., Electrical Pulsed Stimulation of Surfaces Homogeneously Coated with Gold Nanoparticles to Induce Neurite Outgrowth of PC12 Cells. *Langmuir* **2009,** *25* (1), 451-457.https://doi.org/10.1021/la8025683

32. Andrzejewska, A.; Lukomska, B.; Janowski, M., Concise Review: Mesenchymal Stem Cells: From Roots to Boost. *STEM CELLS* **2019,** *37* (7), 855-864.https://doi.org/10.1002/stem.3016

33. Pittenger, M. F.; Mackay, A. M.; Beck, S. C.; Jaiswal, R. K.; Douglas, R.; Mosca, J. D.; Moorman, M. A.; Simonetti, D. W.; Craig, S.; Marshak, D. R., Multilineage potential of adult human mesenchymal stem cells. *Science* **1999,** *284* (5411), 143-147.https://doi.org/10.1126/science.284.5411.143

34. Discher, D. E.; Mooney, D. J.; Zandstra, P. W., Growth Factors, Matrices, and Forces Combine and Control Stem Cells. *Science* **2009,** *324* (5935), 1673-1677.https://doi.org/10.1126/science.1171643

35. Manwaring, M. E.; Walsh, J. F.; Tresco, P. A., Contact guidance induced organization of extracellular matrix. *Biomaterials* **2004,** *25* (17), 3631-3638.https://doi.org/https://doi.org/10.1016/j.biomaterials.2003.10.043

36. Baker, B. M.; Mauck, R. L., The effect of nanofiber alignment on the maturation of engineered meniscus constructs. *Biomaterials* **2007,** *28* (11), 1967-1977.https://doi.org/https://doi.org/10.1016/j.biomaterials.2007.01.004

37. Thostenson, E. T.; Ren, Z. F.; Chou, T. W., Advances in the science and technology of carbon nanotubes and their composites: a review. *Composites Science and Technology* **2001,** *61* (13), 1899-

1912.https://doi.org/10.1016/s0266-3538(01)00094-x

38. Saito, R.; Kataura, H., Optical properties and Raman spectroscopy of carbon nanotubes. In *Carbon Nanotub Es: Synthesis, Structure, Properties, and Applications*, Dresselhaus, M. S.; Dresselhaus, G.; Avouris, P. H., Eds. **2001**; Vol. 80, pp 213-246.

39. Ouyang, M.; Huang, J.-L.; Lieber, C. M., Fundamental Electronic Properties and Applications of Single-Walled Carbon Nanotubes. *Accounts of Chemical Research* **2002,** *35* (12), 1018-1025.https://doi.org/10.1021/ar0101685

40. Troiani, H. E.; Miki-Yoshida, M.; Camacho-Bragado, G. A.; Marques, M. A. L.; Rubio, A.; Ascencio, J. A.; Jose-Yacaman, M., Direct Observation of the Mechanical Properties of Single-Walled Carbon Nanotubes and Their Junctions at the Atomic Level. *Nano Letters* **2003,** *3* (6), 751-755.https://doi.org/10.1021/nl0341640

41. Das, K.; Madhusoodan, A. P.; Mili, B.; Kumar, A.; Saxena, A. C.; Kumar, K.; Sarkar, M.; Singh, P.; Srivastava, S.; Bag, S., Functionalized carbon nanotubes as suitable scaffold materials for proliferation and differentiation of canine mesenchymal stem cells. *International Journal of Nanomedicine* **2017,** *12*, 3235-3252.https://doi.org/10.2147/ijn.s122945

42. Zhou, Z.; Yu, P.; Zhou, L.; Tu, L.; Fan, L.; Zhang, F.; Dai, C.; Liu, Y.; Ning, C.; Du, J.; Tan, G., Polypyrrole Nanocones and Dynamic Piezoelectric Stimulation-Induced Stem Cell Osteogenic Differentiation. *ACS Biomaterials Science & Engineering* **2019,** *5* (9), 4386-4392.https://doi.org/10.1021/acsbiomaterials.9b00812

43. Nadri, S.; Soleimani, M.; Hosseni, R. H.; Massumi, M.; Atashi, A.; Izadpanah, R., An efficient method for isolation of murine bone marrow mesenchymal stem cells. *International Journal of Developmental Biology* **2007,** *51* (8), 723-729.https://doi.org/10.1387/ijdb.072352ns

44. Baghaei, K.; Hashemi, S. M.; Tokhanbigli, S.; Asadi Rad, A.; Assadzadeh-Aghdaei, H.; Sharifian, A.; Zali, M. R., Isolation, differentiation, and characterization of mesenchymal stem cells from human bone marrow. *Gastroenterol Hepatol Bed Bench* **2017,** *10* (3), 208-213

45. Price, R. L.; Waid, M. C.; Haberstroh, K. M.; Webster, T. J., Selective bone cell adhesion on formulations containing carbon nanofibers. *Biomaterials* **2003,** *24* (11), 1877-1887.https://doi.org/https://doi.org/10.1016/S0142-9612(02)00609-9

46. Yoon, J.-K.; Misra, M.; Yu, S. J.; Kim, H. Y.; Bhang, S. H.; Song, S. Y.; Lee, J.-R.; Ryu, S.; Choo, Y. W.; Jeong, G.-J.; Kwon, S. P.; Im, S. G.; Lee, T. I.; Kim, B.-S., Thermosensitive, Stretchable, and Piezoelectric Substrate for Generation of Myogenic Cell Sheet Fragments from Human Mesenchymal Stem Cells for Skeletal Muscle Regeneration. *Advanced Functional Materials* **2017,** *27* (48), 1703853.https://doi.org/10.1002/adfm.201703853

47. Yoon, J. K.; Misra, M.; Yu, S. J.; Kim, H. Y.; Bhang, S. H.; Song, S. Y.; Lee, J. R.; Ryu, S.; Choo, Y. W.; Jeong, G. J.; Kwon, S. P.; Im, S. G.; Tae, T. I.; Kim, B. S., Thermosensitive, Stretchable, and Piezoelectric Substrate for Generation of Myogenic Cell Sheet Fragments from Human Mesenchymal Stem Cells for Skeletal Muscle Regeneration. *Advanced Functional Materials* **2017,** *27* (48).https://doi.org/10.1002/adfm.201703853

48. Sugimoto, A.; Miyazaki, A.; Kawarabayashi, K.; Shono, M.; Akazawa, Y.; Hasegawa, T.; Ueda-Yamaguchi, K.; Kitamura, T.; Yoshizaki, K.; Fukumoto, S.; Iwamoto, T., Piezo type mechanosensitive ion channel component 1 functions as a regulator of the cell fate determination of mesenchymal stem cells. *Scientific Reports* **2017,** *7* (1), 17696.https://doi.org/10.1038/s41598-017-18089-0

49. Jaffe, T. L. A. W. Electrospun electroactive polymers for regenerative medicine applications. 2017-05-04.

50. Shuai, C.; Liu, G.; Yang, Y.; Yang, W.; He, C.; Wang, G.; Liu, Z.; Qi, F.; Peng, S., Functionalized BaTiO3 enhances piezoelectric effect towards cell response of bone scaffold. *Colloids and Surfaces B: Biointerfaces* **2020,** *185*, 110587.https://doi.org/https://doi.org/10.1016/j.colsurfb.2019.110587

51. Damaraju, S. M.; Shen, Y.; Elele, E.; Khusid, B.; Eshghinejad, A.; Li, J.; Jaffe, M.; Arinzeh, T. L., Three-dimensional piezoelectric fibrous scaffolds selectively promote mesenchymal stem cell differentiation. *Biomaterials* **2017,** *149*, 51-62.https://doi.org/https://doi.org/10.1016/j.biomaterials.2017.09.024

Chapter 4

1 Conclusions and perspective

1.1 Conclusion

Electrospinning has developed into a simple and effective new processing technology, that can be used for the fabrication of nanofibers with a variety of composition and properties, some of which play a huge role in the area of biological applications. Meanwhile, piezoelectric materials as new smart materials, became interesting for tissue engineering. Specifically, the flexible polymer PVDF and copolymers became popular materials and widely used in various healthcare applications. Moreover, carbon nanotubes are novel materials that have unique mechanical and chemical properties, which have also been incorporated into the biomedical field.

In our project we aimed at producing a device for direct mechanical stimulation of cells, based on the inverse piezoelectric effect from electrospun nanofibers with adequate composition. Then, the device would be tested on a range of suitable cell models, to verify its usefulness or potential for application in the biomedical field. This is a novel use of electrospun nanofibers, since only the direct piezoelectric effect had been used so far and reported in the literature.

For our objectives, we decided to use PVDF as the base for the nanofibers, since it can be produced with the adequate composition for piezoelectric applications. The properties of the PVDF polymer nanofibers were improved with the addition of Multi Walled Carbon Nanotubes (MWCNTs) which resulted on enhanced piezoelectric behavior. Moreover, the MWCNTs are known to possess suitable properties for interaction with biological samples.

After several experiments we were able to find the optimized conditions for the electrospinning process of aligned nanofibers: electrospinning voltage of 20 kV at 15 cm distance (1.33 kV/cm); solvent system composed of DMF and acetone (6:4 by volume); the polymer solution had the concentration of 12% (12 g PVDF by 100 ml

solvent); the MWCNTs had a concentration of 0.5% (weight ratio); rotating collector at 2000 rpm. Using these conditions we obtained highly aligned nanofiber meshes with suitable properties for our objectives, especially the piezoelectric PVDF crystal structure confirmed by XRD, FTIR, mechanical and electrical testing. The fibers characterization was completed with successful *in vitro* cytocompatibility tests, using the L929 fibroblasts cell line. The overall product, the PVDF/MWCNTs nanofibers, indeed show adequate piezoelectric properties as well as the three-dimensional structure and cytocompatibility required for application as scaffolds for tissue engineering.

The PVDF/MWCNTs were successfully applied on interdigitate electrodes which allowed their use for the preparation of a small cell culture vehicle, which supported the inverse piezoelectric stimulation of the cultured cells and thus paving the way for the research on its potential for tissue engineering applications.

For the testing of our device, we decided to use three different cell types: NIH3T3 fibroblasts; PC12 neuroblastic cells; mesenchymal stem cells (MSCs). The rationale for this choice was: first, investigate the effect of our device on the cell morphology, proliferation and migration of fibroblasts, which due to their natural cell function, play an important role in wound healing; secondly, to verify the potential of our device on the proliferation and differentiation of neuroblastic cells since they hold an important role as models for nerve regeneration studies; thirdly, we wanted to investigate the capacity of our device to modulate the proliferation and differentiation of mesenchymal stem cells, which have the potential to derive into several different cell types. On all cell types, the device with aligned PVDF/MWCNTs and inverse piezoelectric stimulation for 30 minutes per day (10 V, 5Hz square wave) was compared to several other combination of materials for control.

The testing with the NIH3T3 cell line allowed us to conclude that the device stimulation resulted in the highest bioactivity, with improved viability, proliferation

and migration, as compared to other materials tested. The cell morphology was directly affected by the fibers' alignment, showing that the cells exhibit growth along the fibers' direction. Moreover, we demonstrated that the enhancement of bioactivity resulted from the mechanical stimulation provided by the inverse piezoelectric effect, other than the electric signal used for driving the fibers.

Regarding the PC12 neuroblastic cells testing, the device resulted on significant enhancement of the cell adhesion and proliferation. The differentiation was also positively influenced, since the cells exhibited increased expression of the NF-200 neurofilament protein and neuron-like shape with extended neurites, when compared to other materials and without stimulation.

The final testing with MSCs revealed that with the level of stimulation used, it was not possible to observe significant differences between the cells' adhesion and proliferation, over the other materials without stimulation. Regarding the MSCs differentiation, the two different experiments yielded different results. For the adipogenic differentiation the stimulation didn't show any enhancement, when compared with other materials and without stimulation. On the contrary, for the osteogenic differentiation, the IPS with aligned PVDF/MWCNTs nanofibers improved the differentiation process.

Overall, we concluded that the mechanical stimulation provided by the inverse piezoelectric effect, from the PVDF/MWCNTs nanofibers, has a positive effect on the behavior of specifically selected cell types, which opens the possibility for its use on fundamental cell biology research and, more importantly, for different tissue engineering applications, such as, wound healing, nerve regeneration and bone regeneration.

1.2 Prospective

For future work we can already envisage several lines of research. The first will be the improvement of our device, with a robust design that allows for more extensive and complex experiments. The new design should allow: an easier handling and experimental setup; the use of different voltage, signals, frequency and stimulation time; autonomous operation inside an incubation chamber, with remote control from a PC. The second line of research should take advantage of the new device design and validate the results from this thesis with a more extensive range of experimental parameters, that would support a better understanding of the effects of mechanical stimulation on cell biology. After that, further testing may include *in vivo* experiments to confirm the in vitro results with a clear target for application in tissue engineering.

Project M1420-01-0145-FEDER-000005-CQM+

Project PROEQUIPRAM - M1420-01-0145-FEDER-000008